UNIVERSITÉ DE SHERBROOKE
Faculté de génie
Département de génie mécanique

ÉTUDE DES CARACTÉRISTIQUES THERMIQUES ET HYDRODYNAMIQUES DE COULIS DE GLACE

Thèse de Doctorat
Spécialité : génie mécanique

Landa C. Onokoko

Jury : Nicolas GALANIS (directeur)
Sébastien PONCET (codirecteur)
Michel POIRIER (codirecteur)
Stéphane HALLÉ (examinateur)
Bernard MARCOS (examinateur)
Hachimi FELLOUAH (rapporteur)

Sherbrooke (Québec) Canada Février 2019

To my wife Bando;

To my children: Elie, Jean, Lydia, Ruth and Philomene;

For their love, support and sacrifices.

RÉSUMÉ

Les matériaux à changement de phase solide-liquide sont de plus en plus utilisés pour le stockage et le transport de l'énergie de manière efficace en bénéficiant de la chaleur latente de changement d'état. Parmi ces matériaux figure le coulis de glace utilisé comme fluide frigoporteur dans les boucles de refroidissement secondaires. Il offre de nombreux avantages vis-à-vis des fluides conventionnels dans le transport de l'énergie et l'amélioration des transferts de chaleur dans les échangeurs. La conception d'installations utilisant le coulis de glace nécessite la connaissance de ses caractéristiques thermo-hydrodynamiques. Plusieurs travaux ont été réalisés, mais une divergence a été observée dans les résultats et opinions étant donné la complexité des mécanismes de transfert de chaleur due aux régimes d'écoulement et à la dynamique de changement de phase. Dans cette thèse, un modèle CFD 3D qui considère le coulis de glace comme un fluide Newtonien monophasique ayant des propriétés effectives qui dépendent de la concentration en glace a été développé et utilisé pour simuler l'écoulement du coulis de glace dans des conduites isothermes et chauffées. Le modèle qui tient compte de la fusion, la flottaison et la diffusion-convection des particules de glace, a été validé à l'aide des résultats de la littérature et des mesures réalisées avec le montage disponible à CanmetENERGY à Varennes, Québec, Canada. Malgré la relative simplicité de ce modèle (comparé aux modèles à deux phases utilisées ailleurs), sa solution numérique donne des résultats qui reflètent correctement les observations expérimentales.

Mots-clés : Coulis de glace, Modèle monophasique, Transfert de chaleur, Changement de phase, Simulation.

ABSTRACT

Solid-liquid phase change materials are increasingly being used for energy storage and transport in an efficient manner, taking advantage of the latent heat of phase change. Among these materials is the ice slurry used as a coolant in the secondary cooling loops. It offers many advantages over conventional fluids in the transport of energy and the improvement of heat transfer in heat exchangers. The design of installations using ice slurry requires knowledge of its thermo-hydrodynamic characteristics. Several studies have been carried out, but a discrepancy has been observed in the results and opinions given the complexity of heat transfer mechanisms due to flow regimes and phase change dynamics. In this thesis, a 3D CFD model which treats the ice slurry as a Newtonian fluid with effective properties depending on the local ice fraction has been developed and used to simulate ice slurry flow in both isothermal and heated pipes. The model, which considers the melting, settling and convection-diffusion of ice particles, has been validated using literature results and measurements made with the test bench available at CanmetENERGY in Varennes, Québec, Canada. Despite the relative simplicity of this model (compared to the two-phase models used elsewhere), its numerical solution gives results which correctly reflect experimental observations.

Keywords: Ice slurry, Single-phase model, Heat transfer, Phase change, Simulation.

REMERCIEMENTS

Je tiens tout d'abord à exprimer ma profonde reconnaissance à mon Directeur de thèse, le Professeur Nicolas GALANIS pour ses conseils, sa disponibilité et pour m'avoir offert cette opportunité.

Je tiens à remercier aussi :

- le Professeur Sébastien PONCET pour son soutien permanent, sa rigueur et son envie de partager ses connaissances.

- Dr Michel POIRIER mon encadreur de thèse à CanmetENERGY pour son support et sa disponibilité.

- les membres du jury pour avoir accepté de participer à l'évaluation de ce travail.

- les membres du personnel de la Faculté pour leur support.

- le CRSNG et la Faculté de Génie de l'Université de Sherbrooke pour le support financier.

- Mme Monique Joyal PAINCHAUD pour son aide précieuse.

Enfin, que tous ceux qui ont contribué à faciliter cette étude trouvent ici le témoignage de ma sincère gratitude et vive reconnaissance.

TABLE DES MATIÈRES

LISTE DES FIGURES

LISTE DES TABLEAUX

LISTE DES SYMBOLES

Nomenclature

a, R	Average ice particle radius (m)
C_p	Specific heat ($kJkg^{-1}K^{-1}$)
d_p	average ice particle diameter (m)
D	internal pipe diameter (m)
f	hindrance function (–)
H_e	Hedström number (–)
h	heat transfer coefficient ($Wm^{-2}K^{-1}$)
Δh_{mix}	heat of mixing ($kJkg^{-1}$)
$\mathrm{J}_{\emptyset}$	diffusion flux for specie Ø (m^2s^{-1})
k	thermal conductivity ($Wm^{-1}K^{-1}$)
K_c, K_μ	constants (-)
L	pipe length (m)
$\mathrm{L_f}$	ice specific latent heat of fusion ($kJkg^{-1}$)
$\mathrm{L_h}$	heated section length (m)
$\dot{m}$	mass flow rate (kgs^{-1})
N	particles flux
P	pressure (Pa)
Q	gravitational acceleration vector
Re	Reynolds Number (–)
$S_{\dot{\gamma}}$	source term of species equation
S_h	source term for heat
$S_{\emptyset}$	source term for specie Ø
T	temperature (℃)
u	velocity vector (ms^{-1})
w	mass fraction (-)
x_i	Cartesian coordinates
z	Axial coordinate (m)
*z**= (z/*D*)/*Re*	

Lettres grecques

α, β, γ	coefficients
$\dot{\gamma}$	magnitude of shear rate (s^{-1})
$\Gamma_{\emptyset}$	diffusive coefficient for specie Ø
μ	dynamic viscosity (Pas)
ρ	density (kgm^{-3})
$\boldsymbol{\tau}$	shear stress tensor (Pa)

$\emptyset$	volume fraction $(-)$
ω_o	terminal velocity of a single ice particle in aqueous solution (ms^{-1})

Indices

a	additive
as	residual aqueous solution
B	Bingham
c	critical
ic	ice particle
in	inlet
is	ice slurry
m	mean value
loc	local
o	initial
w	wall

LISTE DES ACRONYMES

AIE	Agence internationale de l'énergie
ASHRAE	American Society of Heating, Refrigerating, and Air Conditioning Engineers
CANMET	Canada Center for Mineral and Energy Technology
CFD	Computational Fluid Dynamics
DEFRA	Validity of Food Miles as an Indicator of Sustainable Development.
GES	Gaz à effet de serre
HFC	Hydrofluorocarbures
MPG	Monopropylene glycol
PCM	Phase Change Materials
QUICK	Quadratic Upstream Interpolation for Convective Kinematics
RNG	Renormalization-group
RTD	Resistance Temperature Detector
SIMPLE	Semi Implicit Method for Pressure Linked Equations
UDS	User-defined scalar
VOF	Volume of fluid

CHAPITRE 1

INTRODUCTION

La consommation mondiale en énergie augmente avec la croissance de la population et de son économie. Elle crée une augmentation d'émissions de gaz à effet de serre (GES) qui contribuent à la détérioration de la qualité de l'air avec un impact très nocif sur l'environnement. Selon l'AIE (2010), les émissions de gaz à effet de serre (GES) attribuables à la demande mondiale d'énergie augmenterons de 40% d'ici 2030 par rapport à 2007. Devant les conséquences néfastes des rejets de gaz à effet de serre, il est devenu indispensable de développer des systèmes innovants qui permettent une amélioration de l'efficacité énergétique, une meilleure maîtrise de la demande énergétique et une réduction des émissions de CO_2. La consommation d'énergie par les procédés de fabrication, de distribution et de vente (les grandes surfaces) des produits alimentaires est considérée comme la source principale d'émission de CO_2. Environ 7% des émissions totales proviennent de la distribution et de la vente des produits alimentaires (DEFRA, 2005). Les technologies du froid, qui progressivement prennent de l'ampleur dans la transformation et la conservation des aliments, sont aujourd'hui responsables du principal impact de GES sur l'environnement. Selon Coulomb (2008), le froid est responsable de 15 % de la consommation mondiale d'électricité. Selon Cowan et al. (2010), l'impact du secteur de la réfrigération sur le réchauffement climatique est attribuable à 72% à la consommation de l'énergie. D'autre part, la fuite dans l'atmosphère des hydrofluorocarbures (HFC) contenus dans les systèmes de réfrigération a un impact significatif sur le réchauffement climatique. Des récentes recherches ont montré que les émissions globales des hydrofluorocarbures (HFC) ont augmenté de plus de 50 % entre 2007 et 2012 (Lunt et al., 2015). Donc, diminuer la demande d'énergie de réfrigération et l'utilisation de fluides frigorifiques traditionnels dans le secteur alimentaire et la climatisation est devenu l'une des priorités dans la réduction des émissions de GES.

Devant les contraintes environnementales de plus en plus sévères (protocoles de Montréal en 1989 puis de Kyoto en 1997) ainsi que les problèmes grandissant de disponibilités des ressources énergétiques, le secteur de réfrigération est appelé non seulement à rationaliser l'utilisation de son énergie mais aussi à faire évoluer ses technologies vers le développement de systèmes innovants qui permettent une amélioration importante de l'efficacité énergétique. C'est le cas du refroidissement indirect utilisé dans les opérations industrielles de distribution du froid.

Les matériaux à changement de phase (PCM-Phase Change Materials) solide-liquide sont de plus en plus utilisés pour le stockage et le transport de l'énergie de manière efficace en bénéficiant de la chaleur latente de changement d'état. Parmi ces matériaux figure le coulis de glace utilisé comme fluide frigoporteur secondaire dans la distribution de froid. Le coulis de glace offre de nombreux avantages vis-à-vis des fluides conventionnels dans le transport de l'énergie et l'amélioration des transferts de chaleur dans les échangeurs (Bel et Lallemand, 1999). Dans certains pays, les besoins en conditionnement d'air peuvent représenter 60% de la demande globale d'électricité dans les bâtiments commerciaux. L'utilisation d'un système de stockage d'énergie par coulis de glace peut engendrer une économie de 55% (Monteiro et Bansal, 2010). D'autre part, l'utilisation du coulis de glace permet de réduire la charge des hydrofluorocarbures (HFC) dans la réfrigération étant donné qu'il est non polluant, non toxique, ininflammable et facile à manipuler avec sûreté.

La conception d'installations utilisant le coulis de glace nécessite la connaissance de ses caractéristiques thermo-hydrodynamiques telles que le coefficient d'échange thermique et le coefficient de friction. Plusieurs travaux ont été réalisés, mais sans qu'un consensus ne se dégage (Ayel et al., 2003) car les mécanismes de transfert de chaleur sont très complexes (transferts convectifs entre cristaux de glace et fluide porteur, entre coulis de glace et parois de la conduite et par conduction au sein même des cristaux de glace qui sont le siège d'un changement de phase) et dépendent du régime d'écoulement (homogène, hétérogène,

stratification) et de la dynamique de changement de phase (cristallisation ou fusion de la glace).

Des nombreux travaux ont déjà démontré les performances des coulis de glace dans les échangeurs de chaleur (Ayel et al., 2003 ; Kauffeld et al., 2005 ; Egolf et al., 2005 ; Niezgoda-Zelasko, 2006 ; Lee et al., 2006 ; Niezgoda-Zelasko et Zalewski, 2006 ; Renaud-Boivin et al., 2012) mais les avantages technologiques du coulis et son éventuel impact sur l'économie demandent un examen critique des travaux antérieurs afin de suggérer de nouvelles pistes de recherche. Jusqu'à maintenant, peu d'études ont été effectuées sur la chute de pression et le transfert de chaleur dans un écoulement de coulis de glace sujet aux effets combinés de la stratification et de la fusion de glace.

Bien qu'il existe un certain nombre de travaux sur l'étude numérique d'écoulements de coulis de glace, leur caractérisation ne fait pas l'unanimité et les résultats publiés ne s'adressent pas à tous les problèmes détectés de façon expérimentale. La modélisation numérique d'écoulements de coulis de glace est relativement difficile au regard des phénomènes complexes qui les caractérisent (stratification, fusion, etc…). Cependant, avec l'amélioration des modèles mathématiques et l'augmentation des capacités de calcul des ordinateurs, ces écoulements peuvent être étudiés au moyen des méthodes CFD. Ce projet de doctorat consiste à concevoir un modèle numérique simple et efficace capable de fournir, à des coûts de calcul raisonnables, des informations fiables sur la structure des écoulements de coulis de glace dans les tuyaux en tenant compte des effets combinés de la flottaison et de la fusion de glace.
La démarche et les résultats du projet sont présentés dans les chapitres suivants :

Le premier chapitre constitue une introduction au contexte énergétique et aux systèmes de réfrigération. Les défis environnementaux d'aujourd'hui, la situation énergétique du monde, ainsi que les avantages de la réfrigération indirecte et l'utilisation du coulis de glace comme fluide frigorigène sont présentés.

Le deuxième chapitre est une synthèse des notions de base sur les coulis de glace. Le modèle de calcul des propriétés thermophysiques du coulis de glace, la rhéologie, la viscosité et le modèle de flux diffusifs de Phillips et al. (1992) sont présentés. Un aperçu bibliographique et une analyse critique des travaux antérieurs sur les écoulements des coulis de glace avec une attention particulière sur la modélisation numérique sont aussi présentés.

Le troisième chapitre présente l'étude de la stratification du coulis de glace dans une conduite isotherme. Une présentation détaillée du modèle dans le cas d'un écoulement isotherme est faite (phénomènes physiques mis en jeu, mise en équation du modèle, ...).

Le quatrième chapitre présente l'étude de la rhéologie d'un coulis de glace à base de propylène glycol.

Le cinquième chapitre présente l'étude expérimentale et numérique d'un écoulement isotherme de coulis de glace dans une conduite horizontale.

Le sixième chapitre présente l'étude numérique des transferts de chaleur dans un écoulement de coulis de glace dans une conduite horizontale chauffée.

Le dernier chapitre présente la synthèse des résultats obtenus et les perspectives futures pour la poursuite de ces travaux.

CHAPITRE 2

NOTIONS FONDAMENTALES ET REVUE BIBLIOGRAPHIQUE

2.1 Définition

Les coulis de glace sont des suspensions formées de cristaux de glace dispersés dans une solution aqueuse. Ils sont obtenus à partir de solutions aqueuses contenant un additif chargé d'abaisser la température de cristallisation de la solution. Le choix de l'additif est fait de façon à adapter la température de cristallisation du mélange à l'application visée. Les sels, les glycols et les alcools sont les additifs le plus couramment utilisés. Sans additif, les cristaux de glace produits dans l'eau pure sont dendritiques. Ils présentent une surface très rugueuse qui entraîne une faible fluidité, une agglomération facile et un colmatage des conduites.
La taille typique des cristaux de glace se situe entre 0.1 et 1 mm de diamètre. Cette taille dépend du type d'additif, de la concentration en glace et du type de générateur à glace utilisé. Sans additif, la taille des cristaux est généralement supérieure à 1 mm de diamètre (Stamatiou et Kawaji, 2005).

Les coulis de glace, qui peuvent transporter quatre fois plus d'énergie frigorifique que l'eau glycolée, présentent l'avantage de nécessiter une faible consommation énergétique (réduction de la taille des installations ; Inaba, 2005) et d'avoir un impact environnemental très faible.

2.2 Génération et Stockage du coulis de glace

Toutes les techniques de génération de la glace ont le même principe de fonctionnement : échanger de la chaleur entre un fluide frigorigène et un mélange aqueux constituant le frigoporteur diphasique. Elles comprennent généralement les étapes suivantes : la surfusion de la solution aqueuse, la nucléation et la croissance des cristaux. La phase aqueuse est d'abord amenée dans un état de surfusion (Paradis et al., 1989 et Snoek, 1993) c'est-à-dire sans

formation de glace à une température inférieure à sa température de cristallisation théorique. L'état de surfusion (qui est par essence instable) ne peut perdurer ainsi indéfiniment, il cesse à une température dite de nucléation, en dessous de laquelle le liquide cristallise même en l'absence de tout germe de cristallisation et passe alors à un état solide stable : C'est la nucléation. La surfusion peut aussi être rompue au-dessus de cette température (*point de Schaefer)* grâce à la présence d'un germe de cristallisation (cristal du corps manipulé, corps isomorphe…), d'une impureté ou en imposant une perturbation (mécanique, acoustique …). Il s'en suit la croissance de cristaux. Les méthodes de génération de coulis de glace peuvent être classées en deux catégories principales : les méthodes utilisant des pièces mobiles et les méthodes sans pièces mobiles. Une revue détaillée des différents types de générateur a été réalisée par Zhang et Ma (2012).

Le stockage du coulis de glace dans les réservoirs est principalement réalisé selon deux modes, le stockage hétérogène et le stockage homogène (Egolf et al., 2008). Dans la cuve de stockage, la taille et la forme des cristaux sont affectés par les phénomènes de lissage, agglomération et maturation (Stamatiou et al., 2005). Le lissage se produit dans les cuves agitées mécaniquement lorsque les cristaux sont endommagés par rupture ou abrasion par collision avec d'autres objets solides tels que les pales de l'agitateur, la paroi de la cuve ou les autres cristaux. L'agglomération peut se produire pendant la génération ou le stockage du coulis de glace. Les petits cristaux s'entrechoquent et se collent les uns aux autres pour former des cristaux plus larges et stables. Kobayashi et Shirai (1996) ont montré à partir d'expériences faites sur le stockage du coulis de glace que l'agglomération dépend principalement du germe de cristallisation (cluster), la répartition initiale de la taille des cristaux et de la concentration du soluté. En effet un coulis de glace est formé d'un ensemble de petits et de gros cristaux qui n'ont pas la même concentration et la même température d'équilibre. En raison de la contribution d'énergie de surface, les petits cristaux ont une température d'équilibre plus petite ce qui favorise la croissance de grands cristaux à leur détriment (tension superficielle). Ce phénomène qui prévoit une augmentation de la taille moyenne du cristal sur une période

relativement longue est appelé mûrissement d'Ostwald. La Figure 2.1 montre l'évolution de la taille du cristal de glace observée expérimentalement par Pronk et al. (2005).

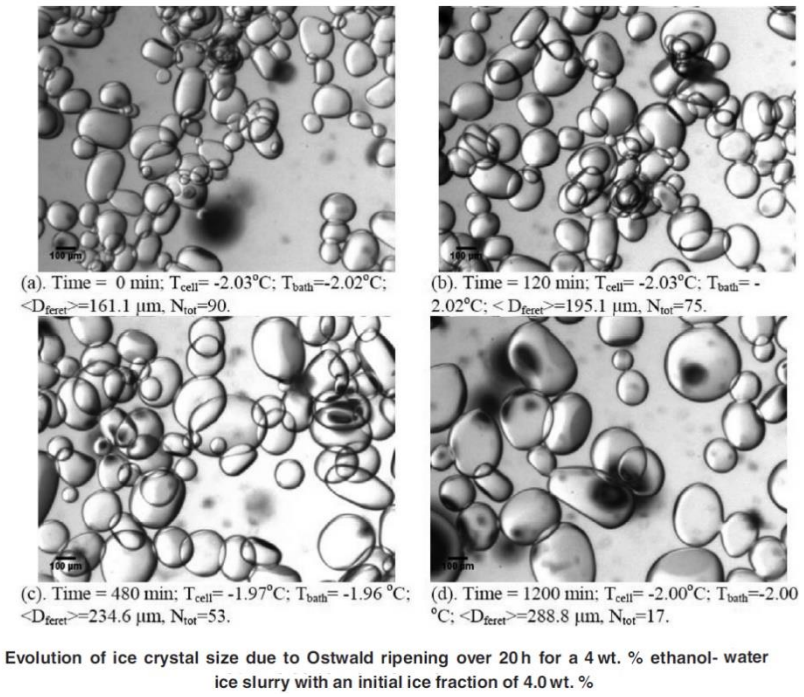

Fig. 2.1 Évolution dans le temps (20 heures) de la taille du cristal de glace dû à la maturation d'Ostwald pour un coulis de glace à base d'éthanol (w_{ao}= 4.0 % et w_{ic}= 4.5 ; Pronk et al., 2005)

2.3 Applications des coulis de glace

Les dernières avancées technologiques dans le domaine de la production, du transport et de la distribution de froid consistent essentiellement à séparer la production de froid et son transport aux utilisateurs par un circuit intermédiaire utilisant le coulis de glace comme frigoporteur. Cette technique permet de transporter une grande partie d'énergie de refroidissement sous forme latente avec comme avantages : la puissance frigorifique élevée, capacité de stockage énergétique accrue, faible énergie de pompage, zéro impact sur l'environnement, etc...

Une revue sur les applications des coulis de glace a déjà été faite (Kauffeld et al., 2010 ; Egolf et Kauffeld; 2005 ; Kauffeld et al., 2005). Ci-dessous, sont identifiés les principaux secteurs d'application des systèmes de refroidissement à coulis de glace :

La climatisation des grands bâtiments : Centres commerciaux, aéroports, grands immeubles, etc…

Un exemple typique d'un système de climatisation de bâtiment au moyen du coulis de glace est donné à la Fig. 2.2.

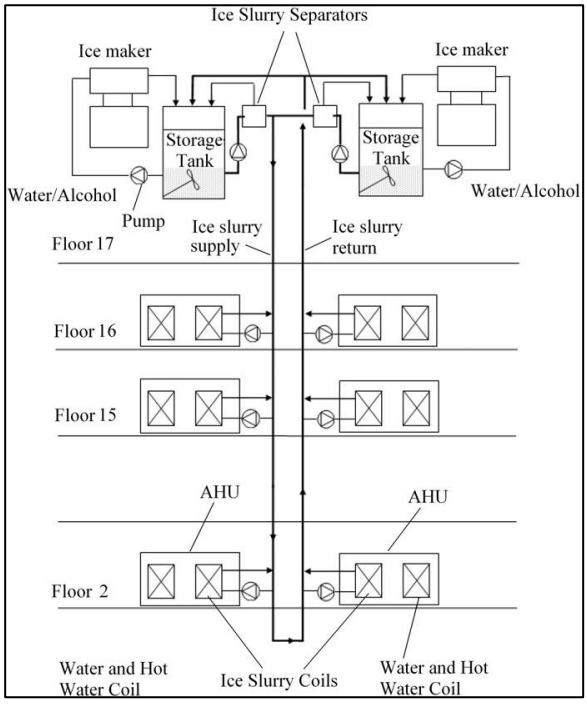

Fig. 2.2 Schéma de principe d'un système de climatisation de bâtiment par coulis de glace (Kauffeld, 1998).

Le froid industriel : Industrie agroalimentaire, entrepôt frigorifique, brasseries…

Les applications spécifiques : refroidissement des mines, pêche, médecine…

2.4 Propriétés Thermo-physiques du coulis de glace

La connaissance des propriétés thermophysiques des coulis de glace est primordiale dans l'étude de leurs comportements thermique et hydrodynamique. Etant donné que le coulis de glace est un mélange d'une solution aqueuse et des cristaux de glace, il est difficile d'évaluer ses propriétés thermophysiques avec précision. Elles dépendent de plusieurs paramètres tels que la géométrie de la structure, le débit massique, les conditions de température et de pression à l'entrée, de la concentration d'additif, de la fraction de glace, etc... Les corrélations

utilisées dans le calcul des propriétés thermophysiques des coulis de glace reposent sur les méthodes semi-empiriques basées sur la détermination de la concentration en glace à partir des mesures de densité et sur l'hypothèse que le coulis de glace est un mélange diphasique non-miscible. Les propriétés du coulis de glace sont obtenues par pondération linéaire des propriétés correspondantes de la glace et de la solution aqueuse (Wasp et al., 1977, Guilpart et al., 1999 ; Kauffeld et al.,2005). Différents modèles pour chaque propriété thermophysique ont été proposés et utilisés pour le dimensionnement des systèmes utilisant le coulis de glace comme fluide frigoporteur (Meewise et Infante Ferreira, 2003). Les données de base et relations intervenant dans la détermination des propriétés des solutions aqueuses pour la plupart des applications industrielles ont été publiées par certains auteurs (Melinder, 1997 ; Lakhdar, 1998 ; ASHRAE, 2005). Les propriétés de la glace sont des fonctions de la température. Elles sont décrites dans le Handbook on Ice Slurries – Fundamentals and Engineering (2005).

2.4.1 Mélange Diphasique Eau-Glace-Additif : Diagramme d'équilibre

Point de congélation commençante

C'est la température à laquelle commence l'apparition des premiers cristaux de glace. Elle est représentée à la Fig. 2.3 par une courbe de congélation qui donne le point de congélation en fonction de la concentration en additif. Pour différentes solutions aqueuses utilisées dans notre travail, les courbes de congélation sont basées sur des valeurs tabulées de l'ASHRAE (2005).

La température de saturation

La température de saturation d'un mélange eau-additif correspond au point de congélation à la concentration massique initiale de l'additif w_{ao} (Fig. 2.3). Au-dessous de cette température, la formation de particules de glace augmente la concentration résiduelle de l'additif dans le liquide.

Concentration massique en glace

La concentration massique en glace w_{ic} est donnée par la relation suivante,

$$w_{ic} = 1 - \frac{w_{ao}}{w_a} \tag{2.1}$$

Cette relation permet de relier directement la fraction massique en glace à la température. Elle est obtenue à partir du bilan de matière du diagramme d'équilibre. Elle n'est valable que si la solution et la glace se trouvent en équilibre thermodynamique.

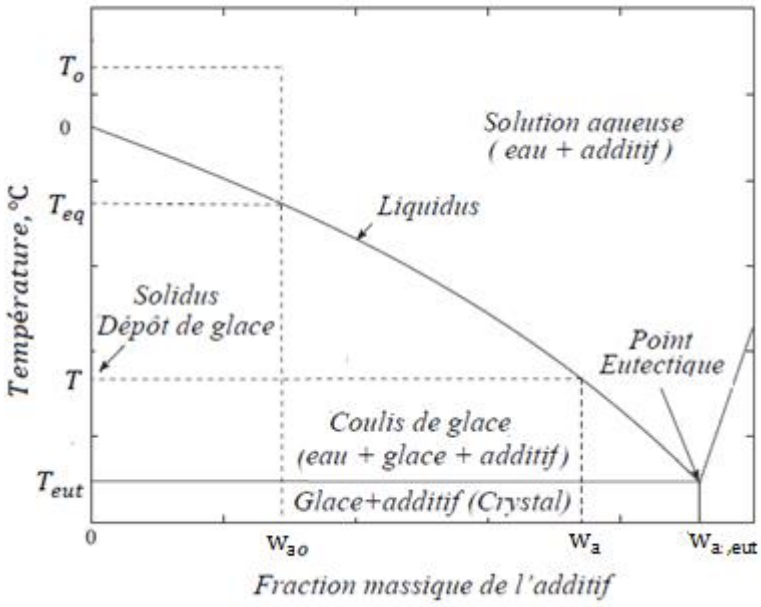

Fig. 2.3 Diagramme d'équilibre eau-additif (Solution aqueuse) adapté de Evans (2007)

La relation qui relie la température *T* à la concentration résiduelle d'additif w_a dans la solution aqueuse peut-être approximée par une équation polynomiale de la forme :

$$w_a = \sum(a_i T^i) \text{ ou } T = \sum(a_i' w_a^i) \tag{2.2}$$

Une équation similaire peut être utilisée pour exprimer la concentration volumique résiduelle en additif en fonction de la température de saturation. Les coefficients a_i et α_i' ont été calculés par Renaud-Boivin et al. (2012) pour des solutions aqueuses de propylène glycol, d'éthylène glycol, de chlorure de calcium et de chlorure de sodium à partir des valeurs tabulées de l'ASHRAE (2005).

A partir du bilan de matière du diagramme d'équilibre, l'équation qui permet de calculer la concentration volumique résiduelle d'additif $\emptyset_a$ dans la solution aqueuse est donnée par :

$$\emptyset_a = \frac{w_{ao}}{1 - w_{ic}} \frac{\rho_{as}}{\rho_a} \tag{2.3}$$

2.4.2 Propriétés du Mélange Diphasique Eau-Glace-Additif : Coulis de glace

Pour déterminer les propriétés thermophysiques du coulis de glace, il faut tenir compte de la concentration résiduelle en additif. Cette concentration résiduelle est supérieure à la concentration initiale d'additif puisqu'une fraction d'eau a cristallisé. Les propriétés du coulis de glace dépendent des propriétés de la solution aqueuse calculées pour une concentration d'additif résiduelle, et des propriétés de la glace, pondérées par leur fraction massique dans le mélange (Wasp et al. 1977, Guilpart et al. 1999).

Les propriétés thermophysiques du coulis de glace peuvent être calculées avec les relations suivantes (Kauffeld et al., 2005) :

$$\rho_{is} = \emptyset_{ic}\rho_{ic} + (1 - \emptyset_{ic})\rho_{as} \tag{2.4}$$

$$\mu_{is} = \mu_{as}\left(1 + 2.5\emptyset_{ic} + 10.05\emptyset_{ic}^2 + 0.00273e^{16.6\emptyset_{ic}}\right) \tag{2.5}$$

$$k_{is} = k_{as}(1 + 3\emptyset_{ic}\beta + 3\emptyset_{ic}^2\beta^2\gamma) \tag{2.6}$$

Où : $\gamma = 1 + \beta/4 + (3\beta/16)\,[(\alpha + 1)/(2\alpha + 3)]$,

$$\beta = (\alpha - 1)/(\alpha + 2), \quad \alpha = k_{ic}/k_{as} \tag{2.7}$$

$$h_{is} = w_{ic}h_{ic} + (1 - w_{ic})h_{as} \tag{2.8}$$

Melinder et Granryd (2005) ont donné les expressions de h_{ic} et h_{as} :

$$h_{ic} = -\mathrm{L_f} + C_{p,ic}T \tag{2.9}$$

$$h_{as} = h_{0,T_{ref}} + \Delta h_{mix} + \int_{T_{ref}}^{T} C_{p,as}\,dT \tag{2.10}$$

Où :

$h_{0,T_{ref}}$ est l'enthalpie de l'eau à la température de référence, $h_{0,T_{ref}}$ =0 kJ/kg à 0°C.

Δh_{mix}, la chaleur de mélange et L_f la chaleur latente spécifique de fusion.

Les corrélations qui relient Δh_{mix} et L_f à la fraction massique résiduelle $\mathrm{w_a}$ peuvent être obtenues de Renaud-Boivin et al. (2012) et de Kumano et al. (2010) respectivement.

Les propriétés de la glace sont obtenues à partir des relations suivantes (Kauffeld et al., 2005) :

$$\rho_{ic} = 917 - 0.13T \quad (2.11)$$

$$k_{ic} = 2.21 - 0.0012T \quad (2.12)$$

$$C_{p,ic} = 2.12 + 0.008T \quad (2.13)$$

Les propriétés de la solution aqueuse sont décrites en détail à la section 2.4.3

2.4.3 Propriétés des Mélanges Binaires Eau-Additif : Solution aqueuse

Plusieurs approches sont proposées dans la littérature pour calculer les propriétés thermophysiques de la solution aqueuse. Parmi les plus importantes, nous avons celles de Melinder (1997), de Bel et Lallemand (1999), de Ben Lakhdar et al. (1999) et de Lugo et al. (2002). Bien que les deux premières approches de calcul permettent de déterminer les propriétés thermophysiques des solutions aqueuses avec une grande précision, elles ne peuvent pas être appliquées à des basses concentrations en additif. Les deux dernières approches basées sur les fonctions d'excès données par Guilpart et al. (1999), permettent de surmonter ce problème par l'évaluation de la divergence entre l'état idéal (état de référence) et l'état réel de la solution aqueuse.

Dans notre travail, les propriétés thermophysiques de la solution aqueuse sont calculées avec les formules obtenues à partir des valeurs tabulées de l'ASHRAE (2005). L'expression générale de l'une quelconque de ces propriétés a la forme suivante :

$$P_{as}(\emptyset_a, T) = \sum_{i=0}^{M} T^i \sum_{j=0}^{N} b_{i,j}\, \emptyset_a^j \quad (2.14)$$

Les coefficients $b_{i,j}$ ont été calculés par Renaud-Boivin et al. (2012) pour des solutions aqueuses de propylène glycol, d'éthylène glycol, de chlorure de calcium et de chlorure de sodium à partir des valeurs tabulées de l'ASHRAE (2005).

2.5 Rhéologie du coulis de glace

La modélisation mathématique d'un écoulement diphasique solide/liquide est très complexe, en particulier lorsque la distribution de la phase solide dans la solution n'est pas homogène.

Le coulis de glace est considéré comme un type spécial de fluide diphasique solide-liquide. Son comportement rhéologique est étroitement lié aux conditions opératoires. Les différents auteurs qui ont étudié les propriétés rhéologiques du coulis de glace s'accordent sur le fait qu'il existe une fraction massique critique en glace en dessous de laquelle le coulis de glace se comporte comme un fluide Newtonien. Au-dessus de cette valeur critique, le coulis a un comportement non-Newtonien. La valeur critique diffère d'un auteur à l'autre et du fluide étudié, mais reste comprise entre 6 % et 15 % (Bel, 1996 ; Ben Lakhdar, 1998 ; Ayel et al., 2003). En tant que fluide non-Newtonien, différents modèles théoriques peuvent être utilisés pour décrire les comportements rhéologiques du coulis de glace. Les modèles les plus utilisés sont résumés dans le tableau 2.1 (Illàn et Viedma, 2009b). Parmi ces modèles, le modèle de Bingham est celui le plus fréquemment utilisé (Kitanovski et al., 2005; Niezgoda-Zelasko et Zalewski, 2006). Le modèle de type loi de puissance et ses dérivés (loi de puissance généralisée ou de second ordre) ont largement été utilisés par les ingénieurs (Wafo Soh et Mureithi, 2006; Sayed-Ahmed, 2000). Ils permettent de modéliser avec succès et simplicité les fluides rhéoépaississants et rhéofluidifiants. Les rhéogrammes obtenus à cet effet ont pu être approchés par la loi de Herschel-Buckley.

Dans ses études expérimentales, Mellari (2016) a supposé que le coulis de glace à base de monopropylène glycol (MPG) obéit à la loi d'Ostwald-de Waele. Elle a obtenu des corrélations pour les indices de consistance (K) et de comportement (n) en fonction des concentrations initiales de MPG et de glace. Les résultats ont confirmé que les coulis de glace peuvent se comporter comme un fluide Newtonien ou non et qu'ils peuvent être rhéofluidifiants ($n<1$) ou rhéoépaississants ($n>1$). Les résultats expérimentaux du coefficient de frottement de Darcy étaient en bon accord avec ceux obtenus par le modèle de Poiseuille.

Doestsch (2001) a proposé le modèle de Casson pour décrire simultanément les deux comportements des coulis de glace. Ses études expérimentales ont été basées sur divers types d'additifs. C'est pour cette raison que son modèle s'applique à une large gamme de solutions aqueuses. Les paramètres du modèle ont été exprimés en fonction de la viscosité de la solution aqueuse et de la concentration en glace.

Tableau 2.1 Modèles rhéologiques non-Newtoniens pour des coulis de glace

Model	Expression
Bingham (1916)	$\tau = \tau_o + \mu_B \dot{\gamma}$
Herschel-Bulkley (1926)	$\tau = \tau_o + k\dot{\gamma}^n$
Ostwald-de Waele (1925)	$\tau = k\dot{\gamma}^n$
Casson (1959)	$\tau^{0.5} = {\tau_o}^{0.5} + (\mu_c \dot{\gamma})^{0.5}$

Illàn et Viedma (2009b) ont mené des études expérimentales sur le comportement rhéologique d'un coulis de glace à base de saumure de NaCl à 9 wt % par des mesures de pertes de charge. Les expériences ont pris en compte des cristaux de glace de diamètre moyen 500 µm, des vitesses variant de 0.2 à 5 m/s et des rapports entre le diamètre du cristal de glace sur le diamètre de la conduite de 0.05, 0.10, 0.15, 0.20 et 0.25. Ils ont constaté que la relation contrainte – vitesse de cisaillement est presque linéaire pour des vitesses de cisaillement faibles et suit une loi de type puissance pour des valeurs plus élevées. Par conséquent, les modèles de Bingham et Casson ne sont pas adaptés pour prédire simultanément les deux comportements du coulis de glace. Un modèle modifié de Herschel-Buckley est proposé à la place. Ben Lakhdar (1998), quant à lui, a estimé que les coulis de glace de fraction massique en glace supérieure à 6 % ont un comportement rhéologique pouvant être modélisé par une loi de type loi de puissance d'Ostwald pour des vitesses de cisaillement comprises entre 20 et 310 s^{-1}. Pour des fractions massiques en glace supérieures à 13 %, il a constaté que la viscosité apparente du coulis diminuait avec l'augmentation du gradient de vitesse, mettant ainsi en évidence le caractère rhéofluidifiant de la suspension. Kumano et al. (2016) ont étudié expérimentalement l'effet de la concentration initiale de l'additif sur le comportement rhéologique du coulis de glace. La concentration initiale du coulis de glace à base d'une solution aqueuse d'éthanol a été considérée comme variable. A partir des mesures de la chute de pression, les auteurs ont constaté que le coulis de glace affichait un comportement pseudo-plastique pour des concentrations initiales en additif de 5 et 10wt % et se comportait comme

un fluide Newtonien pour des concentrations de 2 wt%. Egolf et Kauffeld (2005) ont proposé un modèle de Bingham modifié appelé aussi modèle de Bingham généralisé pour décrire les coulis de glace de fraction massique supérieure à 20 %. Ce modèle décrit le comportement rhéologique du coulis de glace sur toute la gamme de fraction de glace par une simple équation. Ils ont remarqué aussi qu'un fluide non idéal de Bingham peut aussi bien être décrit par un modèle de type loi de puissance. Chilton et Stainsby (1998) ont proposé un modèle rhéologique hybride pour décrire le comportement des coulis contenant des fines particules solides. Ils ont assumé que la rhéologie d'un fluide qui présente une contrainte de seuil peut être représentée par le modèle d'Herschel-Bulkley à des faibles taux de cisaillement et par le modèle de Bingham à des taux élevés. Doestsch (2001), comme il a été rapporté par Illàn et Viedma (2009b), et Trebelsi et al. (2017) ont montré que le modèle d'Herschel-Buckley et celui de Casson sont plus adapté pour décrire de façon acceptable le comportement rhéologique des coulis de glace en particulier à des concentrations importantes d'additif. Le modèle d'Herschel-Buckley a le désavantage d'être ambigu quand il s'agit de son optimisation qui conduit à une variété de solutions satisfaisantes. Doestsch (2001) a conclu que le modèle de Casson est préférable lorsqu'il s'agit de choisir entre le modèle de Casson et celui d'Herschel-Buckley.

Les efforts de modélisation du comportement rhéologique des coulis de glace portent actuellement sur la détermination d'un modèle valable pour toutes les valeurs de concentration en glace et prenant en compte la fraction massique de glace, la viscosité de la solution aqueuse, et éventuellement d'autres paramètres tels que la taille et la forme des cristaux de glace.

2.6 Viscosité d'une suspension

Les coulis de glace sont, avant tout, des suspensions de cristaux de glace. Les conclusions générales concernant les suspensions leur sont donc applicables. Dans cette section, nous allons parler des suspensions en général. On peut se représenter une suspension en écoulement comme un ensemble de particules en mouvement les unes par rapport aux autres

Tableau 2.2 Exemples des modèles rhéologiques les plus utilisés.

Auteurs	Coulis de Glace	Géométries et Débits	Comportement	Modèle
Ben Lakdar (1998)	$w_{ic} < 28$ % $d_p = 0.5$ mm	Tube horizontal L= 0.5 m, D_h =15 mm	Newtonien pour $w_{ic} < 6$ % Non-Newtonien pour $w_{ic} \geq 6$ % Rhéofluidifiant pour $w_{ic} > 13$ %	Loi de puissance d'Ostwald
Doestsch (2001)	$w_{ic} < 45$ %	Tube horizontal D_h =10-22 et 38 mm	Newtonien pour $w_{ic} < 6$ % Non-Newtonien pour $w_{ic} \geq 6$ %	Casson
Illàn et Viedma (2009b)	9 wt % Sol. de NaCl $d_p = 0.5$ mm $w_{ic} = 25$ %	Tube horizontal $0.016 < D_h < 0.035$ mm $0<V<2.5\ m/s$	Newtonien pour $\dot{\gamma}$ faible Non-Newtonien pour $\dot{\gamma}$ élevé	Herschel-Buckley Modifié
Kumano et al. (2010)	5 wt % Sol. d'éthanol $d_p = 0.1$-0.4 mm $w_{ic} \leq 25$ %	L= 2.5 m D_h =4.5, 7.5, 10.2 mm	Pseudo plastique	Loi de puissance d'Ostwald

dans un fluide porteur. La viscosité est associée à la contrainte qu'il faut exercer pour déplacer le fluide et les particules entre elles. Plus on ajoute des nouvelles particules, plus il y a d'interactions entre les particules, plus il y a de dissipation visqueuse et donc plus la viscosité augmente jusqu'à diverger pour une valeur de la fraction volumique maximum $\emptyset_{max}$. Einstein (1906) a développé le premier modèle théorique de viscosité pour des suspensions paru dans un article sur la théorie du mouvement Brownien :

$$\mu = \mu_l(1 + 2.5\emptyset) \tag{2.15}$$

Cette relation est valable pour des suspensions diluées ($\emptyset < 0.02$) de particules sphériques monodispersées ($d_p < 2\ \mu m$) en écoulement laminaire . Elle exprime l'évolution de la viscosité en fonction de la fraction volumique des particules. Elle prend en compte les effets

du mouvement Brownien, aléatoire, lié à l'agitation moléculaire des particules solides dispersées dans la phase liquide. La relation d'Einstein néglige toute éventuelle interaction entre particules et n'est pas valable lorsqu'elles deviennent importantes.

Batchelor (1977) a étendu la relation d'Einstein en ajoutant un terme d'ordre deux en Ø en prenant en compte les interactions hydrodynamiques entre paires de particules :

$$\mu = \mu_l(1 + 2.5\emptyset + 6.2\emptyset^2) \tag{2.16}$$

La relation de Batchelor est valable pour des suspensions semi diluées ($\emptyset \leq 0.15$). Lorsque la concentration d'une suspension devient importante, l'estimation de la viscosité pose beaucoup de problèmes. Les perturbations du champ de vitesse induites par la présence d'une particule aux environs des particules voisines ne sont plus négligeables (Coussot et Ancey, 1999). Aux hautes fractions volumiques, les suspensions présentent une divergence de la viscosité pour des concentrations avoisinant la fraction volumique maximale ($\emptyset_{max} \sim 0.64$).
Thomas (1965) a proposé une relation semi-empirique valable pour des suspensions concentrées ($\emptyset < 0.62$) qui permet de prendre en compte les interactions entre particules :

$$\mu = \mu_l\left(1 + 2.5\emptyset + 10.05\emptyset^2 + 0.00273e^{16.6\emptyset}\right) \tag{2.17}$$

Lorsque la fraction volumique en particule augmente, cette relation prend en compte les phénomènes de collision et de réarrangement des particules les unes par rapport aux autres, grâce aux termes supplémentaires en $\emptyset^2$ et $e^{16.6\emptyset}$ respectivement. De nombreuses approches, théoriques, semi-empiriques ou empiriques ayant été proposées pour estimer la viscosité d'une suspension en fonction de la fraction volumique en particules sont disponibles dans la littérature. Quelques-unes de ces approches sont reprises dans le Tableau 2.3

Tableau 2.3 Exemples de lois de viscosité de suspensions (Bel, 1996 ; Kauffeld, 2005)

Auteur	Expression	Remarques
Einstein (1906)	$\mu = \mu_l(1 + 2.5\emptyset)$	$\emptyset < 0.02$ $d_p < 2\ \mu m$
Batchelor (1977)	$\mu = \mu_l(1 + 2.5\emptyset + 6.2\emptyset^2)$	$\emptyset < 0.20$
Thomas (1965)	$\mu = \mu_l(1 + 2.5\emptyset + 6.2\emptyset^2 + 0.00273e^{16.6\emptyset})$	$\emptyset < 0.62$ $d_p < 435\ \mu m$
Krieger and Dougherty (1959)	$\mu = \mu_l\left(1 - \frac{\emptyset}{\emptyset_{max}}\right)^{-2.5\emptyset_{max}}$	
Maron and Pierce (1956)	$\mu = \mu_l\left(1 - \frac{1.5\emptyset}{\emptyset_{max}}\right)^{-1}$	
Leighton and Acrivos (1986)	$\mu = \mu_l\left(1 - \frac{\emptyset}{1 - \frac{\emptyset}{\emptyset_{max}}}\right)^2$	$\emptyset_{max} = 58\%$
Morris and Boulay (1999)	$\mu = \mu_l\left[1 + 2.5\emptyset\left(1 - \frac{\emptyset}{\emptyset_{max}}\right)^{-1} + 0.1\left(\frac{\emptyset}{\emptyset_{max}}\right)^2\left(1 - \frac{\emptyset}{\emptyset_{max}}\right)^{-2}\right]$	
Zarraga et al. (2000)	$\mu = \mu_l \frac{e^{-2.34\emptyset}}{\left(1 - \frac{\emptyset}{\emptyset_{max}}\right)}$	

$\emptyset_{\max}$ dépend fortement de la forme et de l'interaction des particules, et varie entre 0.58 et 0.72 pour les sphères monodispersées.

2.7 Migration de particules solides dans une suspension en écoulement

2.7.1 Migration de particules induite par cisaillement

Lors d'écoulements de suspensions concentrées, il a été observé une agglomération des particules vers les régions à faible taux de cisaillement entrainant une hétérogénéité dans l'écoulement. Cette migration de particules a été pour la première fois observée par Gadala-Maria et Acrivos (1980) dans une cellule de Couette. Selon les auteurs, la viscosité apparente de la suspension diminuait de façon continue sous l'effet du cisaillement, alors que, dans des conditions identiques de cisaillement, la viscosité du fluide porteur reste constante. Les auteurs n'ont pas pu fournir une explication notable à ce phénomène. Par la suite, des nombreuses études expérimentales ont permis de mettre en évidence ce phénomène. La première étude remarquable a été menée par Leighton et Acrivos (1987a, b) en géométrie de Couette. Dans cette étude, les auteurs ont expliqué que la diminution de la viscosité était liée à la migration des particules dans les régions à taux de cisaillement élevé vers des régions à taux de cisaillement faible. Ils ont ainsi confirmé les observations de Gadala-Maria et Acrivos (1980). Ils ont aussi constaté que le coefficient de diffusion des particules était proportionnel au taux de cisaillement et au carré du diamètre des particules employées et augmentait avec la fraction volumique. Dans la suite, de nombreuses études ont montré des résultats similaires dans différentes géométries. Pour n'en citer que quelques-uns, Gadala-Maria (1979), Phillips et al. (1992), Shapley et al. (2002), Ovarlez et al. (2006) ont utilisé la cellule de Couette dans laquelle les mesures des concentrations de particules par différentes techniques ont montré la présence d'une migration radiale des régions à taux de cisaillement élevé (près du cylindre interne tournant) vers les régions à taux de cisaillement faible (près du cylindre externe stationnaire). Sinton et al. (1991), Hampton et al. (1997), Han et al. (1999) ont quant à eux utilisé des conduites circulaires et Koh et al. (1994) et Lyon et Leal (1998) des tuyaux rectangulaires. Ils ont constaté que les particules migraient vers l'axe de la conduite ou le taux de cisaillement était le plus faible. Contrairement à ces résultats, Chan and Powell (1984), Chapman (1990), Chow et al. (1994) n'ont observé aucune migration au sein d'un rhéomètre à disques parallèles alors qu'il existe pourtant un gradient de cisaillement. Chapman (1990) a constaté une migration des particules vers l'extérieur dans le cas d'une géométrie cône-plan, où le taux de cisaillement imposé était constant, alors qu'aucune diffusion n'était attendu.

2.7.2 Migration de particules induite par flottaison (gravité)

La vitesse de flottaison d'une particule est la vitesse qu'une particule acquiert selon la verticale sous l'effet de la pesanteur. Un examen approfondi du phénomène de flottaison des particules est donné dans Wallis (1969). La vitesse de flottaison est l'une des variables clés dans l'étude des systèmes utilisant le coulis de glace comme fluide caloporteur. Elle joue un grand rôle dans l'analyse et la compréhension du processus de stratification. Vue son importance dans le calcul des flux de particules induits par flottaison, plusieurs auteurs ont tenté de modéliser la vitesse de flottaison en fonction des propriétés physiques de la particule solide (taille, forme, densité, …) et du fluide (densité, viscosité, …) dans lequel il est submergé (Hawley 1982 ; Hill,1996).

Dans un coulis de glace très dilué ($\emptyset_{ic} \approx 0.01$), chaque particule de glace accélère vers le haut sous l'effet de la gravité jusqu'à ce que la force de traînée compense les forces d'Archimède et de pesanteur. A partir de ce moment, la particule se déplace à une vitesse constante appelée vitesse terminale de flottaison (ω_o). Les lois classiques de la mécanique des fluides formulées par Newton et Stokes peuvent être utilisées pour déterminer l'expression de la vitesse terminale de flottaison des particules considérées sphériques et discrètes en régime stationnaire (Tchobanoglous et Burton, 1991). Dans plusieurs applications, la loi de Stokes a été appliquée comme vitesse de flottaison d'une particule lorsque le régime d'écoulement autour de la particule est laminaire ($Re_p \leq 1$). La loi de Stokes est bien adaptée aux coulis de glace peu concentrés dans lesquels la flottaison de chaque particule n'est pas influencée par la présence des autres particules.

Bien que la loi de Stokes puisse fournir une indication représentative des ordres de grandeur de la vitesse terminale de flottaison, elle ne peut malheureusement pas prédire avec précision les phénomènes de flottaison réels dus aux effets combinés d'agglomération, de re-suspension et de turbulence (Cheng, 1997b ; Nikora et al., 2004). En outre, la loi de Stokes ne peut pas s'appliquer à toutes les dimensions de particules en flottaison dans un fluide. Plusieurs chercheurs ont montré que pour maintenir les particules en ligne droite, elles doivent avoir un

diamètre supérieur à 0.5 μm (Carver, 1971) et théoriquement, ne pas dépasser 50 μm ($Re_p \approx 1$) (Oseen, 1927 ; Carver, 1971 ; Clift et al, 1978). Dans la vie réelle, la plupart des particules d'intérêt pratique n'ont pas une forme régulière. La formulation de la loi de Stokes ayant été basée sur l'hypothèse d'une particule de forme sphérique, un facteur de forme (Corey shape factor) a été défini pour tenir compte de la forme des particules (Graf, 1971). Pour surmonter ces obstacles, plusieurs chercheurs ont proposé des équations de la vitesse terminale de flottaison applicables sur un large éventail de nombres de Reynolds (Rubey, 1933 ; Albertson, 1953 ; Graf, 1971 ; Clift, et. Al., 1978 ; Hallermeier, 1981 ; Van Rijn, 1993 ; Cheng, 1997a ; Ahrens, 2000 ; Jimenez et Madsen, 2003 ; Brown et Lawler, 2003 ; Nikora, et al., 2004).

Au fur et à mesure que la concentration en particules solide augmente, le champ de vitesse autour de chaque particule est affecté par la présence des particules voisines. Les lignes de courant de la phase liquide circulant autour des particules individuelles commencent à se chevaucher et augmentent la traînée. Par conséquent, la présence d'autres particules constitue un frein (réduction de la vitesse de flottaison) à la stratification (Bond, 1959). La vitesse de flottaison devient alors une fonction de la concentration volumétrique des particules en suspension (Burt, 1986). Pour tenir compte de ce phénomène, deux approches ont été utilisées. La première approche consiste à modifier la vitesse terminale de flottaison en y introduisant une **fonction de freinage** $\mathbf{f}(\emptyset_{ic})$ qui tient compte de l'augmentation de la concentration en particules solides (Richardson et Zaki, 1954 ; Batchelor, 1972 ; Davis et Gecol,1994 ; Di Felice,1999 ; Landman et White, 1992). La seconde approche consiste à modifier la relation de Stokes en remplaçant la viscosité du liquide par **la viscosité effective de la suspension** (Shojaei et Arefinia, 2006). Cette approche prend en compte la collision de particules lors de la flottaison car les nombreuses collisions entre particules observées pendant la flottaison apparaissent comme une augmentation de la viscosité de la suspension qui est une fonction de la fraction volumique de particules donnée dans diverses corrélations (Thomas, 1965 ; Krieger et Dougherty, 1959 ; Leighton and Acrivos, 1986).

Modèle de flux diffusifs de Phillips et al. (1992)

Dans la présente étude, le modèle de Phillips et al. (1992) a été choisi pour modéliser le transport de l'espèce ∅ dans l'écoulement de coulis de glace dans des conduites horizontales de section circulaire. Le modèle de Phillips et al. (1992), appelé aussi modèle de flux diffusifs, est un modèle phénoménologique basé sur les expressions de flux de particules initialement proposé par Leighton et Acrivos (1987b). Phillips et al. (1992) ont introduit ces expressions dans l'équation globale de bilan (flux convectif et diffusif) dans laquelle la diffusion de particules est le résultat du gradient du taux de cisaillement et de la variation spatiale de la viscosité. Le modèle de Phillips et al. (1992) est un modèle constitutif. Il ne tient pas compte de tous les mécanismes qui interviennent dans la migration des particules. En fait, la migration des particules est l'action de diverses forces telles que les forces visqueuse (hydraulique), de flottabilité (gravitationnelle), de cisaillement, inertielle, et Brownienne. En choisissant les conditions d'écoulement appropriées, les effets Brownien (Pe $\sim 10^{+9}$) et inertiel ($Re_p \sim 10^{-6}$) peuvent être négligés par rapport aux effets visqueux. C'est le cas de l'écoulement de coulis de glace correspondant à notre travail où les seules forces en action sont les forces visqueuses, de cisaillement et de flottabilité. Le modèle de Phillips et al. (1992) et les travaux antérieurs n'ont pas pris en compte les forces de flottabilité, ils ont souvent considéré des écoulements à flottabilité neutre (dimensions de particule $a < 1\ \mu m$). Pour les dimensions de particules plus grandes ($a > 1\ \mu m$), la flottabilité devient un mécanisme important et ne peut être négligée.

2.8 Écoulement du coulis de glace dans les tuyaux horizontaux de section circulaire

Au cours des dernières années, de nombreux travaux ont étudié l'influence de certains paramètres, du moins les plus importants, sur les comportements hydrodynamiques et thermiques des coulis de glace. En raison de la diversité d'additifs employés pour la production des coulis de glace et des nombreux autres facteurs tels que la taille moyenne des cristaux de glace, les caractéristiques de la tuyauterie utilisée et surtout les conditions opératoires, une grande variété de résultats et de conclusions a été publiée (Kitanovski et al., 2005). Comme souligné au début de ce travail, le coulis de glace présente des nombreux avantages vis-à-vis

des frigoporteurs monophasiques (Bel et Lallemand, 1999). Il possède une densité énergétique de stockage élevée et une excellente capacité de transfert de chaleur (Kauffeld et al., 2010). Ces avantages font que le coulis de glace est largement utilisé dans les systèmes de refroidissement secondaires (Zhang et Ma, 2012 ; Chung et al., 2014). Cependant, à cause des particules de glace contenues dans le coulis de glace, le phénomène de stratification est inévitable dans les écoulements de coulis de glace qui sont généralement hétérogènes (Kitanovski et al., 2002). Cette hétérogénéité affecte largement l'écoulement et le transfert de chaleur dans les échangeurs de chaleur. Elle crée, par exemple, une répartition non uniforme des contraintes de cisaillement près des parois rendant la détermination du coefficient de frottement difficile. Une revue des études antérieures sur la chute de pression et du coefficient de transfert de chaleur dans les écoulements de coulis de glace a déjà été réalisée (Ayel et al., 2003 ; Monteiro et Bansal; 2010 ; Zhang et Ma, 2012). Dans cette section, nous présentons une vue d'ensemble des récents travaux, avec plus des détails sur la modélisation numérique.

2.8.1 Régimes d'écoulement

Le comportement global d'un coulis de glace dépend également du régime d'écoulement en présence. Classiquement, on distingue les régimes homogène, hétérogène et stratifié (Doron et Barnea, 1996). Ces différents régimes d'écoulements se distinguent par la répartition des particules solides dans la section transversale de la conduite (Fig. 2.4). Dans un l'écoulement homogène, le coulis de glace a une vitesse élevée et la distribution des particules solides est presque uniforme. Ce régime d'écoulement s'approche de celui de la phase continue seule. En effet, quelle que soit la concentration en particule solide, il a été observé des interactions uniformes entre les particules, et que le comportement du coulis de glace se rapproche de celui d'un fluide Newtonien (Kitanovski et al., 2002). Le régime d'écoulement hétérogène apparaît lorsque la vitesse d'entraînement du fluide porteur est de l'ordre de grandeur de la vitesse de glissement de la phase solide par rapport à la phase liquide. La répartition des particules solides dans la section transversale présente un gradient de distribution verticale lié à un rassemblement des particules vers le haut de la conduite. Le comportement du coulis de

glace s'écarte de celui d'un fluide Newtonien. Parmi les écoulements stratifiés qui apparaissent à de faibles vitesses, on peut distinguer l'écoulement avec lit mobile et l'écoulement avec lit stationnaire. Si la vitesse du coulis diminue, un lit mobile apparaît lorsque la fraction maximale possible de la glace se produit dans la partie supérieure de la conduite. Les particules solides sont toutes en contact et se déplacent à la même vitesse. Dans le reste de la conduite, l'écoulement reste hétérogène. À de très faibles vitesses, un lit stationnaire apparaît lorsque la vitesse du lit mobile tend vers zéro. Une partie des particules solides formant le lit est immobile à la paroi, l'autre partie se déplace en bloc. Dans le reste de la conduite, l'écoulement est hétérogène. Récemment, Bordet et al. (2018) ont analysé les régimes d'écoulement de coulis de glace à base de propylène glycol (9.5wt%) obtenus par visualisation directe et mesure de pertes de charge. Des nouveaux régimes d'écoulement ont été identifiés et une nouvelle classification à été proposée. Shook (1985) a présenté une étude expérimentale sur l'influence de la taille des particules sur le régime d'écoulement du coulis de glace. Il a considéré des particules de glace de diamètre 0.3 et 1.4 mm ayant une masse volumique proche de celle du liquide porteur (densité relative~1.05) en écoulement dans un tube de diamètre 52.2 mm. Les résultats expérimentaux ont permis de constater que le diamètre des particules a une influence sur le comportement du mélange.

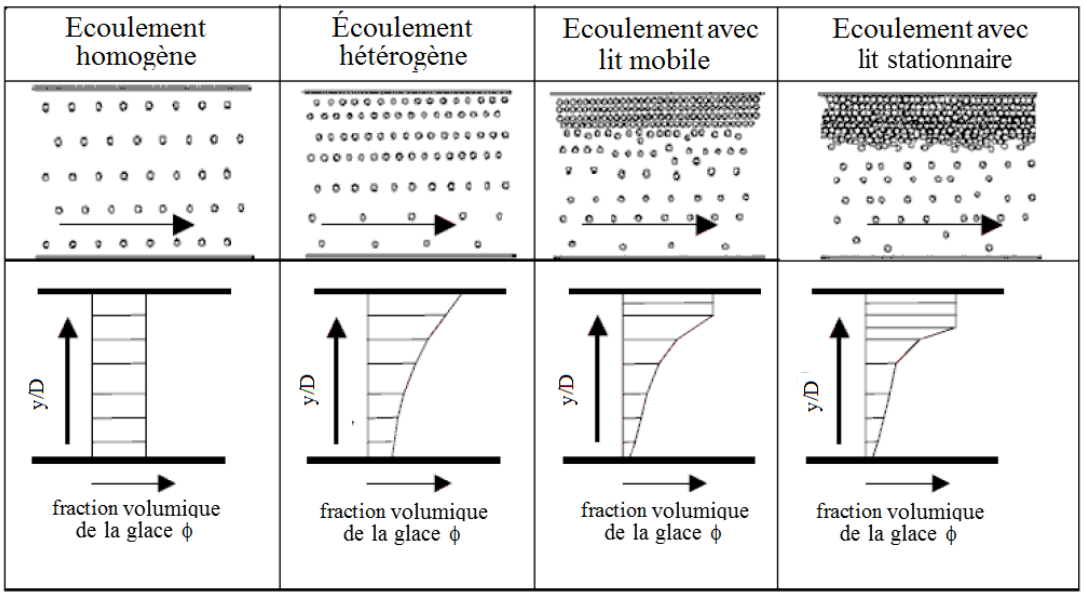

Fig. 2.4 Régimes d'écoulement, adapté de Hu (2006)

2.8.2 Etudes expérimentales sur la perte de pression

Le dimensionnement des conduits transportant les coulis de glace est très complexe. Il demande la connaissance des profils de vitesse, de concentration, la chute de pression et la vitesse de déposition. Ces paramètres ont été déterminés, au fil des années, sur la base de données expérimentales. Les travaux antérieurs sur la détermination du coefficient de perte de charge dans les écoulements de coulis de glace n'ont pas été faits sur la base de modèles rhéologiques. Seules les corrélations empiriques ont été développées et appliquées à cet effet. Pour la plupart des auteurs, la chute de pression augmente avec la fraction en glace. Aux faibles vitesses, plusieurs auteurs (Onokoko et Galanis, 2013 ; Wang et al., 2013b) ont observé une agrégation des particules de glace dans la partie supérieure de la conduite. La conséquence de ce phénomène est l'augmentation du coefficient de perte de charge par frottement. Pour les vitesses élevées (> 1 m/s), le coefficient de perte de charge par frottement reste constant et se rapproche de celui du fluide porteur à la même vitesse. La taille des particules solides joue aussi un grand rôle dans la perte de pression des écoulements de coulis de glace. Pour une même concentration, les mélanges constitués de particules de faible diamètre présentent un coefficient de perte de charge inférieur à ceux contenant des particules de grand diamètre. Jensen et al. (2000) ont constaté, pour les fractions en glace inférieures à 0.1-0.15, que la chute de pression ne varie pas avec l'augmentation de la fraction en glace mais augmente avec la vitesse moyenne du fluide. Au-dessus de ces valeurs, la chute de pression augmente sensiblement avec la fraction en glace mais reste moins influencée par la vitesse moyenne du fluide. Bellas et al. (2002) ont mesuré la chute de pression dans l'écoulement d'un coulis de glace à base d'une solution aqueuse de 5 % en propylène glycol dans un échangeur de chaleur à plaques. Ils ont pris en compte des fractions massiques en glace allant de 0 à 0.25 et des débits variant de 1.0 à 3.7 m^3/h. Pour un accroissement de la fraction massique en glace de 0 à 0.2 et pour la même plage de débit, ils ont constaté que la chute de pression se trouvait augmentée d'environ 15 %. Dans leurs études sur l'écoulement des coulis de glace dans une conduite horizontale, Knodel et al. (2000) ont constaté que la chute de pression diminue avec la fraction en glace et redevient constante pour des fractions en glace supérieures à 4 %. Ils

ont justifié cette diminution par la réduction de la turbulence dans l'écoulement provoquée par l'interaction entre la phase liquide et les particules solides (relaminarisation). Selon eux, il existe une fraction en glace au-delà de laquelle la chute de pression est constatée (30 % dans le cas d'espèce). Frei et Egolf (2002) sont les premiers à avoir trouvé que la chute de pression dans les écoulements de coulis de glace varie avec le temps. Les auteurs ont remarqué que malgré les précautions prises pour éviter la surfusion et la surchauffe du fluide porteur, la chute de pression diminue dans le temps vers une valeur asymptotique due à l'influence du temps sur la taille et la forme des cristaux. Plus tard, ce phénomène a été expliqué par différents mécanismes tels que l'agglomération des particules solides et le phénomène de maturation d'Ostwald. Grozdek et al. (2009a) ont réalisé des études expérimentales sur la chute de pression dans l'écoulement du coulis de glace à base d'une solution aqueuse de 10.3 % en alcool dans un tube circulaire horizontal. Ils ont pris en compte des fractions en glace allant de 0 à 30 %. Ces études ont montré, pour des fractions en glace et des vitesses élevées, que la chute de pression du coulis de glace est de loin supérieure à celle du fluide porteur. Toutefois, pour des concentrations en glace supérieures ou égales à 15 %, ils ont observé l'existence d'une plage de vitesses dans laquelle le coulis de glace peut présenter des chutes de pression inférieures ou égales à celles du fluide porteur. Niezgoda-Zelasko et Zelasko (2007) ont mesuré les pertes de charge pour des écoulements laminaires et turbulents d'un coulis de glace dans des tuyaux circulaires et rectangulaires. Illàn et Viedma (2009a, 2009b) ont étudié l'influence du rapport diamètre de la particule sur le diamètre du tuyau sur la chute de pression dans les tuyaux lisses et ondulés. Les pertes de pression dépendent significativement du régime d'écoulement comme l'illustre la Fig. 2.5, le gradient de pression de la suspension est plus grand que celui du liquide porteur, cette différence diminue avec le degré d'hétérogénéité.

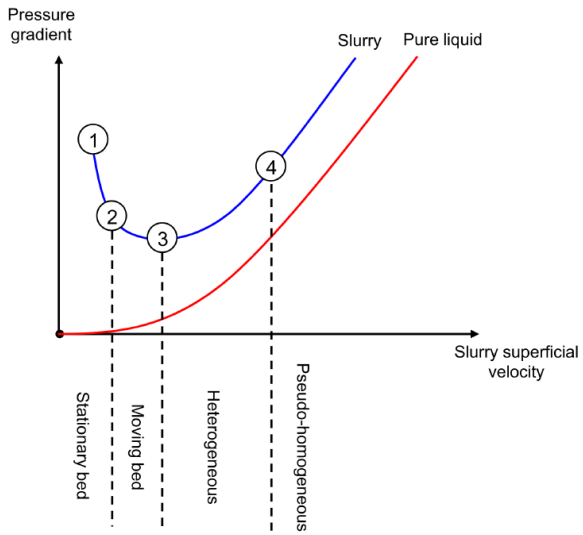

Fig. 2.5 Régimes d'écoulement identifiés dans la courbe gradient de pression vs vitesse d'écoulement dans un tuyau horizontal, d'après Abulnaga (2002).

2.8.3 Etudes expérimentales sur le transfert de chaleur

Les études expérimentales sur le transfert de chaleur des écoulements des coulis de glace ont été réalisées par un bon nombre d'auteurs ces dix dernières années. Pour la plupart d'entre eux, le coefficient de transfert de chaleur augmente avec la fraction en glace et la vitesse du fluide, mais est très peu, ou n'est pas du tout, influencé par le flux de chaleur transféré à l'écoulement. Jensen et al. (2000) et Sari et al. (2000) ont observé une augmentation du coefficient de transfert de chaleur avec l'augmentation de la fraction massique en glace et le débit de l'écoulement dans un échangeur de chaleur. D'autre part, Snoek et Bellamy (1997) et Knodel et al. (2000) ont montré que le coefficient de transfert de chaleur diminue avec l'augmentation de la fraction de glace. Ces écarts dans les résultats montrent que le comportement thermique du coulis de glace dépend de plusieurs paramètres tels que le débit, la taille des particules de glace et la fraction massique en glace. Jensen et al. (2000) ont étudié expérimentalement les caractéristiques du coefficient de transfert de chaleur d'un coulis de glace à base d'une solution aqueuse de 19 % en éthanol dans des conduites de 12, 16 et 20 mm de diamètre. Ils ont pris en compte des fractions en glace allant de 0 à 0.3, des vitesses de 0.5, 1.0 et 1.5 m/s et une taille moyenne des cristaux inférieure à 0.2 mm. Ils ont montré que le coefficient de transfert de chaleur augmente avec la fraction en glace et la vitesse. Knodel et

al. (2000) ont étudié expérimentalement le transfert de chaleur d'un coulis de glace à base d'eau pure dans une conduite horizontale en acier inoxydable de 24 mm de diamètre intérieur et 4.60 m de longueur en prenant en compte des vitesses variant de 2.8 à 5 m/s. Ils ont constaté que le nombre de Nusselt diminue avec la fraction en glace pendant la transition du régime turbulent au régime laminaire : phénomène de relaminarisation. Bédécarrats et al. (2009) ont étudié les caractéristiques du coefficient de transfert de chaleur d'un coulis de glace à base d'une solution aqueuse à 10 % d'éthanol dans deux types d'échangeurs coaxiaux (lisse et annelé). Ils ont pris en compte des fractions en glace de 0 à 30 % et des vitesses d'écoulement entre 0.3 et 1.9 m/s. Les résultats montrent l'existence d'une valeur critique de la concentration en glace en dessous de laquelle le coefficient de transfert de chaleur est d'abord constant et puis, diminue progressivement avec la fraction en glace. Au-dessus de cette concentration critique, le coefficient de transfert de chaleur augmente rapidement avec la fraction en glace (phénomène de relaminarisation). La valeur critique de la concentration en glace dépend de la vitesse de l'écoulement. Elle augmente avec la vitesse. Grozdek et al. (2009b) ont étudié les caractéristiques du coefficient de transfert de chaleur du coulis de glace à base d'une solution aqueuse de 10.3 % en alcool dans un tube circulaire horizontal. Ils ont pris en compte des fractions en glace allant de 0 à 22 %. Les mesures ont montré que le coefficient de transfert de chaleur du coulis de glace est supérieur à celui du fluide porteur, particulièrement en régime laminaire et pour des fractions élevées en glace où il peut atteindre des valeurs deux fois plus grandes. Cette augmentation relativement élevée du coefficient de transfert de chaleur peut s'expliquer par un changement de régime d'écoulement, de l'écoulement homogène à l'écoulement hétérogène. Les forces de flottabilité et de frottement agissant sur des cristaux de glace augmentent avec la concentration en glace et rendent le processus de stratification plus intense (Kauffeld et al., 2005). Lee et al. (2006) ont étudié le transfert de chaleur avec coulis de glace à base de 6.5% d'éthylène glycol dans un échangeur de chaleur de diamètre 16.91 mm et de longueur 1.5 m. Le débit du coulis de glace varie de 800 à 3500 $\mathrm{kg.m^{-2}.s^{-1}}$. La concentration en glace varie de 0 à 25%. Ils ont reporté que le taux de transfert de chaleur augmente avec la concentration en glace et le débit massique. Aux

débits faibles, le coefficient de transfert de chaleur augmente rapidement à partir d'une concentration en glace d'environ 15%. Cette concentration critique dépend du débit massique.

L'influence du flux de chaleur imposé au coulis de glace sur le transfert de chaleur n'est pas clairement établie. Christensen et Kauffeld (1997), Niezgoda-Zelasko et Zalewski (2006), Jensen et al. (2000) ont fait remarquer l'absence ou la faible influence du flux de chaleur sur le coefficient de transfert de chaleur. Knodel et al. (2000), par contre, a montré la possibilité d'augmenter le coefficient de transfert de chaleur de 15 à 25 % lorsque la densité de flux est doublée de 4 à 8 kW. m^{-2}.

La taille et la forme des cristaux de glace jouent aussi un grand rôle dans le transfert de chaleur avec coulis de glace. Les particules de petite taille contribuent plus à l'augmentation de la conductivité par les effets micro-convectifs que des grosses particules. Pour une fraction massique donnée, plus les particules sont petites, plus la surface en contact avec le fluide porteur est importante et plus la quantité de fluide entrainée par la rotation des particules est conséquente (Desmales, 2002). Goel et al. (1984) ont observé expérimentalement cette tendance. Ils ont supposé que plus les particules solides étaient grosses, plus elles risquaient de sédimenter, de s'agglomérer et de former une couche isolante au niveau des parois, laquelle ralentissait les échanges thermiques. D'autre part des grands cristaux de glace conduisent au phénomène de surchauffe de la solution aqueuse qui peut influencer de façon significative les résultats sur le transfert thermique. Selon Hansen et al. (2002) et Pronk et al. (2005), la surchauffe de la solution aqueuse peut intervenir lorsque les cristaux de glace contenus dans le coulis de glace sont en fusion, particulièrement lorsque les cristaux de glace sont relativement grands ou lorsqu'un grand pourcentage de glace est en fusion. Ce phénomène de surchauffe peut affecter négativement le coefficient de transfert de chaleur et conduire à sa diminution dans les échangeurs de chaleur.

2.8.4 Simulations numériques

Depuis le début des années 1980, la simulation numérique est considérée par de nombreux chercheurs comme un moyen efficace et rapide d'étudier différentes configurations d'écoulements ou géométries d'échangeurs. Cette approche présente en effet de nombreux avantages par rapport aux études expérimentales telles que l'accès à toutes les grandeurs locales de l'écoulement et la possibilité d'évaluer de nombreuses configurations et géométries sans se préoccuper des aspects de conception mécanique. La prédiction du comportement des écoulements des coulis de glace est relativement difficile au regard des phénomènes complexes mis en œuvre. Cependant avec l'amélioration des modèles mathématiques et l'augmentation des capacités de calcul des ordinateurs, ces écoulements peuvent être étudiés par les méthodes CFD.

Modèle monophasique

Le modèle monophasique part du principe que le fluide porteur et les particules de glace sont en équilibre thermique et se déplacent avec la même vitesse. Cette approche est plus simple et nécessite moins de temps de calcul. Elle a été utilisée dans plusieurs études théoriques d'écoulements de coulis de glace. Toutefois, cette approche est, en général, en bon accord avec les résultats expérimentaux si les propriétés effectives de suspensions sont connues avec précision (généralement des corrélations empiriques).

Certains auteurs se sont basés sur la mécanique des fluides non-Newtoniens pour simplifier l'écoulement du coulis de glace en un écoulement monophasique. Niezgoda-Zelasko & Zalewski (2006) ont développé un modèle monophasique basé sur le fluide de Bingham pour étudier l'écoulement isotherme de coulis de glace. Ils ont montré qu'en régime laminaire, le modèle donnait une meilleure description du transfert de la quantité de mouvement tandis qu'en le couplant avec le modèle de turbulence k-ε RNG en régime turbulent, le modèle était mieux validé par les résultats expérimentaux. Niezgoda-Zélasko (2006) a réalisé des études numériques sur le transfert de chaleur dans les écoulements de coulis de glace dans des conduites horizontales. Ces études ont confirmé que le coefficient de transfert de chaleur est plus influencé par la fraction massique en glace en régime laminaire qu'en régime turbulent par le fait qu'en régime laminaire, les transferts de chaleur et la fusion de glace sont très

importants près des parois. D'autre part, la présence des cristaux de glace s'accompagne d'une augmentation du coefficient de transfert de chaleur par les effets supplémentaires de la micro-convection. Cela n'est pas le cas en régime turbulent où les effets de la micro-convection sont inhibés par la turbulence. Trabelsi et al. (2010) ont réalisé une étude numérique comparative sur les champs hydrodynamique et thermique des écoulements laminaires stationnaires d'un coulis de glace à base d'une solution aqueuse (15 % en éthanol et 12.25 % en glace) et d'une solution binaire homogène à une phase (eau et 17.1 % d'éthanol) entrant de façon identique dans un tube horizontal isotherme (T_w=274.14 K) avec une même température uniforme (T_o=284.16 K) et un même nombre de Reynolds (Re=500). La longueur du tube isotherme est précédée et suivie par deux zones adiabatiques et les deux fluides sont considérés non-Newtoniens. Les résultats montrent des différences significatives entre les valeurs locales de la contrainte de cisaillement à la paroi, le coefficient de frottement, la température du fluide et le nombre de Nusselt pour les deux écoulements. Le nombre de Nusselt local du coulis de glace est plus élevé dans la région développée de l'écoulement, et la température du fluide diminue dans la zone adiabatique aval du tube due à la conduction radiale et à une augmentation axiale de la concentration en glace.

Modèle diphasique

Le modèle diphasique a l'avantage de faire ressortir l'influence de certains paramètres tels que la taille de la particule de glace, la fraction massique de la glace et d'autres propriétés physiques associées à chaque phase. En général, il existe deux grandes catégories d'approches pour modéliser les écoulements des fluides diphasiques : l'approche Lagrangienne-Eulérienne et l'approche Eulérienne-Eulérienne. Pour des faibles fractions volumiques en particules solides, l'approche Lagrangienne-Eulérienne est la plus adaptée. Cette approche analyse le fluide porteur par le modèle d'Euler, tandis que la particule solide l'est par le modèle de Lagrange. Cependant, à cause du nombre élevé des particules de glace contenu dans le coulis de glace (faibles dimensions des particules) et à la limitation de l'outil informatique, l'approche Lagrangienne-Eulérienne n'est pas appropriée (Jiang et Zhang, 2012 ; Ekambara et al., 2009). L'approche Euler-Euler dispose en générale de trois modèles : le modèle VOF (volume of fluid),

le modèle Mixture et le model Eulérien. Le modèle VOF simule les coulis de glace par la résolution d'un seul ensemble d'équations de quantité de mouvement et par un suivi de la fraction volumique de chaque phase dans tout le domaine. Le modèle ''Mixture'' se base sur les équations de conservation du mélange, l'équation de la fraction volumique de la phase solide et de l'expression de la vitesse relative entre les deux phases. Le modèle Eulérien considère des équations de conservation séparées pour chaque phase, la pression étant la même pour les deux phases. Le volume de chaque phase est calculé par l'intégration de sa fraction volumique sur tout le domaine. Les détails sur ces méthodes sont donnés dans ANSYS Fluent Theory Guide (2013). Un nombre croissant de publications (Zhang and Shi, 2015 ; Shi and Zhang, 2016 ; Wang et al., 2017 ; Kaushal et al., 2012 ; Chen, 2009) dans lesquelles le modèle Eulérien basé sur la théorie cinétique des écoulements granulaires a été utilisé ces derniers temps pour simuler le comportement des coulis de glace. Cette théorie est une adaptation de la théorie cinétique des gaz dans laquelle les interactions particule-particule sont quantifiées dans l'écoulement. Cependant, bien que le modèle numérique utilisant cette approche donne de bons résultats dans le cas des écoulements diphasiques solide-liquide, c'est un modèle très complexe, avec des exigences de calcul élevées. Les équations de conservation sont résolues séparément pour chaque phase sur la base de la dynamique de fluide Newtonien. Le nombre élevé d'équations couplées rend la convergence difficile à contrôler. Li et al. (2016) ont utilisé le modèle VOF pour simuler le transfert de chaleur avec coulis de glace dans un tube horizontal. Ils ont trouvé que les résultats numériques obtenus avec le modèle VOF étaient en très bon accord avec les données expérimentales obtenues dans les conditions opératoires similaires. Niezgoda-Zelasko et Zalewski (2006) ont utilisé les modèles ''Mixture'' et Eulérien pour analyser l'écoulement du coulis de glace dans un tuyau horizontal. Ils ont ensuite fait une étude comparative des avantages de chaque méthode. Mika (2013) a utilisé le modèle ''Mixture'' pour simuler l'écoulement de coulis de glace dans une vanne de régulation. Les résultats obtenus ont permis d'optimiser la structure de la vanne. Wang et al. (2013b) ont appliqué le modèle '' mixture '' pour simuler les écoulements de coulis de glace sur la base de différents modèles rhéologiques. Ils ont présenté les résultats numériques sur la vitesse, la concentration des particules de glace et la chute de pression. Ces

résultats ont montré qu'il existe un degré d'asymétrie dans l'écoulement pour différentes conditions d'écoulement. Ils ont aussi conclu que l'équation de Thomas décrit mieux la viscosité du coulis de glace aux vitesses d'écoulement élevées tandis qu'aux vitesses faibles le modèle de Bingham donnait de meilleurs résultats. Tian et al. (2014) ont aussi adopté le modèle ''Mixture'' pour identifier le mécanisme de stratification dans un écoulement de coulis de glace. Wang et al. (2013a) ont appliqué le modèle Eulérien basé sur la théorie cinétique des écoulements granulaires pour analyser les écoulements de coulis de glace sans tenir compte de la fusion de particules de glace. Ils ont validé ce modèle à l'aide de quatre différents résultats expérimentaux avant de l'utiliser pour simuler les caractéristiques importantes de l'écoulement du coulis de glace dans diverses configurations comprenant des tuyaux horizontaux et verticaux et des coudes à 90°. Comparé au modèle ''Mixture'', le modèle Eulérien semble mieux caractériser les écoulements multiphasiques. Zhang et Shi (2015) ont simulé numériquement l'écoulement des coulis de glace dans un tuyau horizontal par le modèle Eulérien. Couplé aux modèles de transfert de chaleur et de masse, le modèle a d'abord été validé avec les résultats expérimentaux de la littérature et ensuite utilisé pour étudier la stratification et la fusion de la glace dans un écoulement de coulis de glace soumis à un flux de chaleur uniforme. Ils ont montré que la stratification était atténuée par la force de dispersion turbulente et que, par conséquent, la concentration de particules était plus uniforme à des vitesses d'entrée plus élevées. Dans le cas chauffé, les résultats montrent que le coefficient de transfert thermique local diminue rapidement dans la région d'entrée comme dans tous les écoulements de convection forcée puis reste à peu près constant dans la région développée thermiquement et commence à augmenter après la fusion complète du coulis de glace.

2.8.5 Problématique et objectif

Une étude bibliographique des travaux expérimentaux et numériques sur l'écoulement des coulis de glace a été réalisée avec un intérêt particulier sur les écoulements avec transfert de chaleur dans des conduites horizontales. A la lumière de cette étude, on constate :

Une divergence de résultats et opinions des différents auteurs. Pour la plupart des travaux publiés, certaines conclusions sont tirées uniquement pour des configurations et conditions bien restreintes et les résultats obtenus ne fournissent pas une explication complète des phénomènes en présence.

Les propriétés thermophysiques des coulis de glace sont difficiles à définir. La mesure de la fraction solide, par exemple, est un problème complexe que beaucoup de chercheurs essaient de résoudre. La majorité des méthodes actuellement utilisées considère le fluide dans son intégralité (mesures de la température, de la masse volumique...) alors que la répartition de la phase solide dans le fluide n'est pas uniforme au sein d'une même section. Il y a non seulement un gradient de concentration mais aussi un gradient de vitesse. La taille et la forme des cristaux changent avec le temps par agglomération des cristaux et surchauffe de la solution aqueuse.

Le rhéologique du coulis de glace varie en fonction des paramètres opératoires (fluide Newtonien ou non-Newtonien).

Le régime d'écoulement qui influence considérablement la chute de pression dépend des paramètres opératoires.

Un manque de corrélations fiables et largement acceptées pour le calcul des coefficients de perte de charge et de transfert de chaleur. Les corrélations classiques proposées, établies à partir des modèles rhéologiques classiques (Bingham, Ostwald, Herschel-Bulkley ou Casson), ne tiennent pas compte de l'influence des effets de la flottaison et de la fusion de la glace sur l'écoulement.

Les modèles numériques disponibles actuellement sont très complexes et ont des exigences de calcul élevées.

Partant de ces faits, l'objectif principal de cette thèse est de concevoir un modèle numérique simple et efficace capable de fournir, à des coûts de calcul raisonnables, des informations fiables sur la structure des écoulements de coulis de glace dans les tuyaux (isothermes ou chauffés) en tenant compte des effets combinés de la flottaison et de la fusion de glace. Cet

objectif est divisible en sous-objectifs qui, lorsqu'articulés ensemble, permettront l'atteinte de l'objectif principal. Ces sous-objectifs sont définis ci-dessous :

Développer un modèle numérique 3D CFD applicable à l'étude de coulis de glace en régimes laminaire et turbulent.

- Développer une équation de transport des particules de glace basée sur le modèle proposé par Phillips et al (1992) qui incorpore la migration des particules par cisaillement et flottaison.
- Développer un modèle de fusion de glace basé sur les échanges de masse et d'énergie à l'interface entre les particules de glace et le liquide environnant.

Incorporer les propriétés thermophysiques de coulis de glace à l'aide des relations décrites dans le Handbook on Ice Slurries-Fundamentals and Engineering (Kauffeld et al., 2005) et des corrélations établies par Renaud-Boivin et al. (2012) pour des solutions aqueuses.

Valider le modèle à l'aide des résultats de la littérature et des mesures réalisées avec le montage disponible à CanmetENERGY à Varennes, Québec, Canada.

Utiliser le modèle pour simuler et analyser l'effet des paramètres opératoires tels que la température, le débit, la concentration, et la vitesse du coulis de glace à l'entrée du tuyau, les conditions thermiques sur la paroi, sur les caractéristiques de l'écoulement (coefficient de friction, coefficient de transfert de chaleur, distribution de la concentration, distribution de la température, distribution de la vitesse).

CHAPITRE 3

STRATIFICATION IN ISOTHERMAL ICE-SLURRY PIPE FLOW

Auteurs et affiliations :

Landa ONOKOKO : étudiant au doctorat, Université de Sherbrooke, Faculté de Génie, Département de Génie mécanique.

Nicolas GALANIS : professeur, Université de Sherbrooke, Faculté de Génie, Département de Génie mécanique.

Référence : Onokoko C. L. & Galanis N., (2013). Stratification in isothermal ice-slurry pipe flow. ASME Int. Mech. Eng. Congress & Expo, paper IMECE2013-63801, San Diego (USA), November 15-21.

Date d'acceptation **:** Mai 2013

Titre en français : La stratification dans un écoulement de coulis de glace dans un tuyau isotherme.

.

RÉSUMÉ

Un modèle monophasique tridimensionnel d'un écoulement isotherme (laminaire et turbulent) du coulis de glace a été développé pour analyser l'influence des conditions d'entrée (vitesse et concentration), considérées comme uniformes, sur l'évolution axiale de la distribution de la vitesse et de la concentration dans un tuyau horizontal. Le coulis de glace est considéré comme un fluide Newtonien ayant des propriétés locales effectives qui dépendent de la concentration locale de la glace. Malgré sa simplicité comparativement aux modèles multiphasiques disponibles, sa résolution numérique donne des résultats qui reflètent correctement les observations expérimentales. Plus précisément, ces résultats montrent que lorsque le fluide se déplace vers l'aval, la concentration de glace augmente dans la partie supérieure du tuyau et diminue dans la partie inférieure. Le profil de vitesse est essentiellement influencé par la croissance de la couche limite proche de l'entrée, mais plus en aval, il devient asymétrique par rapport au plan de symétrie horizontal avec des vitesses plus élevées dans la partie inférieure du tuyau. Les différences entre les valeurs dans les parties supérieure et inférieure du tuyau sont beaucoup plus importantes dans le cas d'un écoulement laminaire. Les résultats sont analysés en considérant les phénomènes influençant le mouvement des particules de glace (flottabilité et diffusion) et la relation entre la concentration de glace et les propriétés thermophysiques du coulis de glace.

ABSTRACT

A single-phase 3D model for isothermal laminar and turbulent flow of an ice slurry in a horizontal pipe is used to investigate the effects of the uniform inlet velocity and ice concentration on their axial evolution. The slurry is modeled as a Newtonian fluid with effective local properties depending on the local ice concentration. Despite the relative simplicity of this model (compared to the two-phase models used elsewhere) its numerical solution gives results which correctly reflect experimental observations. Specifically, these results show that as the fluid moves downstream the ice concentration increases in the upper part of the pipe and it decreases in the lower part. The velocity profile is principally influenced by the boundary layer growth close to the inlet but further downstream it becomes asymmetrical with respect to the horizontal symmetry plane with higher velocities in the lower part of the pipe. The differences between the values in the upper and lower parts of the pipe are much more important in the case of laminar flow. The results are analyzed by considering the phenomena influencing the ice particle movement (buoyancy and diffusion) and the relation between ice concentration and the thermophysical properties of the slurry.

3.1 Introduction

Ice slurries are mixtures of small ice particles (typically 0.1 to 1 mm of diameter) and a carrier liquid (a mixture of water and an additive such as glycol, sodium chloride or calcium carbonate which lowers the freezing temperature). They offer the possibility of enhanced energy transport density and energy storage due to the combined effects of sensible and latent heat. Applications include comfort cooling of buildings, food processing and the replacement of secondary refrigerants in ice rinks or supermarkets. Their thermophysical properties can be derived from linear weighing of the corresponding properties of the ice (which are essentially determined by the temperature) and the carrier liquid (which vary with the temperature and the concentration of the additive) (Kauffeld, 2005).

The behavior of ice slurries in heat transfer installations is complex. Thus, in horizontal pipes separation of the solid ice particles and carrier liquid occurs with any particle size at very low velocities and with large particles at high velocities. Various flow patterns can be encountered in ice slurry pipelines that affect the hydrodynamics of the flow and the mechanism of heat transfer. The different experimentally observed flow patterns are classified as homogeneous, heterogeneous, sliding bed and stationary bed (Kauffeld, 2005). Kitanovski & Poredos (2002) calculated the concentration distribution of ice in horizontal pipe flow by integrating the one-dimensional diffusion equation with constant values of the diffusion coefficient and the hindered settling velocity of the ice particles. They then calculated the average ice slurry viscosity by integrating the well-known Thomas equation applied locally with the calculated concentration profile. They concluded that for high average velocities and very low ice concentrations “the ice slurry viscosity is almost independent of velocity as for Newtonian fluids”. On the other hand, ice slurries exhibit a non-Newtonian behavior for ice concentrations exceeding approximately 20 % but this threshold value is also influenced by parameters such as the size of the ice particles and the nature of the additive. Several experimental studies have determined values of the effective viscosity of ice slurries and compared them with different rheological models (Kitanovski, 2005).

Several CFD analyses of slurry flow with or without heat transfer have been published in recent years. Thus, Wang et al. (2013a) applied an Euler-Euler model and calculated profiles of velocity and ice particle concentration as well as pressure drop for turbulent isothermal flow in horizontal, vertical and 90º elbow pipes. Their numerical predictions are within 20% of corresponding measured values. NiezgodaZelasko & Zalewski (2006) obtained numerical results using a single-phase model with a Bingham fluid and multiphase models (mixture and Eulerian models). They found that for laminar flows both the Bingham and mixture models gave a correct description of the flow field. For low Reynolds number turbulent flows, they found that the best agreement between numerical and experimental results (for the single-phase and the multiphase Eulerian models) was obtained by using the RNG k-ε turbulence model with the enhanced wall treatment.

In the present study we consider the isothermal, steady, laminar and turbulent flows of ice slurry in the entrance region of a horizontal pipe. The ice slurry is treated as a single-phase Newtonian fluid with effective properties. A model consisting of the three-dimensional differential equations of motion for the slurry, the realizable k-ε turbulence model as well as the conservation equation for the ice particles is proposed and solved numerically. These equations are coupled since the viscosity and density of the slurry depend on the ice concentration which changes from the assumed uniform distribution at the inlet due to the opposing effects of buoyancy and diffusion. The results illustrate the axial evolution of the ice concentration and the velocity profiles which depend on the flow regime (laminar or turbulent) and are in good qualitative agreement with experimental observations.

3.2 Description and modeling of the problem

The ice slurry under consideration is an aqueous solution of ethylene glycol and ice particles of mean diameter d. It is flowing in a horizontal adiabatic pipe of diameter D and length L = 300 D. At the pipe inlet the velocity V_0, the temperature T_0 and the volumetric concentration $\emptyset_0$ of the ice particles are uniform. The outflow condition is applied at the pipe outlet. The no-slip and no-ice particle-flux are applied at the pipe wall. The origin of the coordinates system

is at the pipe inlet. The z axis coincides with the pipe axis while the x and y axes are horizontal and vertical respectively.

3.2.1 Laminar flow

The governing equations are based on the continuum approach. The ice particles migration that includes several mechanisms (Brownian motion, particle settling, shear-induced, and viscosity gradients migration) is described by an additional transport equation.

The steady state continuity and momentum conservation equations are given respectively by:

$$\boldsymbol{\nabla} \cdot (\rho_{is}\boldsymbol{u}) = 0 \tag{3.1}$$

$$\boldsymbol{\nabla} \cdot (\rho_{is}\boldsymbol{uu}) = -\boldsymbol{\nabla}p + \boldsymbol{\nabla} \cdot \boldsymbol{\tau} \tag{3.2}$$

The steady state species conservation equation, based on the particle diffusive model proposed by Phillips et al. (1992), is

$$\boldsymbol{\nabla} \cdot (\rho_{is}\boldsymbol{u}\emptyset) = -\boldsymbol{\nabla} \cdot \boldsymbol{N_t} \tag{3.3}$$

This equation represents a balance between the convective and diffusive particle flux. Neglecting Brownian motion, we model the diffusive particle flux as:

$$\boldsymbol{N_t} = \boldsymbol{N_c} + \boldsymbol{N_\mu} + \boldsymbol{N_s} \tag{3.4}$$

Where $\boldsymbol{N_c}$ is the flux induced by the gradients of shear rate, $\boldsymbol{N_\mu}$ is the flux due to spatial variation in viscosity, and $\boldsymbol{N_s}$ is the flux due to particle settling. Based on the scaling arguments of Leighton & Acrivos (1987), Phillips et al. (1991) proposed the following expressions:

$$\boldsymbol{N_c} = -\rho_{is}K_c a^2(\emptyset^2\boldsymbol{\nabla}\dot{\gamma} + \dot{\gamma}\emptyset\boldsymbol{\nabla}\emptyset) \tag{3.5a}$$

$$\boldsymbol{N_\mu} = -\rho_{is}K_\mu a^2\dot{\gamma}\emptyset^2\frac{1}{\mu_{is}}\frac{d\mu_{is}}{d\emptyset}\boldsymbol{\nabla}\emptyset \tag{3.5b}$$

The values of the coefficients are $K_c = 0.41$ and $K_\mu = 0.62$.

For the settling particle flux we adopt the following form proposed by Richardson & Zaki (1954):

$$\boldsymbol{N_s} = \rho_{is}\omega_{\mathbf{0}} f(\emptyset)\emptyset\boldsymbol{Q} \tag{3.5c}$$

Where ω_0 is the terminal settling velocity of a single particle in the aqueous solution and $f(\emptyset)$ is the hindrance function. For the latter we adopt the form suggested by Revay & Higdon (1992):

$$f(\emptyset) = (1-\emptyset)^{6.55}(1 + 3.458\emptyset^2 + 8.990\emptyset^3) \tag{3.5d}$$

With these relations the species conservation equation becomes

$$\boldsymbol{\nabla}\cdot\{\rho_{is}[\boldsymbol{u} + \omega_0 f(\emptyset)\boldsymbol{Q}]\emptyset\} = \boldsymbol{\nabla}\cdot(\Gamma\boldsymbol{\nabla}\emptyset) + \boldsymbol{S} \tag{3.6a}$$

The diffusive coefficient Γ and the source term $\boldsymbol{S}$ are:

$$\Gamma = \rho_{is}a^2\emptyset\dot{\gamma}\left(K_c + K_\mu\emptyset\frac{\partial\mu_{is}}{\mu_{is}\partial\emptyset}\right) \tag{3.6b}$$

$$\boldsymbol{S} = \boldsymbol{\nabla}\cdot(\rho_{is}\mathrm{K_c a^2}\emptyset^2\boldsymbol{\nabla}\dot{\gamma}) \tag{3.6c}$$

3.2.2 Turbulent flow

For steady state conditions the averaged equations of mass conservation and momentum are:

$$\frac{\partial}{\partial x_i}(\rho_{is}\bar{u}_i) = 0 \tag{3.7}$$

$$\frac{\partial}{\partial x_j}\left(\rho_{is}\bar{u}_i\bar{u}_j\right) = -\frac{\partial\bar{P}}{\partial x_i} + \frac{\partial}{\partial x_j}\left[\mu_{is}\left(\frac{\partial\bar{u}_i}{\partial x_j} + \frac{\partial\bar{u}_i}{\partial x_i} - \frac{2}{3}\delta_{ij}\frac{\partial\bar{u}_i}{\partial x_i}\right)\right] + \frac{\partial}{\partial x_j}\left(-\rho_{is}\overline{u_i'u_j'}\right) \tag{3.8}$$

The turbulence model adopted in the present study is the realizable *k-ε* model. It was preferred to the standard *k-ε* model because it includes an improved equation for *ε* and uses a variable coefficient in the expression of the turbulent viscosity. It is appropriate for boundary

layers with strong adverse pressure gradients such as those encountered near the inlet in the problem under consideration. The corresponding equations are:

$$\frac{\partial}{\partial x_i}(\rho_{is} k \bar{u}_i) = \frac{\partial}{\partial x_i}\left[\left(\mu_{is} + \frac{\mu_t}{\rho_k}\right)\frac{\partial k}{\partial x_i}\right] + G_k + G_b - \rho_{is}\varepsilon - Y_m + S_k \quad (3.9a)$$

$$\frac{\partial}{\partial x_i}(\rho_{is} \varepsilon \bar{u}_i) = \frac{\partial}{\partial x_i}\left[\left(\mu_{is} + \frac{\mu_t}{\rho_\varepsilon}\right)\frac{\partial \varepsilon}{\partial x_i}\right] + \rho_{is} G_1 S_\varepsilon - \rho_{is} C_2 \frac{\varepsilon^2}{k+\sqrt{\nu\varepsilon}} + C_{1\varepsilon}\frac{\varepsilon}{k} C_{3\varepsilon}\ G_b + S_\varepsilon \quad (3.9b)$$

The particle diffusive model proposed by Phillips et al. (1992) is also valid for turbulent conditions according to Bui et al (2003). When associated with the motion created by the density difference between the liquid and solid phases it results in the following expression for the species conservation equation:

$$\frac{\partial}{\partial x_i}\left[\rho_{is}\left(\bar{u}_i + \delta_{i3}\omega_0 f(\emptyset)\right)\emptyset\right] = \frac{\partial}{\partial x_i}\left[\Gamma_\emptyset\left(\frac{\partial \emptyset}{\partial x_i}\right)\right] + S_\emptyset \quad (3.10)$$

The diffusive coefficient $\Gamma_\emptyset$, the source term $S_\emptyset$, the hindrance function $f(\emptyset)$ and the values of the coefficients K_c and K_μ are identical to those for laminar flow.

3.2.3 Ice slurry properties

The fusion temperature of aqueous solutions of additives such as ethylene glycol decreases as the concentration of the additive (X_0 in kg of additive per kg of mixture or $\emptyset_0$ in m^3 of additive per m^3 of mixture) increases. For temperatures above this fusion temperature the mixture does not contain any ice particles. For temperatures below this fusion temperature the mixture contains solid particles which are considered to be pure water; as a result, for such temperatures, the concentration of additive in the liquid mixture is higher than X_0 (and $\emptyset_0$).

According to the Handbook on Ice Slurries (2005) the density of the ice (subscript *i*) can be calculated from the expression:

$$\rho_i = 917 - 0.13T \quad (3.11)$$

The density and the viscosity of the liquid mixture of water and additive (subscript l) depend on the temperature and on the volumetric concentration of the additive (subscript a). They can be calculated from the following formulas:

$$\rho_l(\emptyset_a, T) = \sum_{i=0}^{M} T^i \sum_{j=0}^{N} b_{i,j} \emptyset_a^j \quad (3.12a)$$

$$\mu_l(\emptyset_a, T) = \sum_{i=0}^{M} T^i \sum_{j=0}^{N} b_{i,j} \emptyset_a^j \quad (3.12b)$$

The coefficients $b_{i,j}$ were calculated by Renaud-Boivin et al. (2012) by polynomial curve-fitting of tabulated data published in the ASHRAE Handbook of Fundamentals (2005).

Finally, the density and viscosity of the ice slurry (subscript is) can be calculated from the following equations:

$$\rho_{is} = \emptyset \rho_i + (1 - \emptyset)\rho_l \quad (3.13a)$$

$$\mu_{is} = \mu_l\left(1 + 2.5\emptyset + 10.05\emptyset^2 + 0.00273e^{16.6\emptyset}\right) \quad (3.13b)$$

In all the above expressions the density is in kg/m^3, the viscosity is in mPas while *T* is the temperature in ºC.

3.3 Solution and validation

The coupled differential equations of the model were solved using the software package Ansys-Fluent which is based on the finite volume technique. The ice particle conservation equation was introduced using the user-defined scalar (UDS) functionality. The SIMPLE algorithm was employed to resolve the pressure-velocity coupling in the momentum equation. The QUICK scheme was used to approximate the convection term. The validation of the model was obtained by simulating the steady laminar forced convection of water in a horizontal tube. The mesh independence was examined by refining a coarser size until results were unchanged. Table 1 shows the calculated values of the non-dimensional velocity (V/V_0) at different axial positions ($z^*=(z/D)/Re$) for three mesh sizes and compares them with those obtained by Nascimento et al. (2006) and Liu (1974). The fine mesh with approximately 7.1 10^6 cells which

gives results in very good agreement with those in the literature has been used to obtain all the results presented in the subsequent sections of this paper. For further validation the predicted velocity for a slurry with solid polypropylene spheres is compared in Fig. 3.1 with experimental results by Stutz et al (2013). The agreement is good. The differences are due to the fact that simulations were carried out by assuming that the carrying fluid is a mixture (water and 10% ethanol) while in the experiments it was pure water.

Table 3.1: Mesh independence tests and validation (Re=500, Water Flow)

mesh	z* = 0.0002116	z* = 0.005288	z* = 0.06281	z* = 0.08993
Coarse (2169000 cells)	1.0359	1.4150	1.9777	1.9872
Medium (3481885 cells)	1.0108	1.3924	1.9791	1.9987
Fine (7117986 cells)	1.0094	1.4119	1.9802	1.9998
Liu (1974)	1.100	1.439	1.989	1.999
Nascimento et al (2006)	1.113	1.427	1.961	1.972

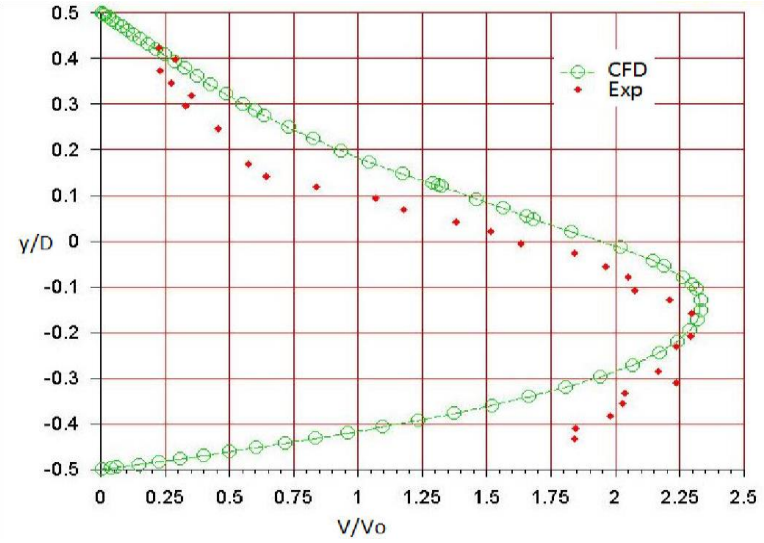

Fig. 3.1: Experimental and numerical velocity profiles

3.4 Results and discussion

Two series of simulations were carried out with different combinations of the inlet velocity and the inlet ice concentration. In all cases the additive is ethylene glycol with a mass concentration in the absence of ice equal to 14% (the corresponding fusion temperature is 268.24 K). The average diameter of the ice particles is d= 0.4 mm and the length of the pipe is L = 3 m for all simulations. The combinations of inlet velocity and inlet ice concentration are chosen so that the corresponding Reynolds number Re_0 is clearly in the laminar or turbulent regime. Specifically, Re_0 is always less than 1000 for the first series and always more than 3000 for the second one.

3.4.1 Results for laminar flow

Figure 3.2 shows the axial evolution of the ice particles concentration distribution along the vertical diameter of the pipe for V_0 = 0.2 m/s and $\emptyset_0$ = 0.1 (which corresponds to a temperature of 267.56 K, i.e. slightly lower than the fusion temperature). Under the effect of buoyancy, the ice particles whose density is smaller than that of the liquid mixture rise towards the top of the pipe. As a result of this phenomenon the ice particle concentration increases in the upper part of the pipe and it decreases in its lower part. The ensuing concentration gradient creates a downwards flux of ice particles which eventually becomes equal to the upward one sustained by buoyancy. Therefore, the concentration profile eventually reaches a form which is independent of the axial position as illustrated by the fact that the profile at z = 1.50 m is identical to the one at z = 2.95 m.

Figure 3.3 shows the corresponding profiles of the axial velocity which also evolve with the distance from the inlet. Near the inlet (z = 0.005 m) we observe the well-known overshoot phenomenon caused by the rapid development of the boundary layer. Further downstream the velocity profile is not symmetrical with respect to the pipe axis. This is due to the influence of the ice particle concentration on the viscosity of the slurry. Thus, in the lower part of the pipe where the ice concentration is low the viscosity decreases and the velocity increases. On

the other hand, in the higher part of the pipe where the ice concentration is high the viscosity increases and the velocity decreases. Eventually the velocity profile reaches a form which is independent of the axial position as illustrated by the fact that the profile at z = 1.50 m is identical to the one at z = 2.95 m.

It is therefore evident that for the conditions under consideration the flow field is fully developed beyond z=1.5 m.

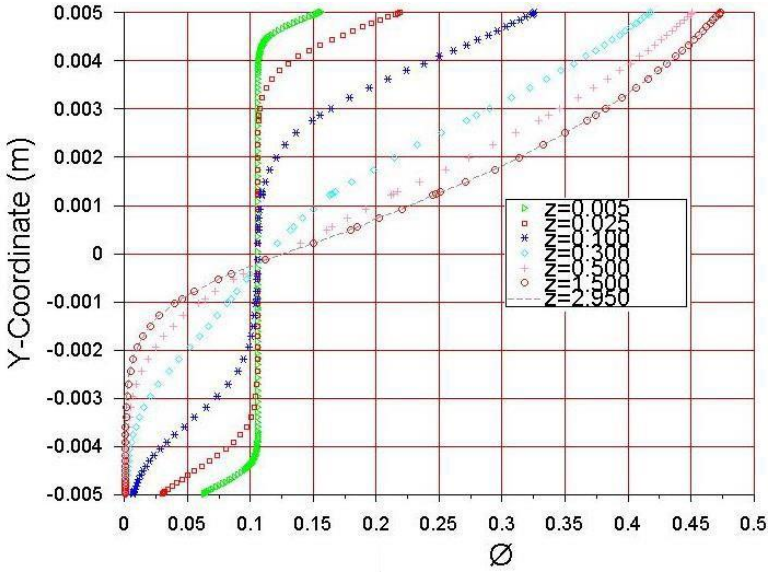

Fig. 3.2: Axial evolution of the concentration profile for V_0 = 0.2 m/s and $\emptyset_0$ = 0.1

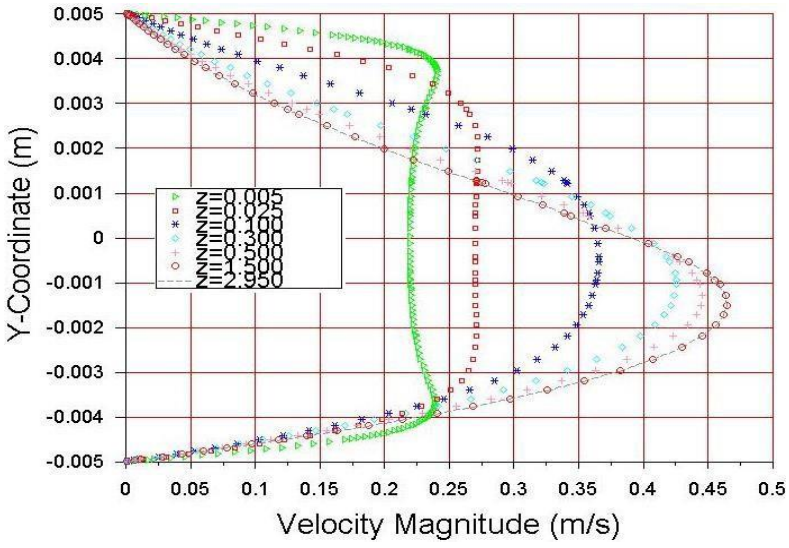

Fig. 3.3: Axial evolution of the velocity profile for V_0 = 0.2 m/s and $\emptyset_0$ = 0.1

In order to test the validity and precision of these results we calculated the average concentration of the ice particles for different cross sections normal to the pipe axis. This quantity was obtained by first integrating the product of the local ice concentration (function of x and y) and the local mass flowrate (also a function of x and y) over the circular cross section; this product was then divided by the mass flowrate of the ice slurry which is of course independent of the axial position. The comparison of the calculated values of the average concentration shows that this quantity is essentially independent of the axial position (see Table 3.2). This result was of course anticipated since the flow under consideration takes place without heat transfer and therefore the quantity of ice transported downstream should not change. The fact that the numerical results satisfy this condition is therefore an indication that the model and its numerical solution are reliable.

Table 3.2: Validation of the constancy of the average ice concentration for laminar flow

Axial position z (m)	0.05	0.5	1.0	2.0	2.95
Average ice concentration (%)	10.00	9.99	10.00	10.03	10.05

Figure 3.4 illustrates the effect of the inlet ice concentration on the fully developed concentration profile for V_0 = 0.35 m/s. We note that the lower part of the pipe does not contain any ice and that the vertical dimension of this ice-free region decreases as $\emptyset_0$ increases. Furthermore as $\emptyset_0$ increases the maximum concentration, which occurs at the top of the pipe, increases as well. These tendencies are consistent with experimental observations (Kauffeld, 2005).

Figure 3.5 illustrates the effect of the inlet ice concentration on the fully developed velocity profile for V_0 = 0.35 m/s. We note that the increase of $\emptyset_0$ causes the increase of the maximum axial velocity and a downward shift of its position. Specifically, the ratio V_{max}/V_0 is approximately 1.8, 1.94 and 2.28 for $\emptyset_0$ equal to 0.1, 0.15 and 0.2 respectively. The form of these profiles is similar to that obtained by Stutz et al (2013). who measured the velocity of a slurry (water with polypropylene spheres having a diameter of 3 mm and a density relative to

water equal to 0.869) using a Pitot tube. Quantitative comparisons were not possible because this article does not specify the values of V_0 and $\emptyset_0$ for the reported experiments.

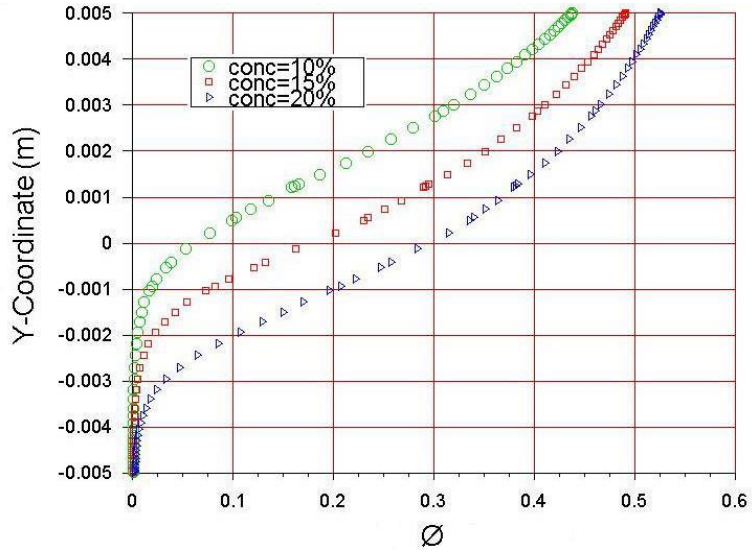

Fig. 3.4: Effect of $\emptyset_0$ on the fully developed concentration profile for V_0 = 0.35 m/s

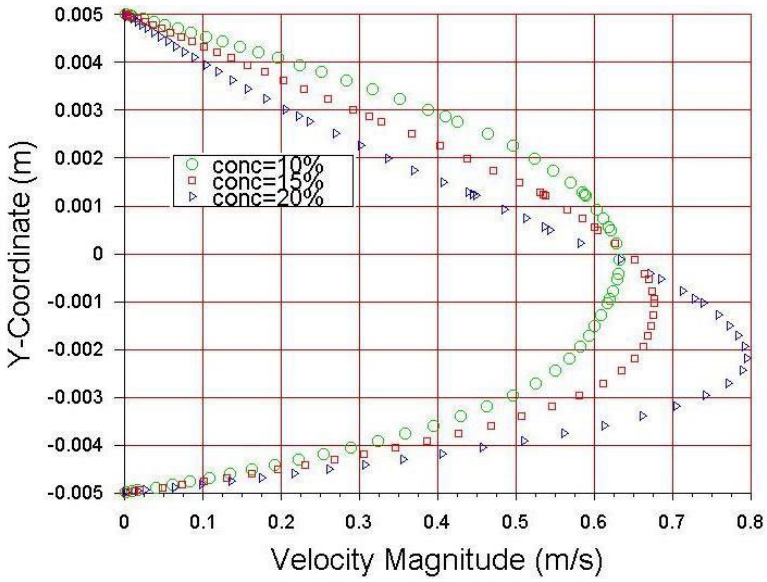

Fig. 3.5: Effect of $\emptyset_0$ on the fully developed velocity profile for V_0 = 0.35 m/s

3.4.2 Results for turbulent flow

Figure 3.6 shows the axial evolution of the ice particles concentration distribution along the vertical diameter of the pipe for V_0 = 2 m/s and $\emptyset_0$ = 0.1 (as before this corresponds to a temperature of 267.56 K, i.e. slightly lower than the fusion temperature). The qualitative explanation of the corresponding results for laminar flow still apply and justify the increase of the ice concentration in the upper part of the pipe as well as its decrease in the lower part. It is important however to note that in the present case the concentration profile has not reached a form independent of the axial position as indicated by the difference between the profiles for z = 1.5 m and z = 2.95 m. This result shows that in the present case the development length for ice concentration is longer than the length of the pipe used in this study (L = 3 m).

Figure 3.7 shows the corresponding iso-concentration lines at z = 2.95 m which as expected are symmetrical with respect to the vertical diameter of the pipe. Figure 3.8 shows the corresponding axial evolution of the velocity profiles along the vertical diameter of the pipe. The overshoot is again present near the pipe inlet but beyond approximately z = 1.5 m the profile becomes independent of the axial position and attains a fairly flat form characteristic of turbulent flows. The hydrodynamically developed profile is very similar to the experimental and numerical results of Wang et al (2013a). According to Figure 3.8 the ratio V_{max}/V_0 is approximately equal to 1.25 in the hydrodynamically developed region.

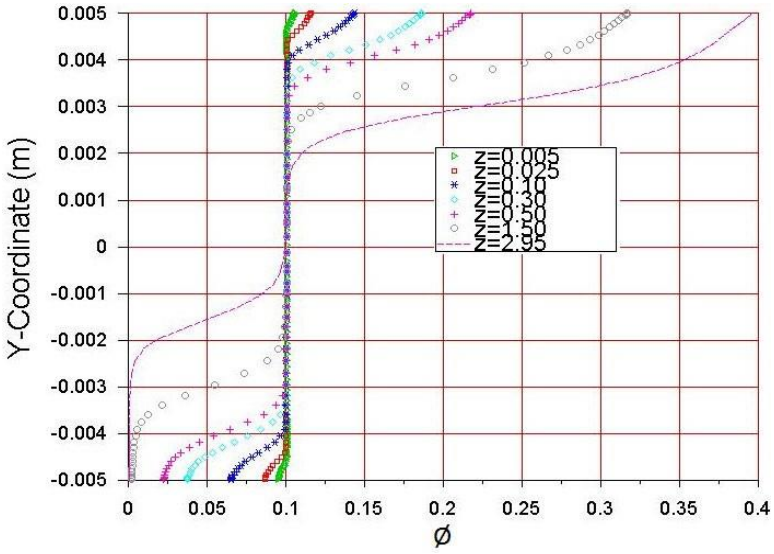

Fig. 3.6: Axial evolution of the concentration profile for V_0 = 2 m/s and $\emptyset_0$= 0.1

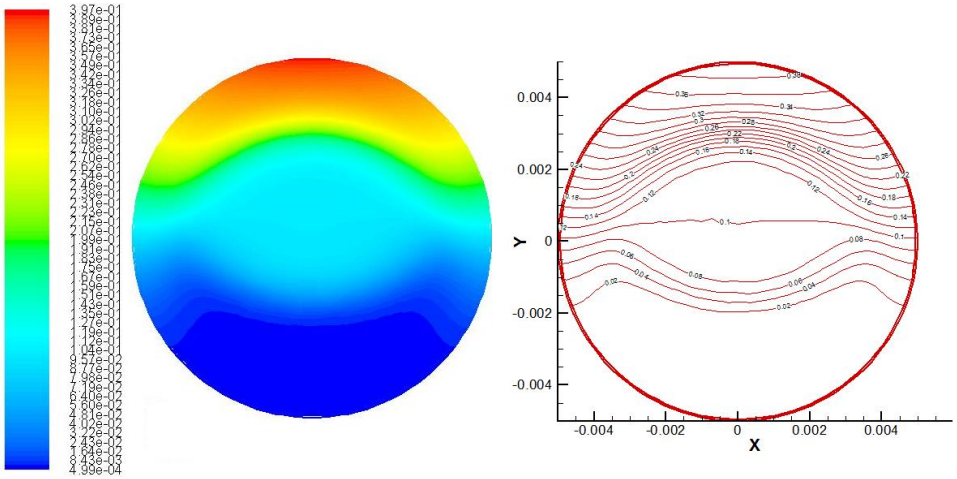

Fig. 3.7: Concentration distribution at z = 2.95 m for V_0 = 2 m/s and $\emptyset_0$= 0.1

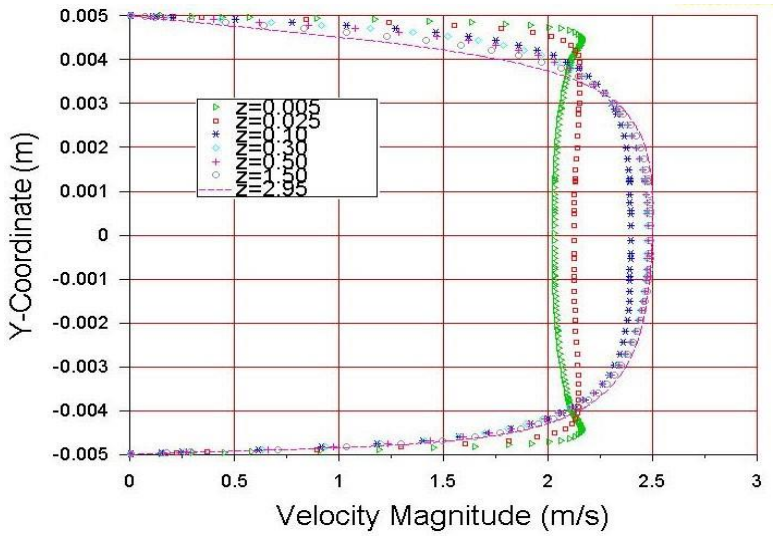

Fig. 3.8: Axial evolution of the velocity profile for V_0 = 2 m/s and $\emptyset_0$= 0.1

Figure 3.9 shows the lines of constant velocity at z = 2.95 m which indicate that the velocity field is not symmetrical with respect to the horizontal diameter of the pipe. Specifically, for symmetrical positions with respect to this diameter the velocity in the upper part is slightly smaller. This is due to the increased concentration of ice particles in the upper part which causes an increase of the molecular viscosity. The corresponding decrease of the velocity is however small since the molecular viscosity is small compared to the turbulent viscosity.

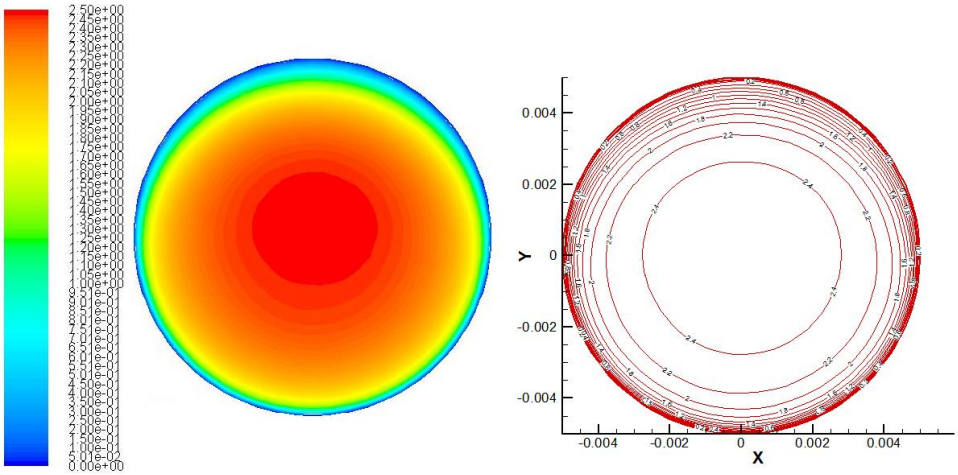

Fig. 3.9: Velocity distribution at z = 2.95 m for V_0 = 2 m/s and $\emptyset_0$= 0.1

Figure 3.10 illustrates the effect of the inlet ice concentration on the concentration profile at z = 2.95 m for V_0 = 2 m/s. We note that the difference between the maximum concentration (which occurs at the top of the pipe) and the minimum concentration (which occurs at the bottom) is greatest for the smallest value of $\emptyset_0$ and smallest for the greatest value of $\emptyset_0$. Complete elimination of the ice from the bottom part of the pipe occurs only for the smallest value of $\emptyset_0$. Qualitatively these results are consistent with experimental observations (Kauffeld, 2005).

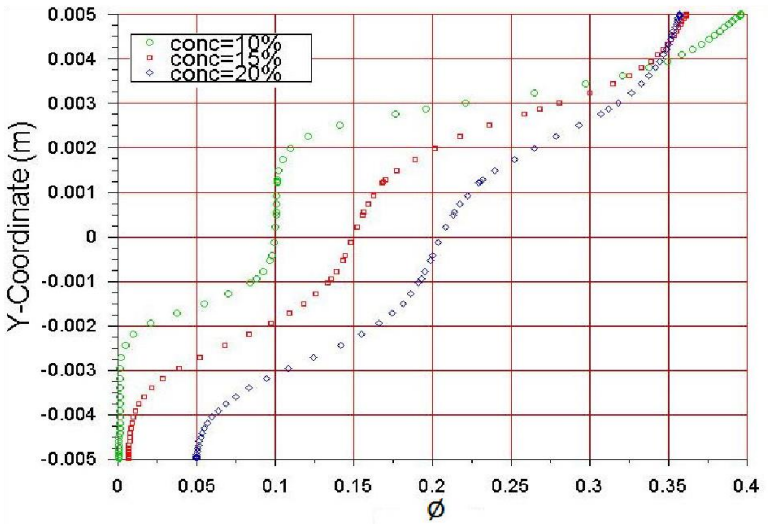

Fig.3.10: Effect of $\emptyset_0$ on the concentration profile at $z = 2.95\ \mathrm{m}$ for $V_0 = 2\ \mathrm{m/s}$

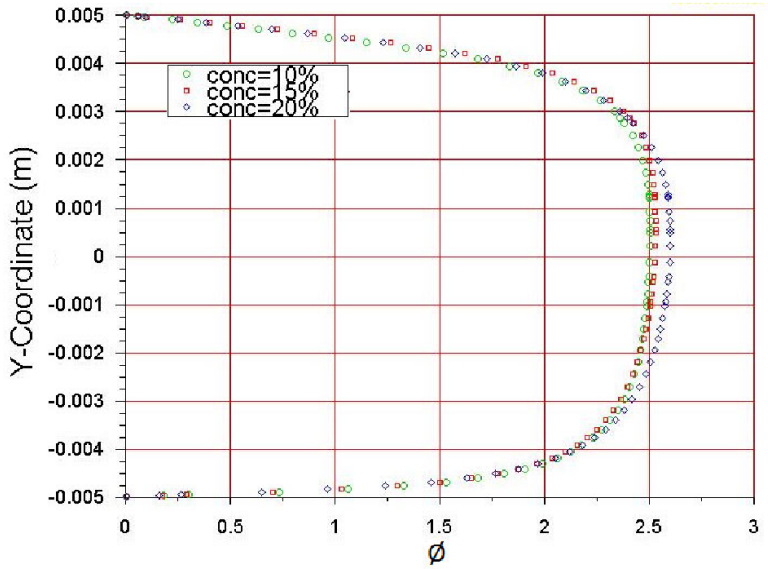

Fig.3.11: Effect of $\emptyset_0$ on the velocity profile at $z = 2.95\ \mathrm{m}$ for $V_0 = 2\ \mathrm{m/s}$

The maximum velocity increases slightly as the inlet concentration increases. It should be noted that the velocity at y = 0.004 m is smaller than at y = - 0.004 m. These results clearly illustrate that this profile is not symmetrical with respect to the pipe axis for the reasons explained in the discussion of Figure 3.9.

Table 3.3 shows the average concentration of the ice particles for different cross sections normal to the pipe axis for turbulent flow with V_0 = 2 m/s and $_0$ = 0.1. These values were calculated as explained earlier in the case of laminar flow. Even though they increase slightly in the direction of flow they are everywhere within less than 2% of the exact value (i.e. the concentration at the inlet). Therefore, we consider that the model and its numerical solution are reliable.

Table 3.3: Validation of the constancy of the average ice concentration for turbulent flow

Axial position z (m)	0.05	0.5	1.0	2.0	2.95
Average ice concentration (%)	10.01	10.05	10.08	10.12	10.16

5.4.3 Comparison of laminar and turbulent results

For all simulations in this section the value of the inlet ice concentration is 10%. The results show velocity and concentration profiles along the vertical diameter of the pipe. Figures 3.12 and 3.13 compare the normalized velocity profiles for laminar (V_0 = 0.2 m/s) and turbulent (V_0 = 2 m/s) flow at z = 0.5 m and z = 2.95 m respectively. The differences at both positions are striking. The maximum normalized velocity in the case of laminar flow is almost twice that of turbulent flow. The asymmetry with respect to the pipe's axis is much more pronounced in the case of laminar flow. Near the top and bottom the velocity increases much faster in the turbulent case. The relative importance of the wall shear stress for the top and bottom of each flow regime cannot be deduced from the corresponding velocity gradients because the viscosity is not the same at these positions. Further calculations are therefore required to

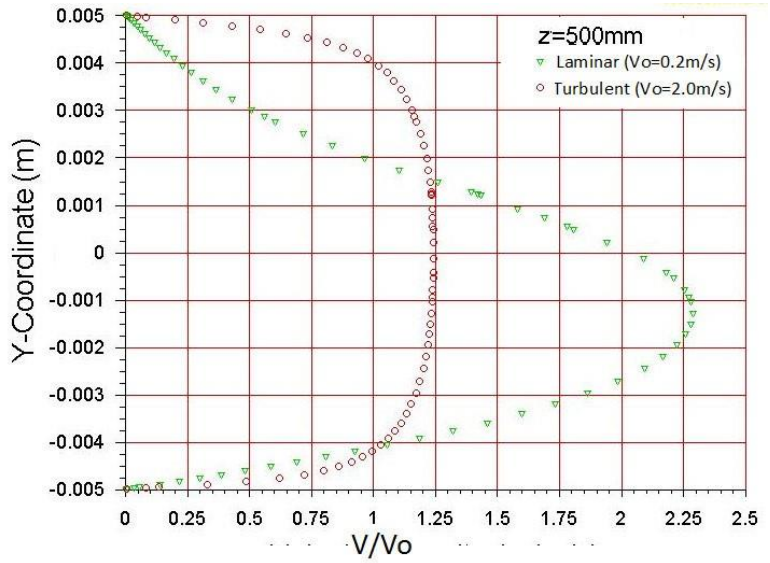

Fig. 3.12: Comparison of normalized velocity profiles for laminar and turbulent (z=0.5m)

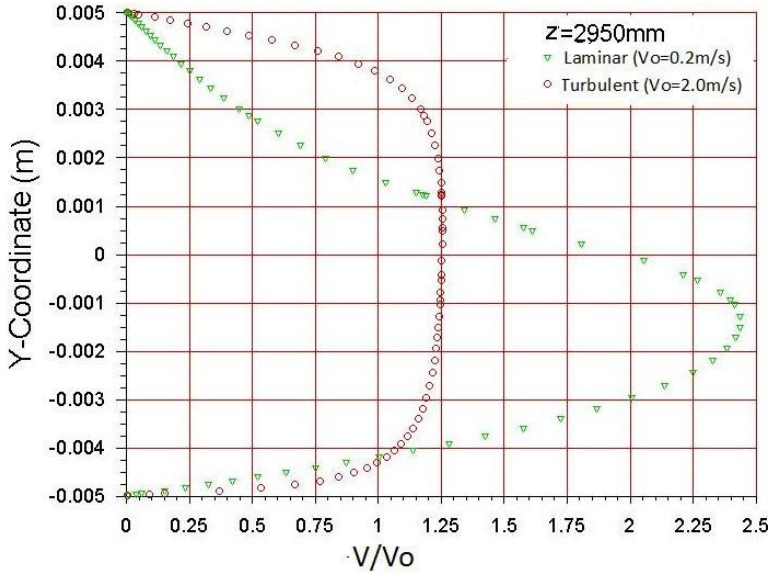

Fig. 3.13: Comparison of normalized velocity profiles for laminar and turbulent flow (2.95m)

evaluate the circumferential and axial distributions of the wall shear stress for each flow regime.

Figures 3.14 and 3.15 compare concentration profiles for laminar (V_0 = 0.2 m/s) and turbulent (V_0 = 2 m/s) flow at z = 0.5 m and z = 2.95 m respectively. Again, the differences between laminar and turbulent results are striking. For laminar flow the lower part of the pipe does not contain any ice and elsewhere it increases almost linearly. For turbulent flow the

concentration remains equal to the inlet value over an important part of the profile (more than half at z = 0.5 m and approximately 20% at z = 2.95 m). At z = 0.5 m the minimum ice concentration is still positive. At both positions the differences between the maximum and minimum concentrations are considerably higher in the case of laminar flow. These observations indicate that the ice concentration profile evolves much faster in the case of laminar flow. It therefore appears that turbulence slows down the effects of buoyancy and diffusion which act alone in the case of laminar flow and tends to maintain a relative uniformity of the ice concentration.

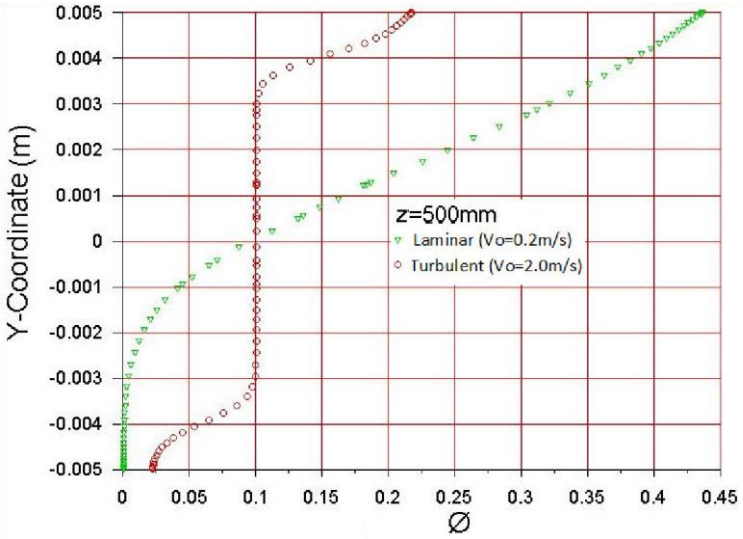

Fig. 3.14: Comparison of concentration profiles for laminar and turbulent flow (0.5m)

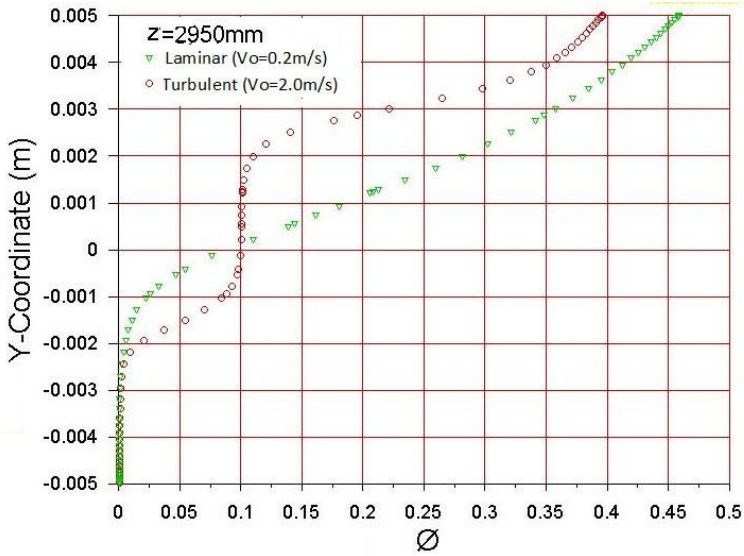

Fig. 3.15: Comparison of concentration profiles for laminar and turbulent flow (2.95m)

3.5 Conclusions

The adopted single-phase model of isothermal ice slurry flow in a horizontal pipe is simpler than the two-phase models used in most other studies of this problem. Nevertheless, its numerical predictions correctly reflect the experimentally determined effects for both laminar and turbulent conditions. Specifically, for laminar flow the model shows that:

- The velocity distribution is not symmetrical with respect to the horizontal symmetry plane; the maximum velocity occurs below the pipe axis and increases significantly with the inlet ice concentration.
- As the slurry moves downstream the ice concentration increases in the upper part of the pipe; in the lower part ice particles eventually disappear completely; the difference between the maximum and minimum concentrations in a fixed cross-section increases with the inlet ice concentration.

For turbulent flow the model shows that:

- The shape of the velocity profile is essentially determined by the turbulence although it is not exactly symmetrical with respect to the horizontal symmetry plane; the effect of the inlet ice concentration on the hydrodynamically developed velocity distribution is very small.
- The ice concentration increases in the upper part of the pipe and it decreases in its lower part; the difference between the maximum and minimum concentrations in a fixed cross-section decreases when the inlet ice concentration increases.

The differences between the behavior of laminar and turbulent flows have been explained by considering the effect of ice concentration on the molecular dynamic viscosity of the slurry and its magnitude relative to the turbulent viscosity.

Acknowledgments

This project is part of the R&D program of the NSERC Chair in Industrial Energy Efficiency established in 2006 at '*Université de Sherbrooke*'. The authors acknowledge the support of the

Natural Sciences & Engineering Research Council of Canada, Hydro Québec, Rio Tinto Alcan and CanmetENERGY Research Center of Natural Resources Canada.

CHAPITRE 4

RHEOLOGY OF A POLYPROPYLENE-GLYCOL ICE SLURRY

Auteurs et affiliations :

Landa ONOKOKO : étudiant au doctorat, Université de Sherbrooke, Faculté de Génie, Département de Génie mécanique.

Nicolas GALANIS : professeur, Université de Sherbrooke, Faculté de Génie, Département de Génie Mécanique.

Sébastien PONCET : professeur, Université de Sherbrooke, Faculté de Génie, Département de Génie Mécanique.

Michel POIRIER : CanmetENERGY Natural Ressources Canada, Varennes, Québec, Canada.

Référence : Onokoko, C.L., Poirier, M., Galanis, N., Poncet, S., 2017. Rheology of a propylene-glycol ice slurry. In: Proceeding of 26th CANCAM, Victoria, BC, Canada, May 29-June 1.

Date d'acceptation **:** Mars 2017

Titre en français : La rhéologie d'un coulis de glace a base de polypropylène-glycol

.

RÉSUMÉ

Les coefficients de friction d'un écoulement de coulis de glace à base de propylène glycol (point de congélation -1,29 ° C) obtenus à partir de mesures de pertes de charge pour différents débits et fractions de glace sont comparés aux valeurs correspondantes obtenues à partir d'un modèle numérique qui considère le coulis de glace comme un fluide Newtonien. Les résultats sont en bon accord en régime turbulent et non en régime laminaire. Les mesures expérimentales sont ensuite utilisées pour établir en fonction de la concentration, les expressions de la contrainte seuil et de la consistance du coulis de glace considéré cette fois-ci comme un fluide de Bingham. Couplé à la corrélation laminaire de Danish-Kumar, le modèle rhéologique obtenu donne des coefficients de friction en excellent accord avec les valeurs déterminées expérimentalement.

Mots-clés : Fluide newtonien, fluide de Bingham, limite d 'élasticité, indice de consistance, fraction de masse de glace, coulis de glace

ABSTRACT

Friction factors for the flow of a particular propylene glycol ice slurry (freezing point -1.29 °C) obtained from measurements of pressure drops with different flowrates and ice fractions are compared with corresponding values from CFD simulations which assume Newtonian behavior. The agreement between these sets of values is good for turbulent conditions but very poor for laminar flows. The experimental data are therefore used to obtain expressions for the yield stress and the viscosity consistency as a function of the ice fraction. When coupled with the Danish-Kumar laminar correlation the obtained Bingham rheological model produces friction factors in excellent agreement with the experimentally determined values.

KEYWORDS: Newtonian fluid, Bingham fluid, yield stress, viscosity consistency, ice mass fraction, ice slurry.

4.1 Introduction

Ice slurries are mixtures of small ice particles (typically 0.1 to 1 mm of diameter) and a carrier liquid (a mixture of water and an additive, such as glycol or sodium chloride, which lowers the freezing temperature). They improve energy transport density and energy storage due to the combined effects of sensible and latent heat. Applications include cooling of buildings, food processing and the replacement of secondary refrigerants in ice rinks or supermarkets. Their thermophysical properties can be derived from linear weighting of the corresponding properties of the ice (essentially determined by the temperature) and the carrier liquid (which vary with temperature and additive concentration) (Kauffeld et al., 2005).

The flow behaviour of ice slurries is complex. Thus, in horizontal pipes, separation of the ice particles and carrier liquid occurs with any particle size at very low velocities and with large particles at high velocities. Various flow patterns (homogeneous, heterogeneous, sliding bed and stationary bed) are encountered and affect the hydrodynamics of the flow and the mechanism of heat transfer (Kauffeld et al., 2005). Kitanovski & Poredos (2002) used a 1D approach to calculate the concentration distribution of ice and applied it to obtain the average ice slurry viscosity by integrating the Thomas equation. They concluded that for high average velocities and very low ice concentrations “the ice slurry viscosity is almost independent of velocity as for Newtonian fluids”. On the other hand, ice slurries exhibit a non-Newtonian behavior for ice concentrations exceeding approximately 20 % but this threshold value is influenced by parameters such as the size of the ice particles and the nature of the additive. Several experimental studies have determined values of the effective viscosity of ice slurries and compared them to different rheological models (Bingham, Ostwald-de-Waele, Casson and Herschel-Bulkley) (Kitanovski et al., 2005). Simulations treating ice slurries as single-phase fluids have used the Bingham model for an ethanol ice slurry (Niezgoda-Zelasko & Zalewski, 2006) and the Newtonian fluid approximation for an ethylene glycol ice slurry (Onokoko & Galanis, 2013) with good results.

These, and other, diverse attempts to characterize the rheology of ice slurries indicate that their exact nature is not yet fully understood. In view of this situation, the present study aims to add new data regarding the behavior of propylene glycol ice slurry for which non-Newtonian behavior has been reported even for low ice concentrations (Mellari, 2016).

4.2 Methodology and results

The ice slurry under consideration is an aqueous solution of propylene glycol whose measured freezing point is -1.29 °C. The pressure loss in a long horizontal pipe ($L_p/D \approx 177$) as well as the inlet and outlet density and temperature of the ice slurry were measured for flow rates between 1 and 38 kg/min and ice fractions of 5 to 20% by mass. Figure 4.1 compares the friction factor for an ice mass fraction of 10% determined from the experimental data with the corresponding numerical results from a 3D CFD model which assumes Newtonian behaviour (Onokoko & Galanis, 2013) and with values determined from published correlations (Renaud-Boivin et al., 2012; Fang et al., 2011). These comparisons (and similar results for other ice mass fractions) indicate a good agreement between the friction factors derived from measurements and the CFD predictions in the turbulent flow regime. In the laminar flow regime however, there are significant differences between the friction factors derived from measurements and the CFD values which are close to the predictions of the Poiseuille expression. On the other hand, the results predicted by assuming a Bingham model are in very good agreement with the measured data for both flow regimes. The details of the calculations with the Bingham model are presented in the following paragraphs.

Experimental pressure drops for laminar flow with three ice mass fractions (5, 15 and 20%) are plotted in Figure 4.2. In all cases, the curves which do not intercept the origin are linear. Therefore, these ice slurry flow situations can be fit by the Bingham model.

Bingham fluids are characterized by two parameters: the yield stress τ_B and the viscosity consistency μ_B. Under steady state and constant temperature and pressure, the relationship between shear stress τ and shear rate γ for Bingham fluids writes:

$$\tau = \tau_B + \mu_B \gamma \tag{4.1}$$

For the purposes of the present study, the velocity from Figure 4.1 is converted into an apparent shear rate ($8u/D$) and the corresponding pressure drop into the wall shear stress ($\tau_w = D\Delta P/\ 4L_p$). The results of this operation is presented in Figure 4.3 together with the best linear correlation of the data.

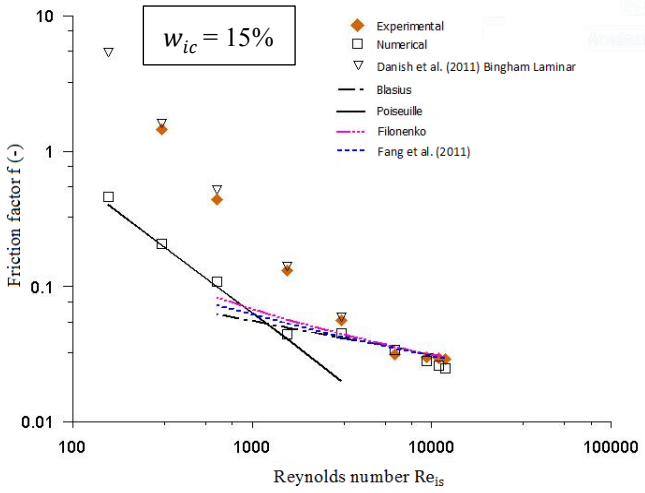

Figure 4.1: Friction factors in a smooth horizontal pipe (ice mass fraction = 15%)

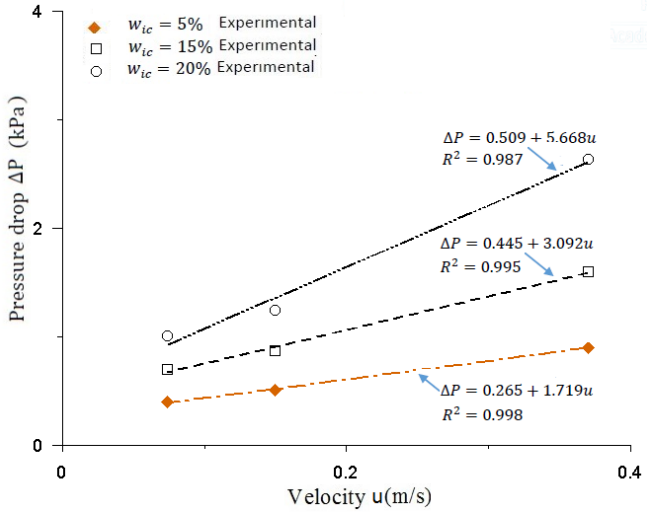

Figure 4.2: Measured pressure loss versus average inlet velocity for three ice mass fractions

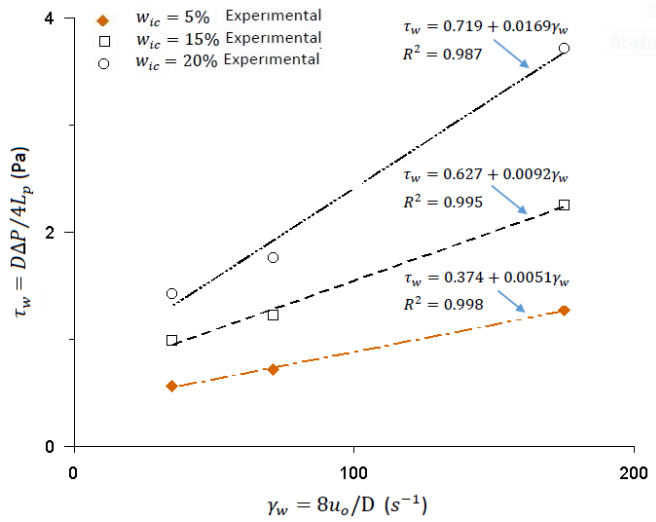

Figure 4.3: Apparent shear stress versus apparent shear rate for three ice mass fractions

From each line in Figure 4.3, one can extract the yield shear stress τ_B from the intercept point and the viscosity consistency μ_B, which is equal to the slope. By applying the curve fitting techniques to these points, one obtains the following expressions for τ_B and μ_B as functions of the ice mass fraction w_{ic} (for ice mass fractions between 5% and 20%):

$$\tau_B = 1.534\, {w_{ic}}^{0.471} \tag{4.2}$$

$$\mu_B = 0.0034\, e^{7.98 w_{ic}} \tag{4.3}$$

Figure 4.4 illustrates the influence of the ice mass fraction on the yield stress and the viscosity consistency. The agreement between the experimental data and the proposed correlations is always very good.

The combination of Equations (4.1), (4.2) and (4.3) provides the general expression of the derived empirical Bingham model in terms of the ice mass fraction (applicable for laminar flow with w_{ic} between 5% and 20%):

$$\tau = 1.534 {w_{ic}}^{0.471} + (0.0034 e^{7.98 w_{ic}})\gamma \tag{4.4}$$

Figure 4.5 illustrates the effect of the ice mass fraction on the relation between the shear stress and the shear rate for the Newtonian and Bingham models. These results reflect the fact that both the yield stress and the viscosity consistency increase with the ice mass fraction as shown in Figure 4.4.

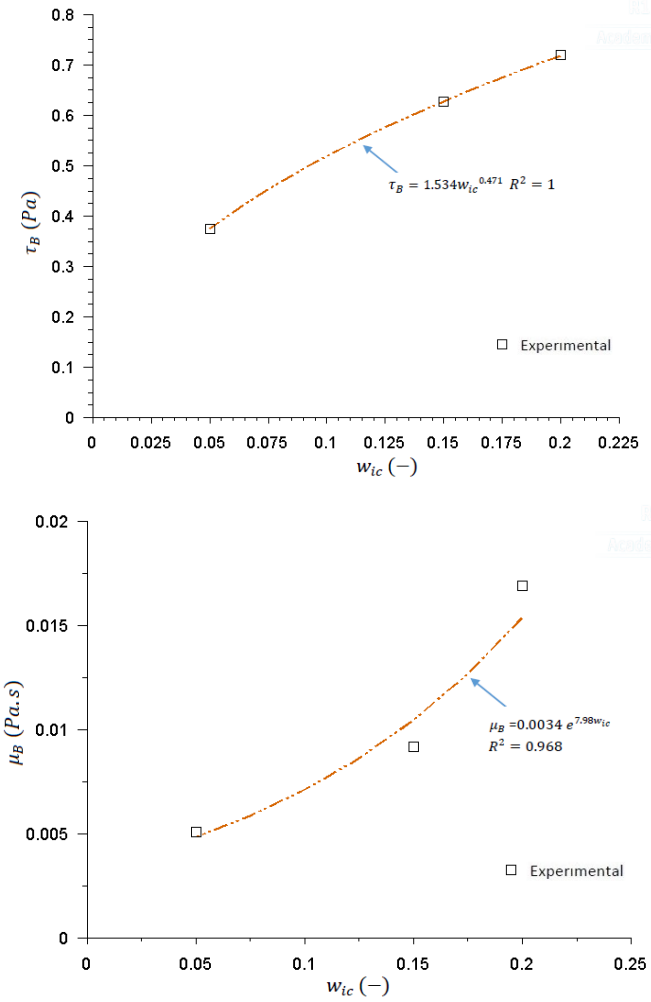

Figure 4.4: Effect of the ice mass fraction on the yield stress and the viscosity consistency

4.3 Validation

Validation is obtained by comparing friction factors derived from the measurements with those predicted using Equation (4.4). For this purpose, one applies the following explicit relation (Danish et al., 2011) for the laminar flow of Bingham fluids in smooth pipes:

$$f = 4K_1 \left\{ \begin{matrix} 1 - 10[K_2/(K_1^4 + 3K_1)]^4 \\ +6[K_2/(K_1^4 + 3K_1)]^3 + K_2/(K_1^4 + 3K_1) \end{matrix} \right\} \quad (4.5)$$

where $K_1 = (16/Re) + (16He/6Re^2)$ and $K_2 = (-16He^2/3Re^8)$. The Reynolds and Hedstrom numbers are calculated using the ice slurry density and the values of τ_B and μ_B from Equations (4.2) and (4.3) respectively.

To ensure that the flow is laminar, this Reynolds number for each combination of measured flow rate (or, equivalently, average velocity) and ice mass fraction is compared with the corresponding critical value obtained from the following relation (Swamee & Aggarwal, 2011), which is valid for $He \leq 10^9$:

$$Re_c = 2100(1 + He/3600)^{0.35} \quad (4.6)$$

Table 4.1 gives the Bingham Reynolds number as a function of the flow mean velocity u_o for different ice mass fractions w_{ic} as well as the corresponding critical Reynolds Re_c and the Hedstrom number *He* for all the flow combinations used in the present study (see Figures 4.1-4.5). It confirms that all these flow combinations are indeed laminar since $Re < Re_c$

It should be noted that these values of the Reynolds number were also used for the evaluation of the friction factors by all of the correlations mentioned in Figure 4.1.

The results of these calculations are shown in Figure 4.1 for w_{ic} = 15% and in Figure 4.6 for w_{ic} = 5% and 20%. The agreement between the experimentally derived values of the friction factor and those calculated by combining equations (4.2), (4.3) and (4.5) is excellent while the predictions of the Newtonian CFD model grossly underestimate the experimental values. In view of these results, one can conclude that Equation (4.4) is valid for the conditions of this study.

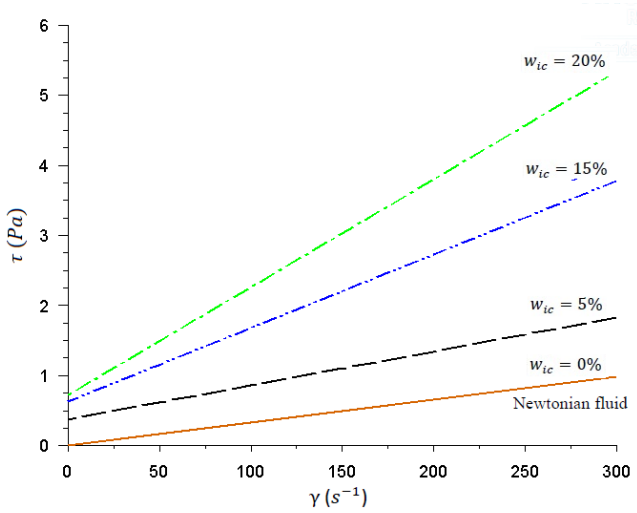

Figure 4.5: Effect of the ice mass fraction on the relation between shear stress and shear rate

Table 4.1: Values of the Bingham Reynolds number

u (m/s)	$w_{ic} = 5\%$ Re_c = 2752 ; He = 4195	w_{ic} = 15% Re_c = 2360 ; He = 1422	w_{ic} = 20% Re_c = 2241 ; He = 732
0.074	248	112	75
0.15	504	226	151
0.37	1242	556	374
0.74	2485	1115	747

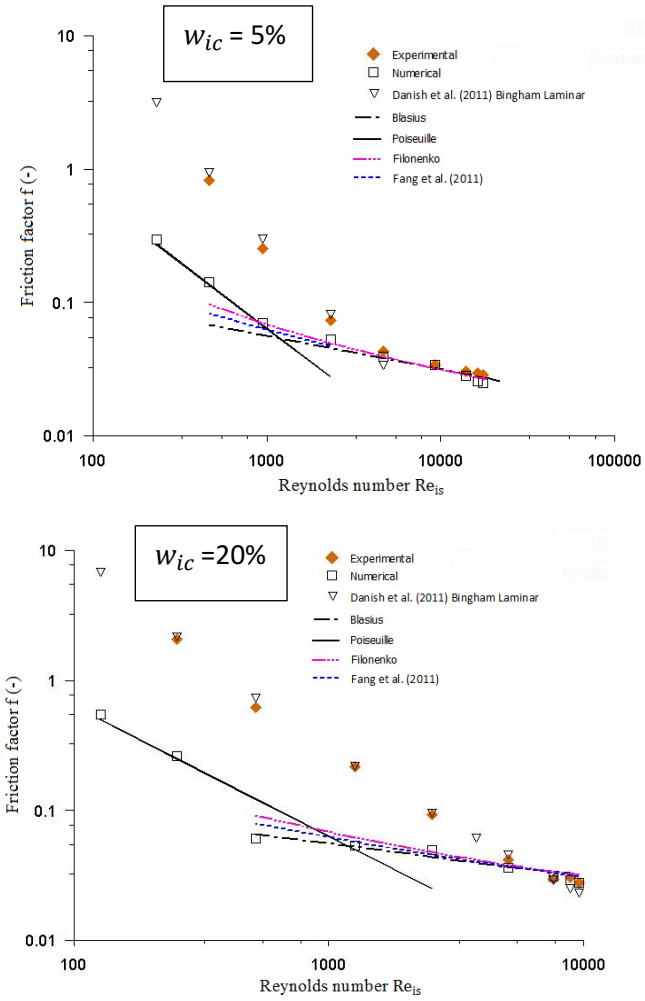

Figure 4.6: Friction factors in a smooth horizontal pipe (ice mass fraction = 5% and 20%)

4.4 Conclusions

Comparisons between friction factors derived from measurements with corresponding values obtained from CFD simulations indicate that the Newtonian behavior is justified for turbulent flows of the polypropylene-glycol slurry under study. For laminar flow a Bingham formulation for the shear stress is developed and produces friction factors in excellent agreement with the experimentally derived values.

Acknowledgments

The authors thank NSERC for its financial support and Natural Resources Canada for making available the instrumented experimental facility at CanmetENERGY in Varennes.

CHAPITRE 5

EXPERIMENTAL AND NUMERICAL INVESTIGATION OF ISOTHERMAL ICE SLURRY FLOW

Auteurs et affiliations :

Landa ONOKOKO : étudiant au doctorat, Université de Sherbrooke, Faculté de Génie, Département de Génie mécanique.

Nicolas GALANIS : professeur, Université de Sherbrooke, Faculté de Génie, Département de Génie Mécanique.

Sébastien PONCET : professeur, Université de Sherbrooke, Faculté de Génie, Département de Génie Mécanique.

Michel POIRIER : CanmetENERGY Natural Ressources Canada, Varennes, Québec, Canada.

Référence : Onokoko, C.L., Poirier, M., Galanis, N., Poncet, S., (2018). Experimental and numerical investigation of isothermal ice slurry flow. International Journal of Thermal Sciences 126, 82-95.

Date d'acceptation **:** Décembre 2017

Titre en français : Etude expérimentale et numérique d'un écoulement isotherme de coulis de glace

RÉSUMÉ

Les caractéristiques d'un écoulement de coulis de glace à base de propylène glycol dans un long tuyau horizontal (L/D ≈ 177) ont été étudiées expérimentalement pour des débits de 1 à 38 kg/min et des fractions de glace de 5% à 24% . La perte de pression, la densité à l'entrée et à la sortie du tube, la température et le débit massique du coulis de glace ont été mesurés et analysés. Un modèle CFD 3D qui considère le coulis de glace comme un fluide Newtonien monophasique ayant des propriétés effectives qui dépendent de la concentration de la glace et de la température est également présenté. Ce modèle inclut la migration de particules de glace induite par cisaillement et flottaison dans l'écoulement. Le modèle a été validé pour des conditions laminaires et turbulentes par les données expérimentales disponibles dans la littérature. Les résultats numériques obtenus sur la chute de pression sont en bon accord avec les données expérimentales issues d'études antérieures. Le modèle proposé a ensuite été utilisé pour établir certaines caractéristiques importantes des écoulements de coulis de glace qui n'ont jamais été obtenues expérimentalement. En particulier, les résultats numériques illustrent la variation axiale et périphérique du coefficient de frottement et expliquent sa variation angulaire par l'analyse des champs de fraction volumique en glace et de vitesse. Les effets des conditions d'entrée sur ces champs sont également illustrés et analysés.

Mots-clés : Tuyau horizontal, fluide monophasique, perte de pression, coefficient de frottement, coulis de glace.

ABSTRACT

The characteristics of propylene glycol ice slurry flow through a long horizontal pipe (L/D ≈177) were investigated experimentally for flow rates between 1 and 38 kg/min and ice fractions of 5%–24% by mass. Pressure losses in the tube, inlet and outlet densities, temperatures and mass flowrates of the ice slurry were measured and analyzed. A 3D CFD model which treats the ice slurry as a Newtonian fluid with effective properties depending on the local ice fraction and includes the shear-induced migration as well as the hindered settling velocity is also presented. It has been validated for laminar and turbulent conditions with data from the literature. The calculated pressure drop is in good agreement with experimental data from the present and previous studies. The proposed model has therefore been used to establish some important ice slurry flow characteristics which have never been obtained experimentally. Notably, the calculated results illustrate the axial and circumferential variation of the friction coefficient and explain its angular variation by analyzing the predicted ice fraction and velocity fields. The effects of the inlet ice fraction on these fields are also illustrated and analyzed.

KEYWORDS: Horizontal pipe, Single-phase fluid, Pressure drop, Friction coefficient, Ice slurry.

5.1 Introduction

Ice slurries are mixtures of small ice particles (typically 0.1–1 mm of diameter) and a carrier liquid (a mixture of water and an additive -such as glycol, alcohol or salt-which lowers the freezing temperature). They offer the possibility of enhanced energy transport density and energy storage due to the combined effects of sensible and latent heat. Applications include comfort cooling of buildings, food processing and the replacement of secondary refrigerants in ice rinks or supermarkets. According to the Handbook on Ice Slurries (Kauffeld, 2005), their thermophysical properties can be derived from linear weighing of the corresponding properties of the ice (which are essentially determined by the temperature) and the carrier liquid (which vary with the temperature and the concentration of the additive).

The rheological behavior of ice slurries is complex. Kitanovski & Poredos (2002) showed that for high average velocities and very low ice concentrations “the ice slurry viscosity is almost independent of velocity as for Newtonian fluids”. On the other hand, ice slurries exhibit a non-Newtonian behavior for ice concentrations exceeding approximately 20% but this threshold value is influenced by parameters such as the size of the ice particles as well as the nature and concentration of the additive (Kauffeld, 2005). Furthermore, separation of the solid ice particles and the carrier liquid increases when the velocity decreases or when the size of the particles and the density of the liquid carrier increase. Under such conditions, ice particles concentrate in the upper side of the tube because their density is smaller than that of the aqueous solution. Thus, various patterns (homogeneous flow, heterogeneous flow, moving bed and stationary bed) are encountered in ice slurry pipe flow which affect the hydrodynamics of the flow and the mechanisms of heat transfer (Ma et Zhang, 2012). In view of this complex situation, research activities in this field are numerous, especially regarding the rheological behavior of ice slurries by pressure drop measurements. Recent published articles include the experimental study by Mellari (2016) who assumed that the monopropylene glycol (MPG) ice slurry follows the Ostwald-de Waele law and obtained correlations for the consistency coefficient and the flow index in terms of the initial MPG concentration and the mass ice concentration. The results confirmed that ice slurries sometimes behave as Newtonian fluids

and other times as non-Newtonian (with a flow index higher or lower than one). Friess et al. (2016) investigated the effect of foreign particles of higher density than ice which can serve as ice forming nuclei. Ideally, this would lead to an increased density of the modified ice particles and would suppress the buoyancy force which leads to the aforementioned non-homogeneous concentration distributions. They reported that it was indeed possible to modify the density of ice particles but that the process was uncontrollable and resulted in sedimentation of the modified ice particles. They concluded that further research is needed in this field using different substances.

Zhang & Shi (2015) investigated numerically the forced convective flow of ice slurries in a horizontal pipe using a 3D Euler-Euler multiphase model based on the kinetic theory of granular flow. The model was validated with experimental data from the literature and used to investigate stratification in isothermal flow and melting of ice for constant wall heat flux. Their results for isothermal flow show that stratification was weakened by the turbulent dispersion force and that therefore the particle concentration was more uniform at higher inlet velocities. In the heated case the results show that the local heat transfer coefficient decreases rapidly in the entrance region as in all forced convection flows. It stays approximately constant in the thermally-developed region and starts increasing after the ice slurry is fully melted. Similar results for laminar and turbulent isothermal flows of ethylene-glycol ice slurries had been reported earlier by two of the present authors (Onokoko et Galanis, 2013) using a simpler single-phase 3D model which treats the ice slurry as a Newtonian fluid with effective local properties depending on the local ice concentration. The predicted axial evolution of the ice concentration and velocity distributions clearly show that laminar results are essentially determined by ice particle movement due to buoyancy and diffusion while turbulence mixing is the controlling parameter for high average velocities. Niezgoda-Zelasko & Zalewski (2006) performed CFD simulations of isothermal ice slurry flow using the single-phase model (Bingham fluid) and multi-phase models (mixture and Eulerian models). They showed that in the laminar region the Bingham and mixture model gave a correct description of momentum transfer. In the turbulent region the best agreement between experimental and numerical

results (for the single-phase and the Eulerian models) was obtained with the RNG k-ε turbulence model and the enhanced wall treatment algorithm. The single-phase model overestimated pressure drops by less than 16%. In the case of the multiphase simulations the introduction of the particle size as a parameter led to agreement better than 10% between the simulations and experiments

The pressure drop due to ice slurry flow is very important for engineering applications and has been investigated extensively, particularly for flow in horizontal tubes. According to Niezgoda-Zelasko & Zalewski (2006), Hagg (2005) and Grozdek et al. (2009a) the pressure drop increases with increasing ice fraction and velocity. On the other hand, Knodel et al. (2000) and Liu et al. (1997) reported a decrease in pressure drop with increasing ice fraction for low values of this parameter. These discrepancies suggest a different behavior of ice slurries for different ice fraction ranges.

In view of this situation the first objective of the present work is to study experimentally the characteristics of isothermal propylene glycol ice slurry flow through a horizontal circular tube. For this purpose, the time evolution of measured temperature, density, and pressure drop as well as the corresponding ice mass fractions are presented and analyzed. Secondly, we wish to further investigate the validity of the proposed single-phase CFD model for ice slurry flow. Hence, its numerical predictions of the velocity and/or ice mass fraction profiles as well as the pressure drop for different flowrates and ice mass fractions are compared to present and previous experimental results. Good agreement is obtained between these sets of data. The model is then used to investigate flow characteristics such as the axial and circumferential distribution of the friction coefficient as well as the effects of the inlet ice fraction on the axial evolution of the velocity and ice fraction fields. The complementarity of experimental and numerical results provides important insights into the flow of isothermal ice slurries.

5.2 Experimental study

5.2.1 Apparatus and procedure

The schematic diagram of the experimental apparatus (designed and built at the CanmetENERGY research center in Varennes, QC, Canada), is shown in Fig. 5.1. Its basic components are an 11 kW refrigeration capacity ice slurry generator (MuellerMaximICE®, Model ORE-3), a measurement loop including the test section and a data acquisition system. An 800 L ice slurry tank separates the ice generator and the measurement loop. It is equipped with a rotary mixer to ensure uniform distribution of the ice particles. The ice slurry is made by mixing water and Dowfrost 50/50 (a commercial product containing water, propylene glycol and corrosion inhibitors). Its measured freezing point is −1.29 °C. The corresponding initial mass fraction of the propylene glycol is 4.24% or 5.35% according to the correlations developed by Renaud-Boivin et al. (2012) and Melinder (2010) respectively; an in-house correlation between the freezing temperature and the propylene glycol mass fraction gives an intermediate value of 4.59%. The test section is a horizontal straight copper pipe with an inner diameter of 0.01692 m and a length of 3.188 m. It is equipped with two pressure taps at a distance of 2.997 m which are connected to a differential pressure transducer. Resistance temperature detectors (RTDs) are installed at the inlet and outlet of the tube and in the ice slurry tank. The mass flowrate and density of the ice slurry are measured before and after the tube with Coriolis flow and density meters. These quantities are measured every 15 s and stored in a monitoring system which also calculates the corresponding ice mass fractions from the in-house correlations. The range and accuracy of measurements are given in Table 5.1. According to the manufacturer of the slurry generator the size of the produced ice crystals ranges from about 150 to 350 μm with an average size of about 200–250 μm. For the numerical part of the present study the ice particles are assumed to be spherical with a diameter equal to 225 μm unless otherwise stated.

Different experiments were carried out by varying the ice slurry flowrate between 1 and 38 kg/min and the ice mass fraction between 5 and 24%. At the beginning of each experiment the slurry generator and the data acquisition system were turned on. The rotary mixer and the test section pump were run continuously to ensure uniform dispersion of ice particles in the tank

and to circulate the slurry through the test section where the pressure difference, the temperature, the density and the flowrate were measured. The ice mass fraction in the circuit and in the tank increased gradually until it reached the desired value at which point the generator was turned off. From then on, the ice mass fraction decreased slowly due to heat gains from the environment.

Table 5.1: Range and accuracy of measurements

Variable	Range	Accuracy
ΔP	0 to 150 kPa	± 0.04 kPa
T	-20 to 20°C	±0.05°C
$\dot{m}$	0 to 41 kgmin^{-1}	±0.1% of reading
ρ	975 to 1030 kgm^{-3}	0.2 to 0.5 kgm^{-3}

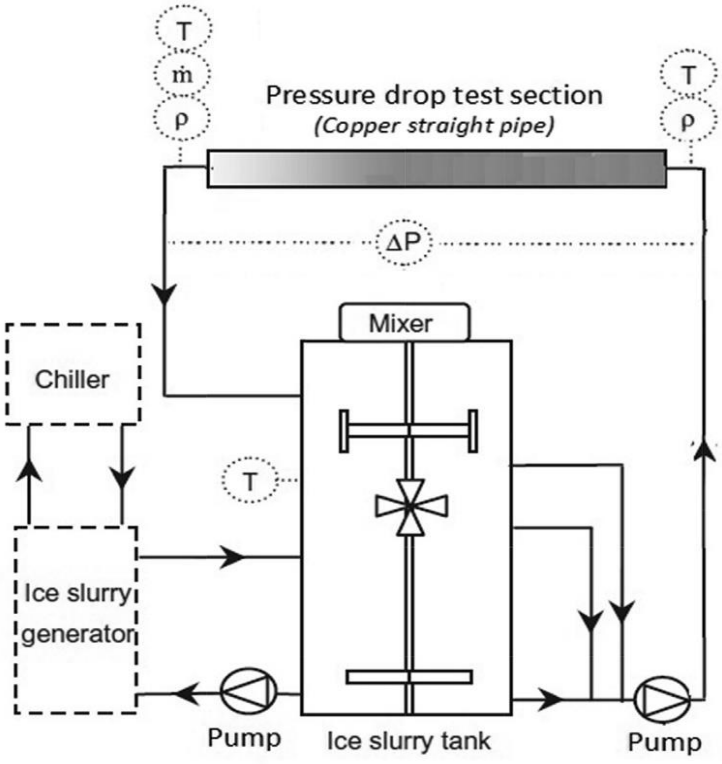

Fig. 5.1. Schematic diagram of experimental apparatus.

5.2.2 Transient results and discussion

Figs. 5.2–5.4 show the transient variations of some important quantities for a typical experiment. Specifically, Fig. 5.2 shows the measured temperatures in the tank as well as at the inlet and outlet of the test section. At any given instant these three values are essentially the same (the difference between the tank and inlet or outlet values is smaller than the uncertainty of the RTD measurements). Therefore, the flow in the test section is, at any given instant, isothermal and heat transfer to the flowing fluid is negligible between the tank and the test section outlet. Fig. 5.3 shows the measured density at the inlet and outlet of the test section as well as a "theoretical density" which was calculated with an in-house correlation using the measured tank temperature. This calculation also yields the corresponding ice mass fraction which is referred to as the "theoretical ice mass fraction" in Fig. 5.3 (the uncertainty of the values for this ice mass fraction is less than 5% based on energy balances involving the measured refrigeration capacity of the ice slurry generator). At any given instant this "theoretical density" is in good agreement with the corresponding values at the inlet and outlet of the pipe since there is no energy input to the fluid between the tank and the test section outlet.

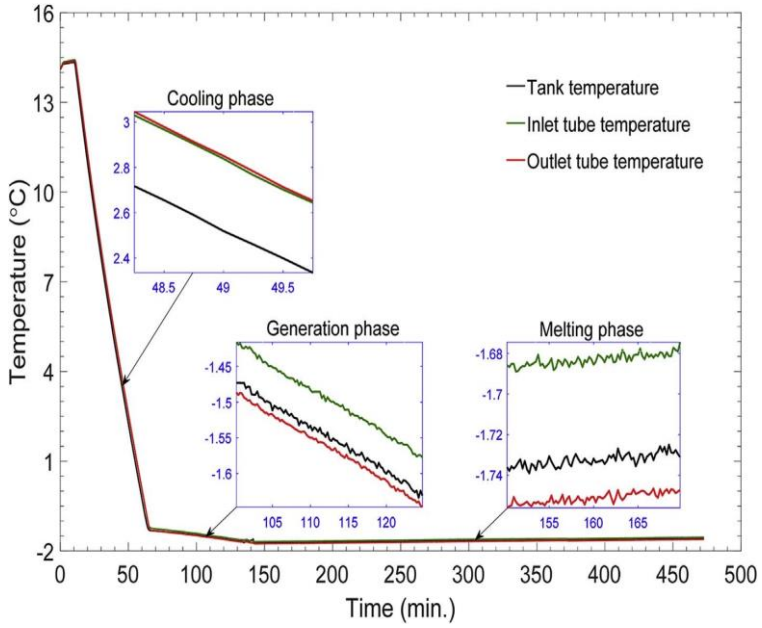

Fig. 5.2. Variation of measured temperature with time.

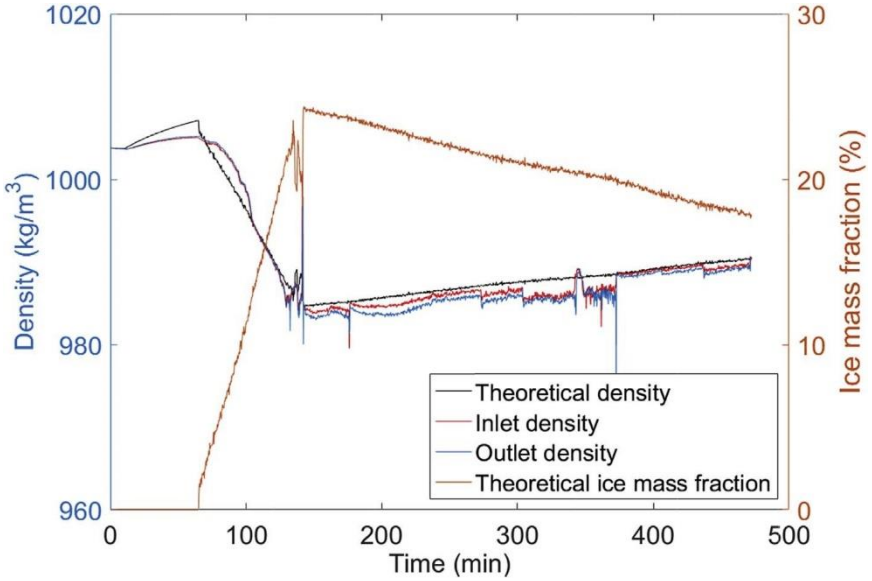

Fig. 5.3. Variation of measured density and calculated ice mass fraction with time.

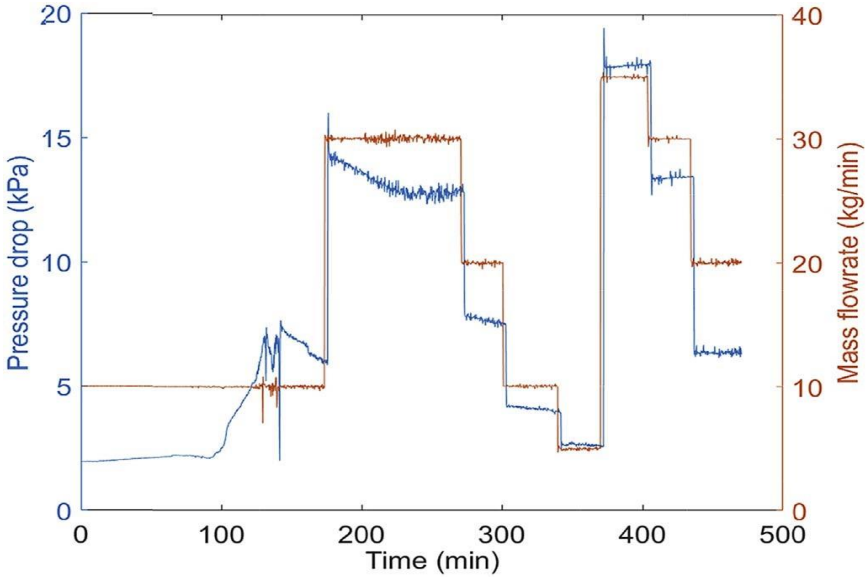

Fig. 5.4. Variation of measured mass flowrate and pressure drop with time.

The important rapid fluctuations depicted in Fig. 5.3 are due to the change in the rotation speed of the tank agitator (at t = 140 min) and to the change in mass flowrate (at t = 176, 274, 303, 342, 372, 406 and 473 min) which is shown in Fig. 5.4.

Figs. 5.2 and 5.3 illustrate the existence of three phases during the initial (t < 176 min) operation with a constant mass flowrate equal to 10 kg/min. The cooling phase takes place from the experiment startup (at t = 0 when the temperature of the mixture was approximately 14 °C) to the moment when the freezing point is reached (at t = 65 min). During this phase the mixture is in the liquid phase, but its density increases slightly (from 1003.8 to 1005.2 kg/m^3) due to the temperature decrease. The corresponding theoretical ice mass fraction is zero while the measured pressure drop is essentially constant at approximately 2 kPa (see Fig. 5.4).

The generation phase starts at t = 65 min when the slope of the temperature curve changes suddenly (see Fig. 5.2). At that instant the ice slurry temperature is −1.29 °C. During this phase the ice mass fraction increases very fast (see Fig. 5.3) and as a consequence the density decreases quickly although not substantially (see Fig. 5.3). The measured and theoretical values of the density become identical from approximately t = 100 min to the end of this second phase which occurs at t = 142 min when the desired ice mass fraction (w_{ic} = 24% for this experiment) is obtained. The increase in ice mass fraction causes an increase of the ice slurry viscosity which in turn results in an important increase of the pressure drop (from approximately 2 kPa to almost 7 kPa, see Fig. 5.4).

As mentioned earlier, when the desired ice mass fraction is obtained the ice generator is turned off. Therefore, from t = 142 min the temperature starts increasing very slowly due to heat transfer from the surroundings and friction. As a result, during this third phase, melting of some ice particles occurs and the ice mass fraction decreases (see Fig. 5.3) while the slurry density increases (see Fig. 5.3). The rate of these variations and the overall property changes are considerably smaller than the corresponding ones occurring during the generation phase. During this melting phase, the ice slurry mass flowrate was changed several times (Fig. 5.4). The difference between measured and theoretical values of the density is greatest between approximately t = 300 min and t = 375 min when the mass flowrate is small (see Fig. 5. 4). The results in Fig. 5.4 indicate that an increase of the mass flowrate causes an increase of the pressure drop (in accordance with the results published by Niezgoda-Zelasko & Zalewski (2006), Hagg (2005) and Grozdek et al. (2009a). Fig. 5.4 also shows that the pressure drop

asymptotically attains a constant value ΔP_∞ after each flowrate change. Since the change of ice mass fraction is extremely small during the time-segments with operation at constant flowrate, it is acceptable to consider that it has a constant value during each of these time-segments. Therefore, the asymptotic value of the pressure drop is a function of the mass flowrate and this essentially constant ice mass fraction. Fig. 5.5 shows this measured asymptotic value of the pressure drop as a function of the average inlet velocity (calculated from the corresponding measured values of the mass flowrate and the inlet density with an estimated uncertainty smaller than 0.5% based on the values in Table 5.1) for three different ice mass fractions in both linear and logarithmic coordinates for better resolution. As in previous studies (Niezgoda-Zelasko & Zalewski, 2006; Shi et al., 2015) these results show that the pressure drop increases with increasing velocity. The rate of increase of ΔP_∞ with u_o is smaller for low velocities than for higher ones. The change in the slope, which is attributed to the transition from laminar to turbulent flow, occurs at approximately 1.25 m s^{-1}, 1.5 m s^{-1} and 1.7 m s^{-1} for w_{ic} = 5%, 15% and 20% respectively. The effect of the Reynolds number on the pressure drop is discussed later, in section 5.4 of the paper. The results of Fig. 5.5 also show that for velocities below approximately 2 m s^{-1} the pressure drop increases significantly with the ice mass fraction. This effect has also been reported by Niezgoda-Zelasko & Zalewski (2006), Hagg (2005) and Grozdek et al. (2009a). On the other hand, for velocities above approximately 2 m s^{-1} the present measurements indicate that for a fixed velocity the effect of ice mass fraction on the pressure drop is very small as reported also by Lee et al. (2002). This behavior can be explained by noticing that for a fixed geometry and a given velocity the pressure drop is proportional to the product of the friction factor and the density. When the ice mass fraction increases the ice slurry density decreases. On the other hand, when the ice fraction increases the Reynolds number decreases (since the density decreases and the viscosity increases) and as a result the friction factor increases. The increase of the friction factor with the ice fraction is more important at low velocities as indicated in Moody's diagram for pure fluids and confirmed for the propylene glycol slurry under study in section 5.5 of the present paper. Therefore, when the ice fraction increases the product of the friction factor and the slurry density increases at low velocities while it is almost constant at high velocities.

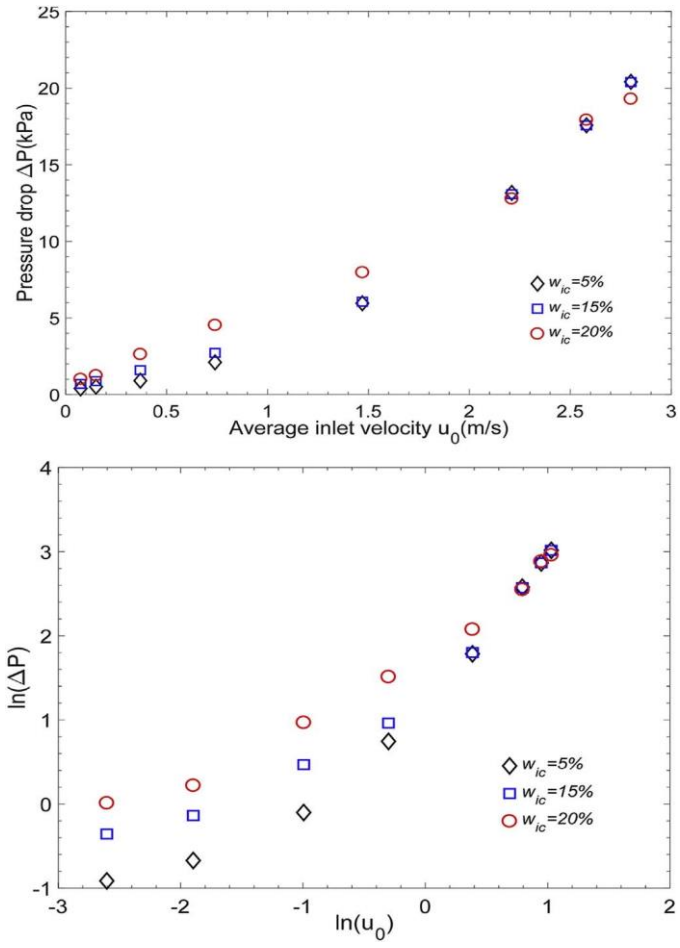

Fig. 5.5. Measured values of pressure drop versus average inlet velocity.

It is reasonable to consider that the slurry temperature is uniform at both the inlet and outlet of the test section and, since at any given instant the measured inlet and outlet temperatures are essentially the same (see Fig. 5.2), the flow is isothermal. It is also probable that the ice mass fraction and slurry density at the test section inlet are also uniform since that position is close to the tank. On the other hand, it is expected that the ice mass fraction and slurry density at the test section outlet are not uniform due to the stratification of ice particles which has been documented both experimentally and numerically (Kauffeld, 2005; Onokoko et Galanis, 2013). Therefore, the density and ice mass fraction values at the test section outlet depicted in Fig. 5.3 should be considered as average values of these properties. Since the measured values of these two properties are at any given instant almost the same at the inlet and outlet

of the test section the corresponding instantaneous average values can be considered as essentially uniform throughout the flow field. Thus, for the present experimental conditions the temperature as well as the average density and ice mass fraction are, to a first approximation, functions of time but independent of the position. Furthermore, since at any instant the measured average values of the density are in fairly good agreement with the corresponding theoretical values they define a state which is close to thermodynamic equilibrium.

5.3 Numerical model

The problem under consideration is the isothermal steady-state flow of an ice slurry in a horizontal straight pipe of constant diameter. The ice slurry is treated as a Newtonian fluid (since, for the numerical calculations, the ice mass fraction does not exceed 20%) with effective local properties depending on the local ice mass fraction. This approach, which was also used successfully in our previous study of ethylene glycol ice slurry flows (Onokoko et Galanis, 2013), is simpler than those adopted by Niezgoda-Zelasko & Zalewski (2006), who treated the ice slurry as a Bingham fluid and Zhang et Shi (2015) who applied a Euler-Euler multiphase model. The origin of the coordinates system is at the center of the pipe inlet. The Z axis coincides with the pipe axis while the X and Y axes are horizontal and vertical respectively.

5.3.1 Laminar flow

The governing equations are derived based on a single-phase approach. The steady state continuity and momentum conservation equations are given respectively by:

$$\frac{\partial}{\partial x_j}\left(\rho_{is} u_j\right) = 0 \tag{5.1}$$

$$\frac{\partial}{\partial x_j}\left(\rho_{is} u_i u_j\right) = -\frac{\partial P}{\partial x_i} + \frac{\partial \tau_{ij}}{\partial x_j} \tag{5.2}$$

The ice particles migration is caused by several mechanisms (shear induced and viscosity-gradients migration as well as particle settling). The species conservation equation is expressed

by the following relation (Onokoko et al., 2013) which is based on the diffusion model proposed by Phillips et al. (1992) for Newtonian fluids and particle fluxes caused by gradients in their volume fraction and in the viscosity (i.e. when the effects of Brownian motion and the inertial lift are negligible):

$$\frac{\partial}{\partial x_j}\{\rho_{is}\emptyset[u_j + \omega_0 h(\emptyset)\delta_{jy}]\} = \frac{\partial}{\partial x_j}\left[\Gamma_\emptyset\left(\frac{\partial \emptyset}{\partial x_j}\right)\right] + S_{\dot{\gamma}} \tag{5.3}$$

where ω_0 is the terminal settling velocity of a single particle in the aqueous solution calculated from Stokes' law and h(Ø) is the hindrance function that represents the reduced mobility of ice particles. Fig. 5.6 shows the variation of h(Ø) with the particles volume fraction. The depicted comparison of experimental data by Buscall et al. (1982) for polystyrene latex (d_p = 3.1μm, settling in 10^{-3} M NaCl aqueous solution) with the correlations of Revay & Higdon (1992), Richardson & Zaki (1954) and Schaflinger (1990) shows that the first correlation is in better agreement with experimental data. We have therefore adopted for h(Ø) the form suggested by Revay and Higdon (1992).

$$h(\emptyset_{ic}) = (1 - \emptyset_{ic})^{6.55}(1 + 3.458\emptyset_{ic}^2 + 8.990\emptyset_{ic}^3) \tag{5.4}$$

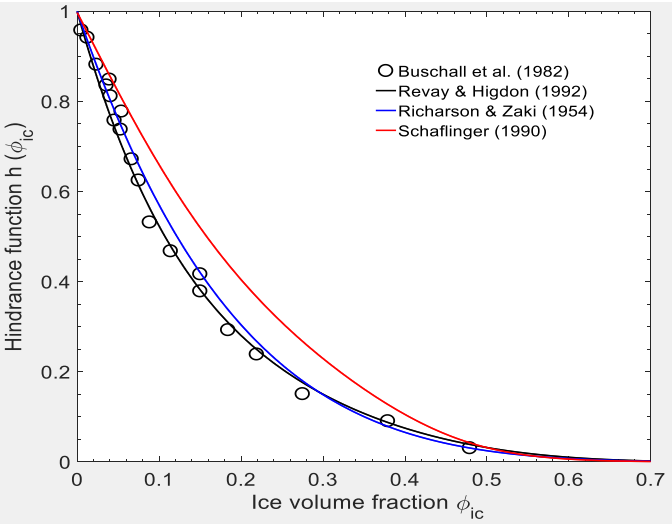

Fig. 5.6. Hindrance function variation with ice volume fraction: (a) Experimental data by Buscall et al. (1982); Correlations of (b) Revay & Higdon (1992), (c) Richardson & Zaki (1954) and (d) Schaflinger (1990).

The diffusive coefficient $\Gamma_{\emptyset}$ and the source term $S_{\dot{\gamma}}$ are given by:

$$\Gamma = \rho_{is} a^2 \emptyset_{ic} \dot{\gamma} \left(K_c + K_\mu \emptyset_{ic} \frac{1}{\mu_{is}} \frac{\partial \mu_{is}}{\partial \emptyset_{ic}} \right) \tag{5.5}$$

$$S_{\dot{\gamma}} = \frac{\partial}{\partial x_j} \left[\rho_{is} K_c a^2 \emptyset_{ic}^2 \left(\frac{\partial \dot{\gamma}}{\partial x_j} \right) \right] \tag{5.6}$$

The values of the coefficients are $K_c = 0.41$ and $K_\mu = 0.62$ as suggested by Phillips et al. (1992).

5.3.2 Turbulent flow

The flow field is calculated by solving the Reynolds-averaged mass and momentum conservation equations expressed by:

$$\frac{\partial (\rho_{is} u_i)}{\partial x_j} = 0 \tag{5.7}$$

$$\frac{\partial (\rho_{is} u_i u_j)}{\partial x_j} = -\frac{\partial P}{\partial x_i} + \frac{\partial \left(\mu_{is} \frac{\partial u_i}{\partial x_j} - \rho_{is} \overline{u_i' u_j'} \right)}{\partial x_j} \tag{5.8}$$

$$-\rho_{is} \overline{u_i' u_j'} = \mu_t \left(\frac{\partial u_i}{\partial x_j} + \frac{\partial u_j}{x_i} \right) - \frac{2}{3} \rho_{is} k \delta_{ij} \tag{5.9}$$

The particle diffusive model proposed by Phillips et al. (1992) is also valid for turbulent conditions according to Bui et al. (2003). Therefore, the species conservation equation which is part of the model is again given by Eq. (5.3). The diffusive coefficient, the source term, the hindrance function and the values of the coefficients are also identical to those for laminar flow.

The presence of ice particles affects the production, dissipation and transport of turbulence. In particular the gradient of the ice mass fraction, which reaches maximum values near the top of the pipe (Onokoko and Galanis (2013), hinders turbulence while turbulent energy is transported by particles motion due to buoyancy and diffusion. The realizable k-ε model with enhanced wall treatment was used in the present study. It was preferred to the standard k-ε

model because it includes an improved equation for the turbulent dissipation and uses a variable coefficient in the expression of the turbulent viscosity. It is appropriate for boundary layers with strong adverse pressure gradients such as those encountered near the inlet in the problem under consideration. The damping influence of stratification on the production of turbulent kinetic energy is expressed as a source term appearing in the transport equation of turbulent kinetic energy k. The expressions of the k and ε equations for the realizable turbulence model used in the present study are in standard form Zhang and Li (2008) and are therefore not reproduced here.

5.3.3 Properties of propylene glycol

The effective properties of ice slurry, such as density and viscosity, are obtained from the relations given in the Handbook on Ice Slurry (Kauffeld, 2005). They involve the volumetric ice fraction, the corresponding properties of ice, and the corresponding properties of the carrier liquid:

$$\rho_{\mathrm{is}} = \emptyset_{ic}\rho_{\mathrm{ic}} + (1 - \emptyset_{ic})\rho_{\mathrm{as}} \tag{5.10}$$

$$\mu_{\mathrm{is}} = \mu_{\mathrm{as}}\left(1 + 2.5\emptyset_{ic} + 10.05{\emptyset_{ic}}^{2} + 0.00273e^{16.6\emptyset_{ic}}\right) \tag{5.11}$$

Relations for the calculation of ice properties are also given in the Handbook on Ice Slurries [1]. In particular:

$$\rho_{\mathrm{ic}} = 917 - 0.13\mathrm{T} \tag{5.12}$$

Properties for different carrier liquids are calculated with the following formulas obtained by polynomial curve-fitting of tabulated data (ASHRAE, 2005):

$$\rho_{\mathrm{as}}(\emptyset_{\mathrm{a}}, \mathrm{T}) = \sum_{\mathrm{i}=0}^{\mathrm{M}} \mathrm{T}^{\mathrm{i}} \sum_{\mathrm{j}=0}^{\mathrm{N}} \mathrm{b_{i,j}} \emptyset_{\mathrm{a}}^{\mathrm{j}} \tag{5.13}$$

$$\mu_{\mathrm{as}}(\emptyset_{\mathrm{a}}, \mathrm{T}) = \sum_{\mathrm{i}=0}^{\mathrm{M}} \mathrm{T}^{\mathrm{i}} \sum_{\mathrm{j}=0}^{\mathrm{N}} \mathrm{b_{i,j}} \emptyset_{\mathrm{a}}^{\mathrm{j}} \tag{5.14}$$

The coefficients $b_{i,j}$ were calculated by Renaud-Boivin et al. (2012). The saturation fraction of additive by volume $\emptyset_a$ is given by the following expression:

$$\emptyset_a = \frac{w_{ao}}{1-w_{ic}} \frac{\rho_{as}}{\rho_a} \tag{5.15}$$

Where w_{ao} is the initial mass fraction of additive and ρ_a the density of propylene-glycol (the term "initial" refers to conditions with temperatures above the freezing point).

5.3.4 Boundary conditions and numerical solution

At the pipe inlet the velocity, the temperature, the mass fraction of the ice particles, the turbulence intensity and the turbulence viscosity ratio are fixed and uniform. The outflow condition is applied at the pipe outlet while the no-slip condition is applied at the pipe wall. Furthermore, the normal particle flux at the wall is set equal to zero.

The coupled differential equations of the model were solved using the commercial software package Ansys-Fluent 15.0 which is based on the finite volume technique. The ice particle conservation equation (Eq. (5.3)) was introduced using the user-defined scalar (UDS) functionality. The domain was divided into 1792917 cells (1688040 hexahedron cells and 1512984 wedge/prism cells). The mesh was generated using Ansys workbench 15.0. A grid independence study has been carried out previously for a pure water flow (Onokoko and Galanis, 2013) and presently for an ice slurry flow at u_0 = 1.48 m/s and w_{ic} = 5%. The chosen mesh was shown to provide grid independent solution for this test case and so has been used for all the other sets of operating conditions. A mesh refinement process near the wall was performed to improve the performance of the wall function and to fulfill the requirement value of y^+ (≈1) for all test cases. The SIMPLE algorithm was employed to resolve the pressure-velocity coupling in the momentum equation. The QUICK scheme was used to approximate the convection term. The numerical calculations were considered as convergent when all the residual was lower than 1.0×10^{-4}.

5.3.5 Model validation with data from previous studies

A partial validation of the model was presented in an earlier paper (Onokoko and Galanis, 2013). Centerline velocities at different axial positions for the laminar flow of water were compared with corresponding values from two published articles. The results were in excellent agreement with the literature. Furthermore, the predicted laminar velocity profile for a slurry with solid polypropylene spheres was in good agreement with corresponding published experimental results by Reghem (2002).

Further comparisons of calculated and published results have now been performed to complement the validation of the proposed model. Thus, the calculated evolution of the velocity profile for laminar flow of pure water is in excellent agreement at all axial positions with the corresponding results by Yu & Ozoe (2001). In particular the present model correctly predicts the overshoot taking place close to the wall near the pipe inlet (these comparisons are not shown here). Furthermore, the calculated fully-developed turbulent velocity profile for flow of water is in very good agreement with both experimental results and the 1/7th power law velocity profile established from pipe flow data. Fig. 5.7 compares the calculated turbulent velocity and ice mass fraction profiles for flow of an ice slurry ($\emptyset_{ic}$ = 10%) with ethylene glycol as the carrier fluid (w_{ao} = 6.3%) with corresponding profiles by Wang et al. (2013a). Again, the agreement between the calculated and measured values is quite satisfactory. As the flow is almost homogeneous, the mixture model of Wang et al. (2013a) and the present results for a single-phase fluid are almost identical. It confirms that the Philipps et al.'s model has been correctly implemented in the ANSYS Fluent flow solver. Finally, Fig. 5.8 compares calculated values of the pressure drop for the flow of an ethanol ice slurry in a 9mm diameter pipe with corresponding measurements by Grozdek et al. (2009a). For the numerical simulation it was assumed that the average ice particle diameter was 100 μm and the properties of the ethanol aqueous solution with w_a = 10.3% were calculated with correlations used by Ben Lakhdar (1998). The agreement between numerical predictions and experimental values is good for all ice mass fractions and inlet velocities included in this figure which encompass both laminar and turbulent flow regimes. This agreement is probably due to the fact that these experimental

conditions satisfy the assumptions made in the formulation of the present model. It should be emphasized that there is no evidence in the literature about the nonNewtonian behavior of the slurry and the multiphase character of the flow for this particular set of operating conditions. In fact, examples to the contrary exist: thus, Kumano et al. (2013) showed that ethanol based slurries for w_{ao} = 10.3% exhibit a Newtonian behavior for w_{ic} up to 20% for Re_{is} = 4500 and D = 7.5 mm, although this is not necessarily true for other pipe diameters or Reynolds numbers.

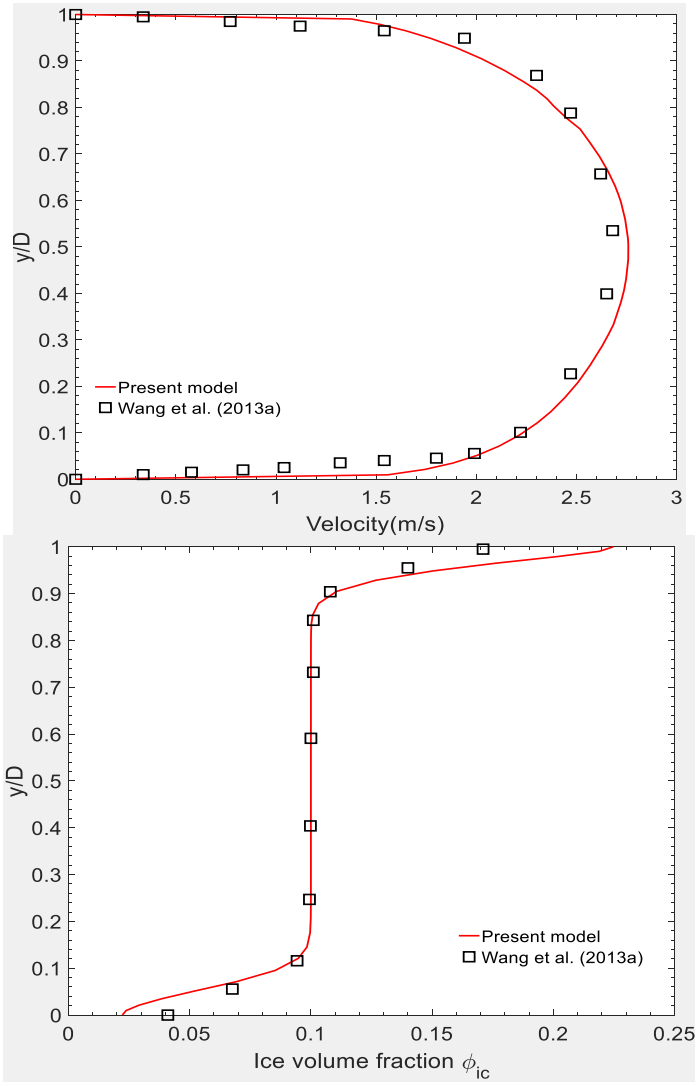

Fig. 5.7. Comparison of predicted and experimental velocity and ice mass fraction profiles for an ethylene glycol ice slurry (D = 2.4 cm, w_{ao} = 6.5%, u_o = 2.25 m s^{-1}, $\emptyset_{ic}$ = 10%).

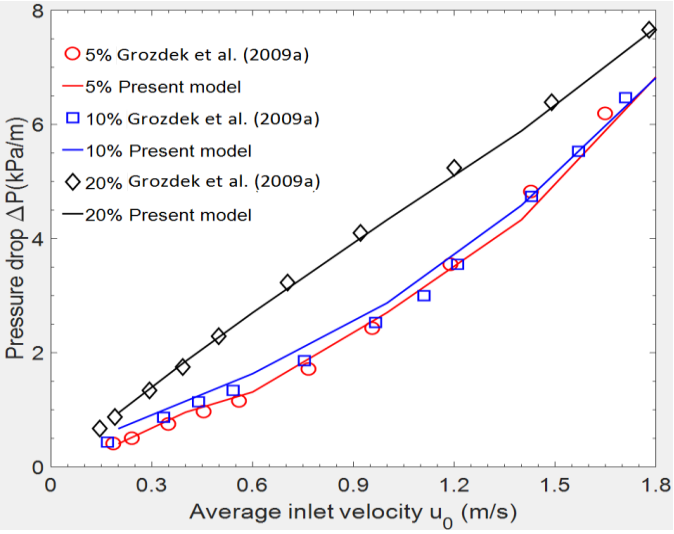

Fig. 5.8. Comparison of predicted and experimental pressure drops for an ethanol ice slurry (D = 9 mm, w_{ao} = 10.3%)

In view of these successful comparisons which include laminar and turbulent flows for water and different slurries we conclude that the proposed single-phase model based on the particles diffusion model by Phillips et al. (1992) is valid despite its relative simplicity compared to the two-phase modeling used in other studies (Zhang and Shi, 2015; Niezgoda-Zelasko and Zalewski, 2006). It can therefore be used to analyze the behavior of isothermal ice-slurry pipe for conditions (geometries, nature and concentration of additive, ice fractions and velocities or mass flow rates) similar to those used for its validation.

5.4 Steady-state pressure drop ΔP_∞

The effects of inlet ice mass fraction and average inlet velocity on the measured time-independent pressure drop attained at the end of each time-segment with constant flowrate (see Fig. 5.4) were presented and analyzed in the last paragraph of section 5.2.2. Here the measured values of this pressure drop are compared with the corresponding predictions of the proposed CFD model and with those obtained from different published correlations.

Fig. 5.9 compares the measured pressure drop over the distance between the two pressure taps (L = 2.997 m) with the corresponding numerical predictions of the present CFD model. The

agreement between the two sets of values is good for each of the three ice fractions under consideration for values of ΔP_∞ higher than 5 kPa while for values of ΔP_∞ lower than 2 kPa it is not as close as in the case of the ethanol ice slurry (see Fig. 5.8). In the region of low pressure drops the present measured values are considerably higher than the corresponding predictions of the proposed numerical model. Since low pressure drops are associated with low velocities (see Figs. 5.5 and 5.8) this difference is, at least partly, due to the fact that at low velocities the fluid is no longer homogeneous; under such conditions one can expect a stratified flow with a bed of ice particles mostly confined at the top of the pipe and higher pressure drops than those predicted for a homogeneous fluid. Other possible reasons for the observed differences in the region of low pressure drops (or, equivalently, low velocities) are the possibility that the fluid may not be Newtonian and/or the effect of the inlet loss which is not identical in the experimental setup and in the numerical model since the inlet velocity profile during the experiments is unknown.

Fig. 5.10 presents the values of ΔP_∞ predicted by the CFD model versus the ice slurry Reynolds number Re_{is}, which is calculated using the inlet conditions ($Re_{is} = \rho_{is} u_o D/\mu_{is}$). It should be noted that, for a fixed velocity, this Reynolds number decreases as the ice mass fraction increases since the slurry density and viscosity depend on the ice mass fraction. This figure also

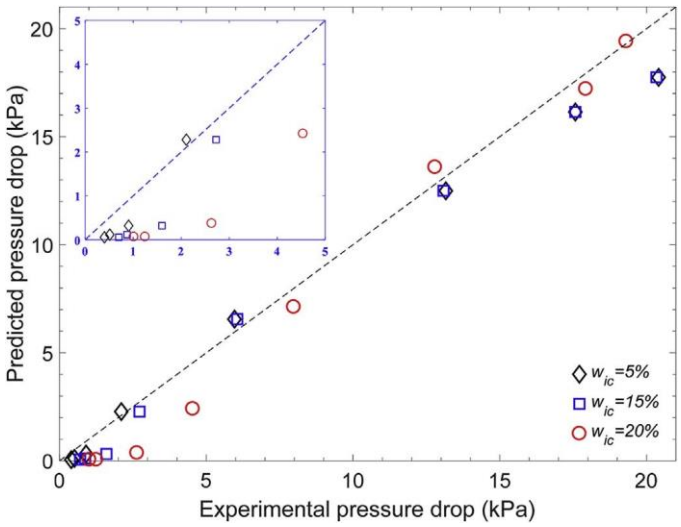

Fig. 5.9. Comparison of experimental and numerical pressure drop for flow of propylene glycol (w_{ao} = 4.24%) ice slurry over a length of 2.997 m

compares the numerically predicted ΔP_∞ with corresponding reference values calculated from:

$$\Delta P = f\,(L/D)\,(0.5\,\rho_{is}\,u_o^2) \qquad (5.16)$$

With the friction coefficient given by the Poiseuille relation ($f = 64/\,Re_{is}$) for laminar flow and by the Blasius correlation ($f = 0.316\,Re_{is}^{-0.25}$) for turbulent flow. The variation of ΔP_∞ with Re_{is} depicted in Fig. 5.10 follows the trend of the reference curves and its values are in practically all cases slightly higher than the corresponding reference values. A systematic exception to this occurs for Reynolds numbers between approximately 2000 and 3500: in this range the CFD prediction of the pressure drop for each of the three ice fractions under consideration is between the two corresponding reference results obtained from the Poiseuille and Blasius relations. This is due to the transition from laminar to turbulent conditions for which the Poiseuille and Blasius correlations respectively under-estimate and over-estimate the friction coefficient.

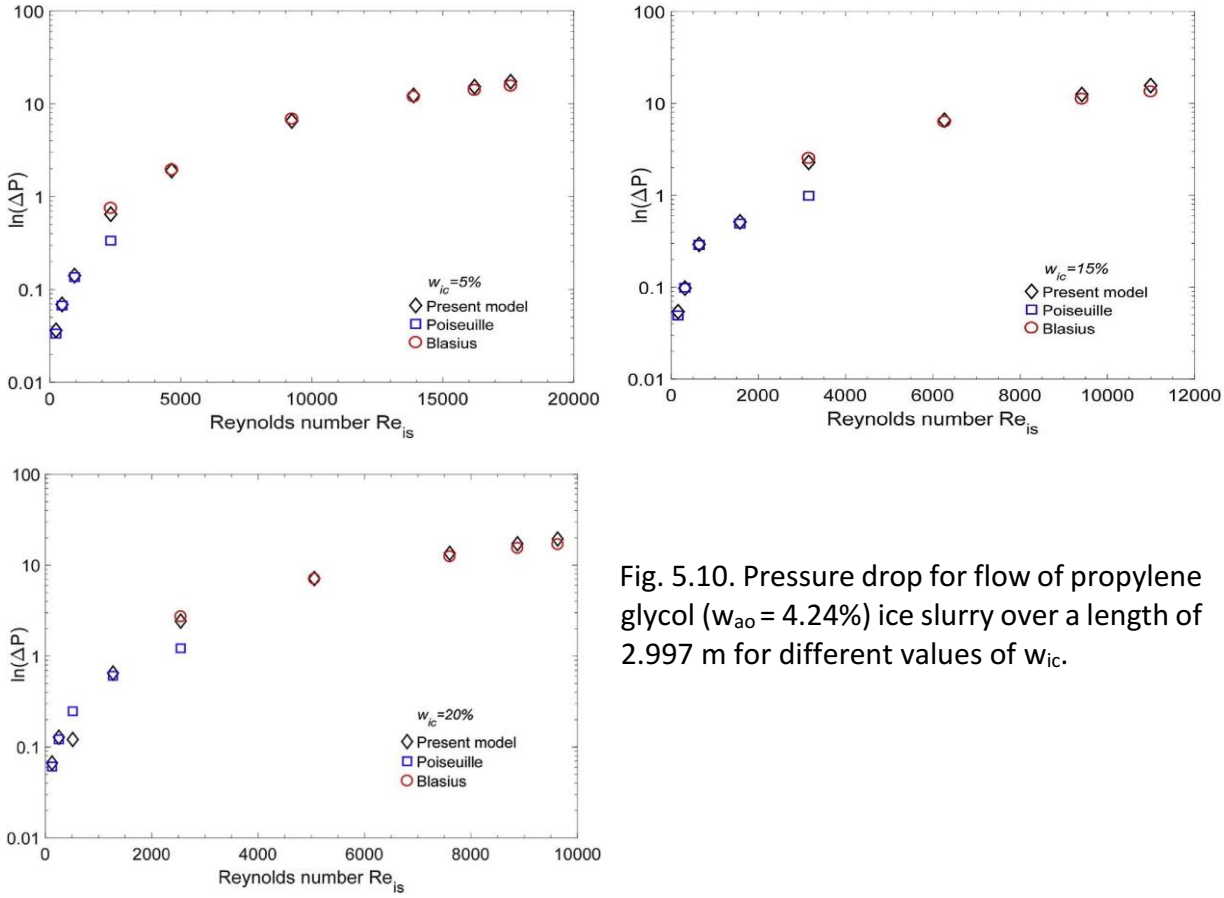

Fig. 5.10. Pressure drop for flow of propylene glycol (w_{ao} = 4.24%) ice slurry over a length of 2.997 m for different values of w_{ic}.

5.5 Flow field analysis

In this section the validated CFD model is used to provide details of the propylene glycol ice slurry flow which could not be obtained with the experimental apparatus and procedure described in section 5.2.1. The results presented here focus on the effects of the inlet velocity on the axial development of the velocity, ice mass fraction and friction coefficient distributions. They complement those in Onokoko and Galanis (2013) which focused on the effects of the inlet ice concentration on the flow of ethylene glycol ice slurries.

Two series of simulations were carried out with w_{ao} = 4.24%, $\emptyset_{ic}$ = 5% and different inlet velocities. The velocity is chosen so that the corresponding Reynolds number Re_{is} is clearly in the laminar or turbulent regime. Specifically, Re_{is} is always lower than 1000 for the first series and always higher than 4500 for the second one. For these simulations the length of the pipe is assumed to be 3.5 m (i.e. greater than that of the experimental test section) to approach fully developed conditions at its outlet but the pipe diameter is equal to that of the experimental test section (D = 0.01692 m).

5.5.1 Laminar flow regime

Fig. 5.11 shows the axial evolution of the ice volume fraction distribution along the vertical diameter of the pipe for average inlet velocities equal to 0.074 m s^{-1} (Re_{is} = 465) and 0.148 m s^{-1} (Re_{is} = 930). Close to the pipe inlet the volume fraction profile is uniform as per the imposed inlet condition. As the fluid moves downstream, the ice particles whose density is smaller than that of the liquid mixture rise towards the top of the pipe under the effect of buoyancy. As a result, the ice volume fraction increases in the upper part of the pipe and it decreases in its lower part. The ensuing concentration gradient creates a downwards flux of ice particles which eventually becomes equal to the upward one sustained by buoyancy. Consequently, the ice fraction profile reaches a form which is independent of the axial position as illustrated by the fact that for u_o = 0.074 m s^{-1} the profiles at Z = 2.5 m and Z = 3.49 m are identical. Therefore, in this case the concentration development length is smaller than 2.5 m. On the other hand,

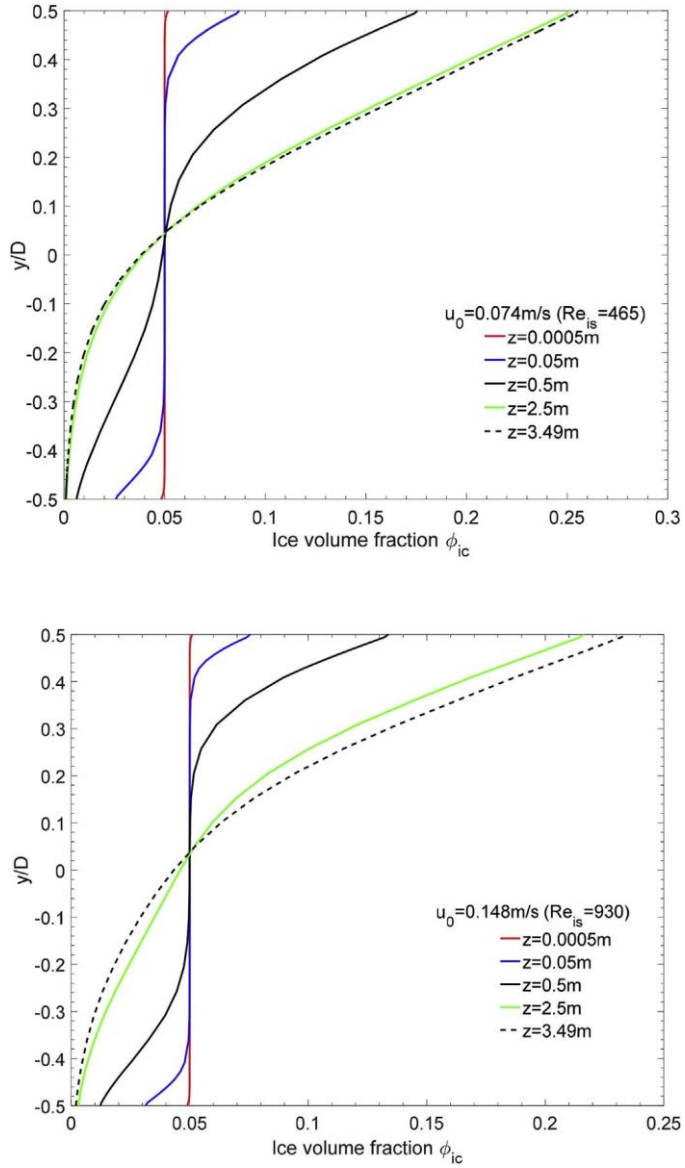

Fig. 5.11. Axial evolution of the ice volume fraction profile along the vertical pipe diameter for laminar flow of propylene glycol ice slurry (w_{ao} = 4.24%, $\emptyset_{ic}$ = 5%).

for u_o = 0.148 m s^{-1}, the profiles at these two axial positions are still somewhat different indicating that in this case the concentration development length is larger than 3.5 m. At Z = 3.49 m the predicted difference between the maximum and minimum volume fractions is smaller in the case of the higher velocity as in Kitanovski and A. Poredos (2002). Furthermore, at this axial position, the ice volume fraction at the bottom of the pipe is zero for the higher velocity. Finally, it should be recognized that, at any point in the region with important

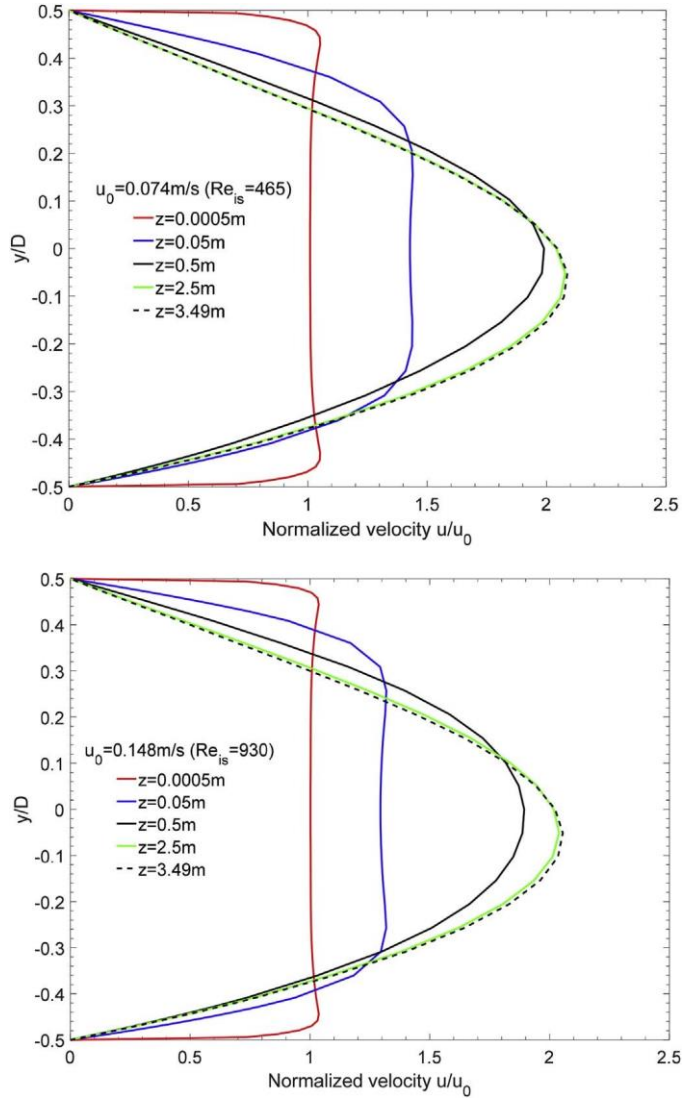

Fig. 5.12. Axial evolution of the velocity profile along the vertical pipe diameter for laminar flow of propylene glycol ice slurry (w_{ao} = 4.24%, $Ø_{ic}$ = 5%)

variations of the ice fraction, the slurry is not in thermodynamic equilibrium; if this was the case, the slurry temperature would have been non-uniform, a situation contrary to both the experimental results and the assumptions of the CFD model.

Fig. 5.12 shows the corresponding profiles of the normalized axial velocity which also evolve with the distance from the inlet. Near the inlet (Z = 0.0005 m) we observe the well-known overshoot phenomenon caused by the rapid development of the boundary layer. Further downstream the velocity profiles are not symmetrical with respect to the pipe axis. This is due

to the influence of the ice fraction distribution on the viscosity of the slurry. Thus, in the lower part of the pipe where the ice fraction is small the viscosity decreases and therefore the velocity increases. On the other hand, in the upper part of the pipe where the ice fraction is high, the viscosity increases and therefore the velocity decreases. As a result, as Z increases the position of the maximum velocity moves downwards. This is clearly illustrated in the case of u_o = 0.148 m s^{-1} by the profiles at Z ≥ 0.5 m. Therefore, the gradient of the velocity at the wall is higher at the bottom of the pipe than at the top. We also note that for both inlet velocities the profiles at Z = 2.5 m and Z = 3.49 m are identical. Therefore, for both cases the hydrodynamic development length is smaller than 2.5 m. The value of the maximum normalized velocity is slightly higher in the case with u_o = 0.148 m s^{-1} and its position is lower than for u_o = 0.074 m s^{-1}. In order to test the validity and precision of these results we calculated the average volume fraction of the ice particles for different cross sections normal to the pipe axis. This quantity was obtained by first integrating the product of the local ice fraction (function of X and Y) and the local mass flowrate (also a function of X and Y) over the circular cross section; this product was then divided by the mass flowrate of the ice slurry which is of course independent of the axial position.

The comparison of the calculated values of the average ice fraction shows that this quantity is essentially independent of the axial position (see Table 5.2). This result was of course anticipated since the flow under consideration takes place without heat transfer and therefore the quantity of ice transported downstream should not change. The fact that the numerical results satisfy this condition to within 0.1% in the worst case (occurring at Z = 3.49 m for u_o =

Table 5.2: Axial evolution of the calculated average ice volume fraction for laminar flow with $\emptyset_{ic}$ = 5% at the inlet.

Axial position Z (m)	0.0	0.076	0.102	0.701	1.300	1.900	2.499	2.883	2.997	3.49
$\emptyset_{ic}$ (%) for u_o = 0.074 m.s^{-1}	5.0	5.0	5.0	4.999	4.998	4.998	4.997	4.997	4.997	4.997
$\emptyset_{ic}$ (%) for u_o = 0.148 m.s^{-1}	5.0	5.0	5.	4.999	4.998	4.997	4.996	4.996	4.995	4.995

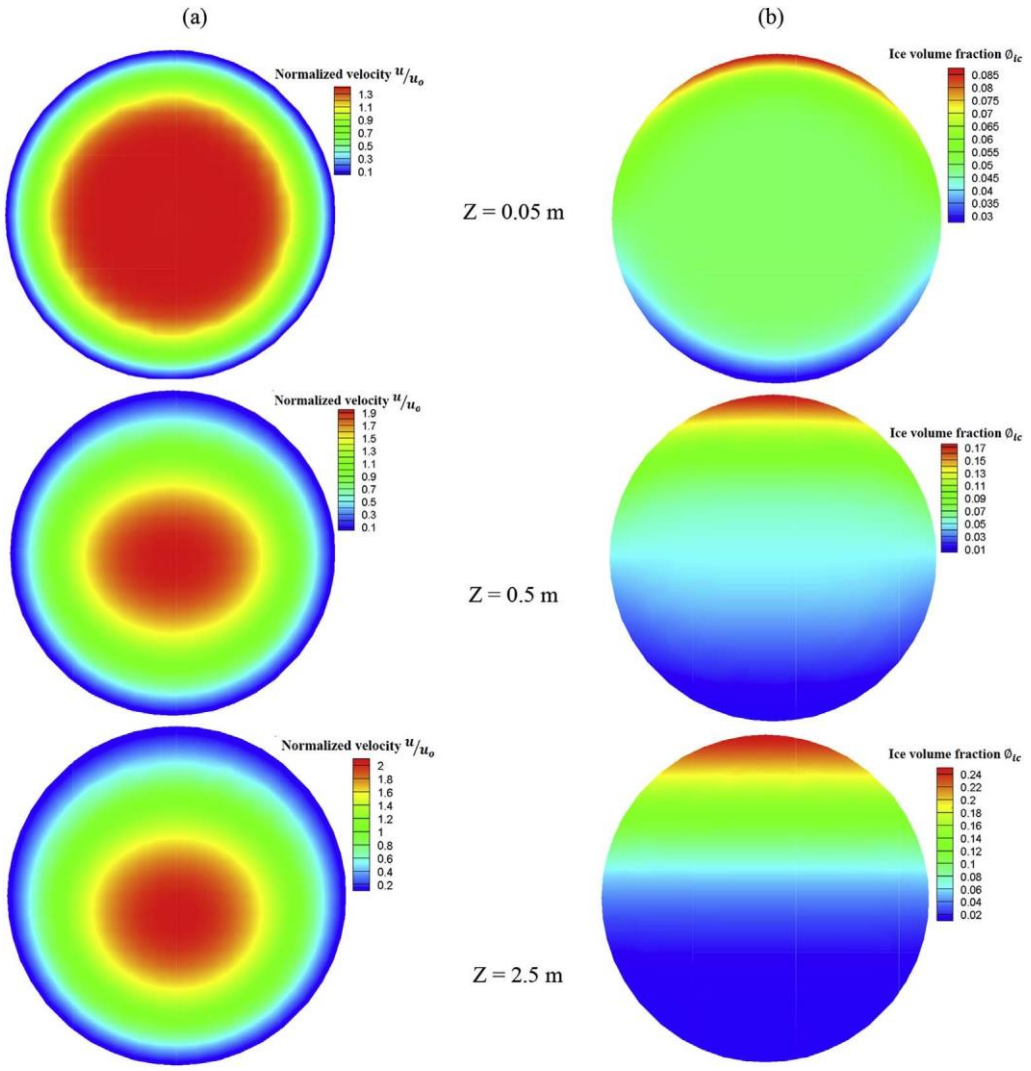

Fig. 5.13. Distributions of (a) normalized velocity and (b) ice volume fraction at different axial positions for laminar flow of propylene glycol ice slurry (wao = 4.24%, Øic = 5%, uo = 0.074 m s−1, Reis = 465).

0.148 m s^{-1}) offers further proof that the model and its numerical solution are reliable and precise.

Fig. 5.13 illustrates the velocity magnitude and ice volume fraction distributions at some selected axial positions for u_o = 0.074 m s^{-1} (Re_{is} = 465). It shows that the velocity field changes earlier than the ice fraction. It also indicates that both distributions are symmetrical with respect to the vertical diameter, a fact which was confirmed by comparing predicted values of

both variables at such symmetrical positions. Furthermore, the velocity distributions show that its gradient at the wall varies all along the circumference from a high value at the bottom to a low value at the top (see Fig. 5.12). This observation suggests that the wall shear stress and the local friction coefficient which depend on the axial position may also vary along the circumference. This is confirmed by the results of Fig. 5.14 which shows the axial variation of the local friction coefficient at the top and bottom of the pipe as well as its circumferential variation at Z = 0.5 m. As is the case for the flow of any fluid, the friction coefficient for Re_{is} = 930 is everywhere smaller than the corresponding value for Re_{is} = 465. The circumferential distributions are symmetrical with respect to the vertical diameter.

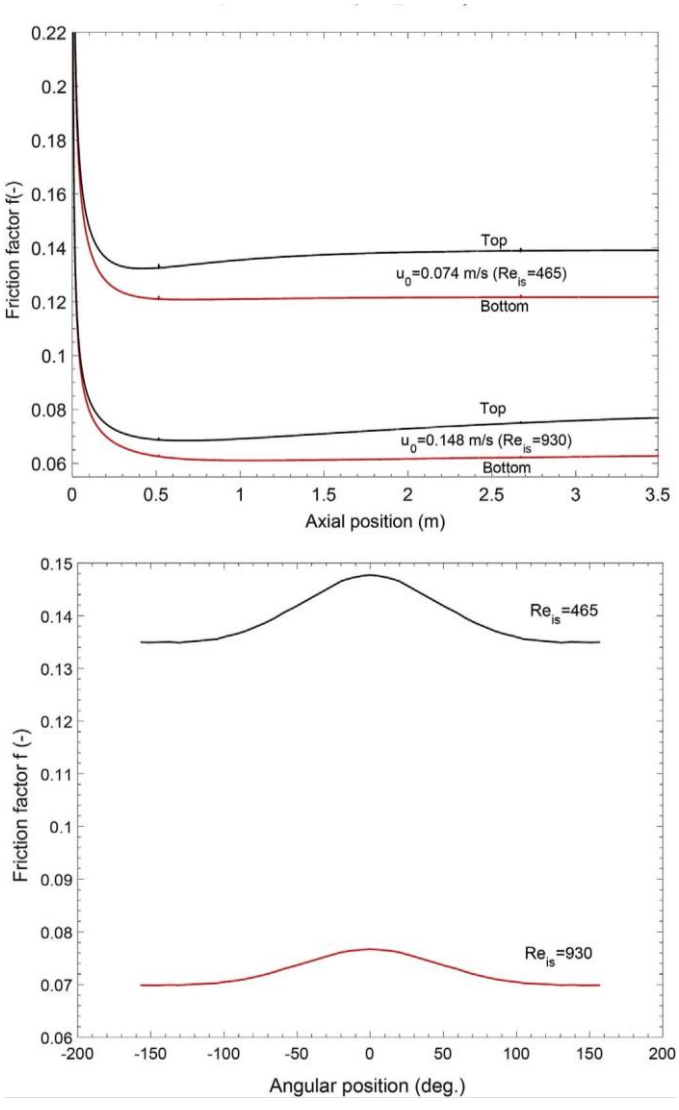

Fig. 5.14. Axial evolution and circumferential variation (at Z = 0.5 m) of the friction coefficient for laminar flow of propylene glycol ice slurry (w_{ao} = 4.24%, $\emptyset_{ic}$ = 5%).

The maximum friction coefficient is always at the top of the pipe but the minimum does not always occur at the bottom as in the presented case. Additional results not included here for lack of space, show that, for example, in the case u_o = 0.148 m s^{-1} (Re_{is} = 930) the minimum friction coefficient at Z = 3.49 m occurs at an angle of approximately 100°, that is just below the horizontal diameter. The dependence of the friction coefficient on u_o and Z can be explained from its following expression:

$$f = 8\,\tau_w / (\rho_{is}\,u_o^2) = [8 / (\rho_{is}\,u_o^2)]\,[\mu_{is}\,(\partial u/\partial r)_w] \qquad (5.17)$$

The derivative of the velocity and the local density (which depends on the ice fraction) vary monotonically along the pipe circumference (from a maximum at the bottom to a minimum at the top) while the local viscosity (which depends on the ice fraction) is minimum at the bottom and maximum at the top. Therefore, the behavior of the friction coefficient is determined by the velocity and ice fraction distributions which as shown in Figs. 5.11 and 5.12 depend on u_o and Z. Fig. 5.14 also shows that at any axial position the difference between the maximum and minimum values of the friction coefficient is higher for the lower of the two Reynolds numbers under consideration. For both velocities under consideration the friction factor for fully developed flow of a homogeneous fluid (f = 64/Re) is between the corresponding values shown in Fig. 5.14. Results analogous to those for the ice fraction depicted in Figs. 5.11 and 5.13 and Table 5.2 were also obtained for the slurry density but are not shown here for the sake of brevity. They indicate that at any given axial position the local density field is symmetrical with respect to the vertical diameter but not symmetrical with respect to the horizontal one. Its maximum value occurs at the bottom of the pipe since the corresponding ice fraction is the lowest and depends on the axial position. On the other hand, the average density for any cross-section perpendicular to the pipe axis is independent of the axial position. The fact that the average values of the ice fraction and of the slurry density are independent of the axial position is also consistent with the experimental results presented in section 5.2.2 which showed that their measured values at the inlet and outlet of the test section are essentially the same. This

observation validates the interpretation of these measured values as being average values of the corresponding quantities.

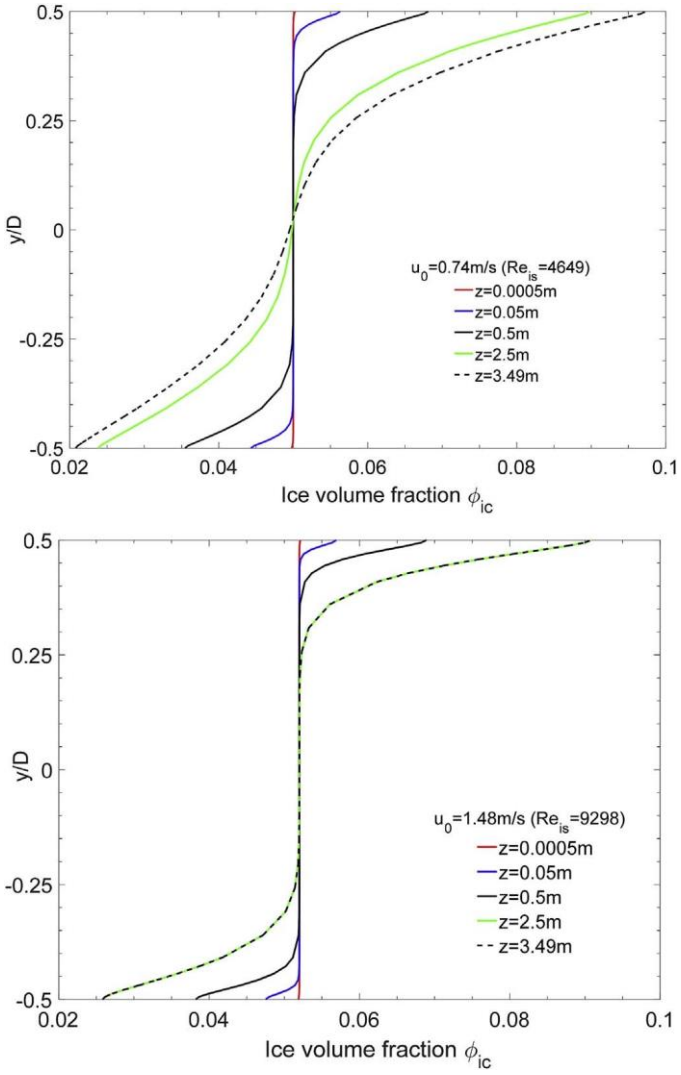

Fig. 5.15. Axial evolution of the ice volume fraction profile along the vertical pipe diameter for turbulent flow of propylene glycol ice slurry (w_{ao} = 4.24%, $\emptyset_{ic}$ = 5%)

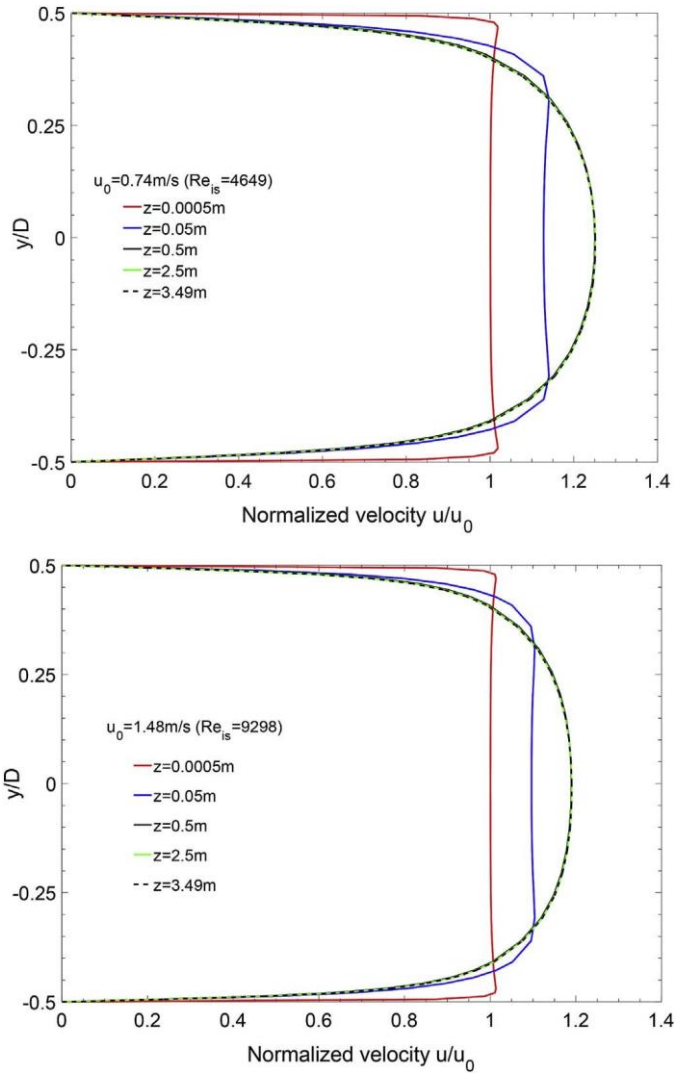

Fig. 5.16. Axial evolution of the velocity profile along the vertical pipe diameter for turbulent flow of propylene glycol ice slurry (w_{ao} = 4.24%, $\emptyset_{ic}$ = 5%)

5.5.2 Turbulent flow regime

Fig. 5.15 shows the axial evolution of the ice volume fraction distribution along the vertical diameter of the pipe for average inlet velocities equal to 0.74 m s^{-1} (Re_{is} = 4649) and 1.47 m s^{-1} (Re_{is} = 9298). Buoyancy and diffusion caused by concentration gradients are again responsible for creating non-uniform ice distributions which in both cases tend towards a fully developed condition. These results as well as those of Fig. 5.11 confirm the validity of the statement in the last paragraph of section 5.2.2 which postulated such a non-uniformity. The present

profiles are however very different from those for laminar flow in Fig. 5.11. Thus, the difference between the maximum and minimum ice fractions is in the present case 0.09 and essentially independent of u_o while in the case of laminar flow it was 0.24 for $u_o = 0.148$ m s^{-1} and 0.14 for $u_o = 0.074$ m s^{-1}. Contrary to the laminar case with $u_o = 0.148$ m s^{-1} the ice fraction at the bottom of the pipe does not become equal to zero in any of the two cases in Fig. 5.15. In the case of the higher of the two Reynolds numbers in Fig. 5.15 we note that in the developed region the ice fraction remains equal to its inlet value over approximately half of the diameter. A similar profile was obtained experimentally by Wang et al. (2013a) for an ethylene glycol slurry (see Fig. 5.7). We conclude that turbulence diminishes the effects of buoyancy and diffusion and therefore reduces the range of the ice fraction values in cross-sections normal to the pipe axis.

Fig. 5.16 shows the corresponding axial evolution of the velocity profiles. The overshoot is again observed near the pipe inlet but from approximately Z = 0.5 m the profiles for both inlet velocities are independent of the axial position. Thus, the hydrodynamic development length is quite short compared with its value for the laminar cases illustrated in Fig. 5.12. In the present case it is also essentially independent of the inlet velocity. The hydrodynamically developed profiles are quite similar to each other and to the experimental one in Fig. 5.7. The most significant differences between the turbulent and laminar velocity profiles are those regarding the maximum velocity. In the present case it occurs only slightly below the pipe axis and is hardly influenced by the inlet velocity while in the laminar case its position is clearly lower and its distance from the pipe axis increases with u_o. Furthermore, the maximum normalized velocity which is greater than 2 in the laminar case (Fig. 5.12) is just 1.4 for $u_o = 0.74$ m s^{-1} and approximately 1.3 for $u_o = 1.48$ m s^{-1}. Therefore, these velocity profiles exhibit the same properties as those of simple fluids such as pure water. We conclude that the presence of the ice with an inlet volume fraction of 5% has very little influence on the velocity field which is essentially determined by the level of turbulence and the average velocity. This is attributed to the fact that the presence of ice particles influences the molecular viscosity which is small compared to the turbulent viscosity.

Table 5.3 shows the corresponding average volume fraction of the ice particles at different axial positions calculated as explained in section 5.1 for the laminar case. Again, this quantity is, as expected, essentially independent of the axial position. Even in the worst case which occurs at Z = 3.49 m for u_o = 0.74 m s^{-1} the calculated value is within 1.2% of the inlet value. Although the agreement between the calculated and inlet values is not as good as for laminar flow (see Table 5.2) it is deemed satisfactory in view of the more complex calculations undertaken for the determination of the turbulent field.

Table 5.3: Axial evolution of the calculated average ice volume fraction for turbulent flow with $\emptyset_{ic}$ = 5% at the inlet

Axial position Z (m)	0.0	0.076	0.102	0.701	1.300	1.900	2.499	2.883	2.997	3.49
$\emptyset_{ic}$ (%) for u_o = 0.74 m.s^{-1}	5.0	5.001	5.001	5.011	5.021	5.033	5.042	5.050	5.052	5.062
$\emptyset_{ic}$ (%) for u_o = 1.47 m.s^{-1}	5.0	5.001	5.001	5.007	5.010	5.015	5.024	5.030	5.032	5.037

Fig. 5.17 illustrates the velocity and ice volume fraction distributions at some selected axial positions for u_o = 0.74 m s^{-1} (Re_{is} = 4649). They indicate that both fields are symmetrical with respect to the vertical diameter. They also show that the velocity field starts changing closer to the inlet and that the extreme values of both quantities are not as distant as in the laminar case. The velocity field again indicates that its derivative at the wall varies along the pipe circumference while the ice volume field indicates that the corresponding density and viscosity are also non-uniform. Consequently, the local friction coefficient varies along the pipe circumference as illustrated in Fig. 5.18 which shows the axial variation of its extreme values occurring at the top and bottom of the pipe. These values decrease with increasing Reynolds number and are always smaller than the ones for laminar flow (see Fig. 5.18).

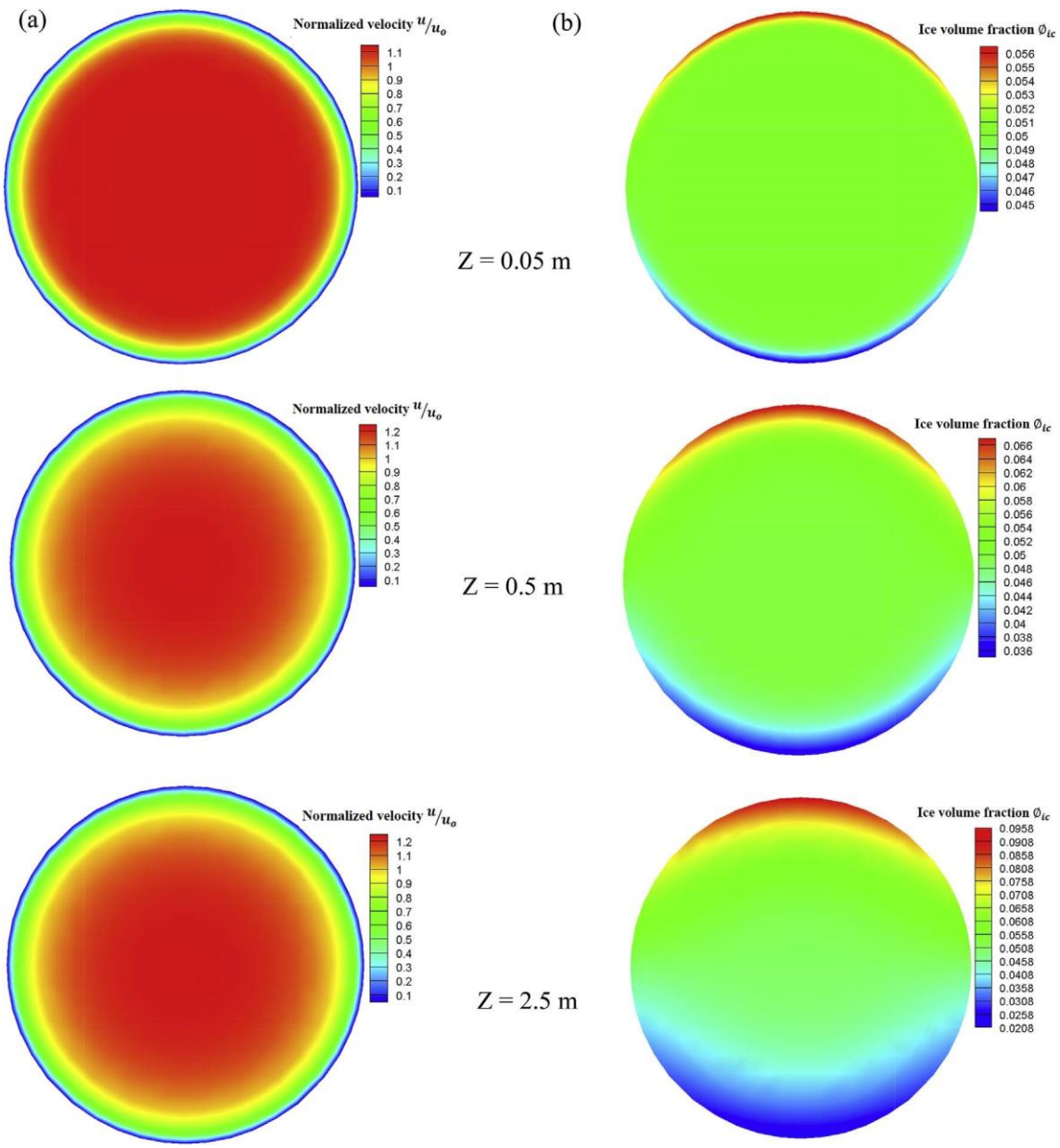

Fig. 5.17. Distributions of (a) normalized velocity and (b) ice volume fraction at different axial positions for turbulent flow of propylene glycol ice slurry (w_{ao} = 4.24%, $\emptyset_{ic}$ = 5%, u_o = 0.74 m s^{-1}, Re_{is} = 4649).

It should be noted that the doubling of the velocity in the turbulent regime (Fig. 5.18) results in a considerably smaller decrease of the friction coefficient than in the laminar regime (Fig. 5.14); this observation substantiates the argument explaining the effect of ice mass fraction on the pressure drop stated in section 5.7. The axial evolution of the friction factor is

qualitatively the same for laminar and turbulent flows as illustrated in Figs. 5.14 and 5.18 respectively. Its behavior can be explained by noting that, as illustrated in Figs. 5.1 and 5.11–5.13 and 5.5-5.17, the velocity distribution undergoes significant changes closer to the pipe inlet than the ice concentration. In the region immediately after the inlet the flow field is in fact conditioned by the boundary layer growth whose thickness does not depend on the angular position. The friction factor in this region is therefore essentially uniform around the pipe circumference and decreases rapidly from its infinite value at Z = 0 (where the fluid velocity goes to zero from the imposed finite inlet value). Its decrease is similar to that experienced by any pure Newtonian fluid in the hydrodynamic entry length. Beyond this velocity-dominated entry region the ice concentration increases near the top of the pipe and decreases near its bottom. As a result of this stratification the velocity distribution is modified and at any axial position the friction factor at the top of the pipe is higher than at its bottom. The distribution of the density exhibits the same qualitative behavior as in the laminar case but its lack of symmetry with respect to the horizontal diameter is less pronounced.

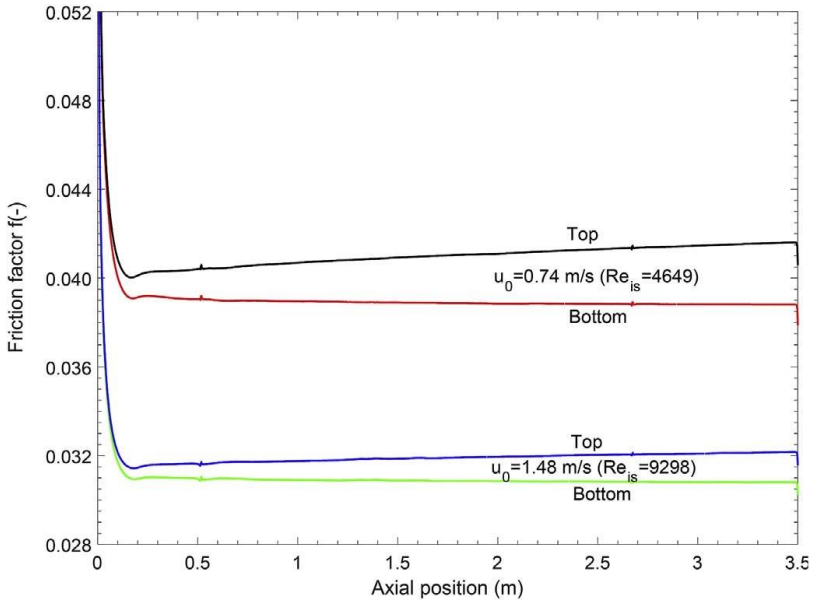

Fig. 5.18. Axial evolution of the friction coefficient for turbulent flow of propylene glycol ice slurry (w_{ao} = 4.24%, $\emptyset_{ic}$ = 5%)

5.6 Conclusion

The proposed CFD model of isothermal ice slurry flow in a horizontal pipe which treats the ice slurry as a Newtonian fluid with effective properties depending on the local ice fraction is simpler than the models used in most other studies of this problem. Nevertheless, its predictions are in excellent agreement with velocity and ice fraction profiles for the turbulent flow of an ethylene glycol slurry published by Wang et al. (2013a) and with the pressure drop for the flow of an ethanol slurry measured by Grozdek et al. (2009a) for a wide range of average inlet velocities and ice mass fractions corresponding to both laminar and turbulent flows. Its numerical predictions for the pressure drop in a 2.997 m long pipe for a propylene glycol slurry for different mass flowrates and ice concentrations encompassing laminar and turbulent flows are also in good agreement with present experimental values except at very low velocities when different flow regimes (annular or stratified) may occur. In view of these comparisons we consider that the proposed model is particularly suited for the simulation of turbulent ice slurry flows for which the ice fraction distribution is almost uniform. More reliable quantitative and local measurements for other additives, additive concentrations and pipe diameters are required to further validate the present model (especially for laminar flows in order to explain the fact that it correctly predicts pressure drops for ethanol ice slurries but not for propylene glycol ones) and all the forthcoming ones.

The model has been used to validate the interpretation of experimental slurry density and ice fraction values which are essentially equal at the inlet and outlet of the 2.997 m long pipe as being the corresponding local average values. This is based on the model predictions, which show that their average values are constant throughout the flow field despite the fact that the local density and ice fraction depend on all three spatial coordinates.

The three-dimensional variations of the slurry velocity, of the local ice fraction and of the friction coefficient have been illustrated for laminar and turbulent flow conditions and have been explained based on the predicted ice fraction variation which is caused by the opposing effects of buoyancy and diffusion generated by ice fraction gradients. Thus, in the top half of

the pipe the ice fraction increases and therefore the molecular viscosity and the friction coefficient increase while the density and the velocity decrease. All the fields are symmetrical with respect to the vertical diameter and the extreme values of the first two quantities (velocity and ice fraction) always occur on this diameter. The distortion of the corresponding profiles from the uniform inlet conditions is less important for turbulent flows since in that case the molecular viscosity which depends on the ice fraction distribution is smaller than the turbulent viscosity.

Acknowledgements

This project is part of the R&D program of the NSERC Chair in Industrial Energy Efficiency established in 2006 at 'Université de Sherbrooke'. The authors acknowledge the support of the Natural Sciences and Engineering Research Council of Canada, Hydro-Québec, Rio Tinto Alcan and CanmetENERGY Research Center of Natural Resources Canada.

CHAPITRE 6

HEAT TRANSFER OF ICE SLURRY FLOWS IN A HORIZONTAL PIPE: A NUMERICAL STUDY

Auteurs et affiliations :

Landa ONOKOKO : étudiant au doctorat, Université de Sherbrooke, Faculté de Génie, Département de Génie mécanique.

Nicolas GALANIS : professeur, Université de Sherbrooke, Faculté de Génie, Département de Génie Mécanique.

Sébastien PONCET : professeur, Université de Sherbrooke, Faculté de Génie, Département de Génie Mécanique.

Michel POIRIER : CanmetENERGY Natural Ressources Canada, Varennes, Québec, Canada.

Date de soumission : November 2018

État de l'acceptation : en évaluation

Revue : International Journal of Thermal Sciences

Titre en français : Etude numérique de transfert de chaleur dans un écoulement de coulis de glace dans un tuyau horizontal

ABSTRACT

The thermal behavior of ethylene glycol-water ice slurry flowing through a horizontal heated tube is investigated numerically. The ice slurry is assumed to behave as a Newtonian fluid with effective properties depending on temperature and ice fraction. The 3D steady-state model includes the mass, momentum and energy conservation equations for the liquid-solid mixture as well as a transport equation for the ice particles, which characterizes the balance between convective and diffusive fluxes. The diffusive flux includes those induced by the shear rate gradients, the spatial variation in viscosity and the particle settling. The heat and mass exchanges between the ice particles and the carrier liquid are modeled through source terms. The model is validated against experimental data from the open literature and applied to laminar and turbulent flows. Some important heat transfer characteristics of melting are obtained including the axial distributions of the heat transfer coefficient, the bulk and wall temperatures, the ice volume fraction and the melting rate. They show significant differences from corresponding distributions for non-melting flows. The effects of the wall heat flux and other operating parameters on these quantities are presented and analyzed.

Keywords: ice slurry; melting; heat and mass transfer; laminar and turbulent flows.

RÉSUMÉ

Le comportement thermique d'un coulis de glace à base d'éthylène glycol en écoulement stationnaire dans un tuyau horizontal chauffé est étudié numériquement. Le coulis de glace est considéré comme un fluide Newtonien ayant des propriétés effectives qui dépendent de la concentration de la glace et de la température. Le modèle 3D qui comprend les équations de conservation de masse, de quantité de mouvement et de l'énergie pour le mélange liquide-solide contient aussi une équation de transport obtenue à partir du bilan des flux convectifs et diffusifs des particules de glace. Les flux diffusifs sont ceux induits par le gradient du taux de cisaillement, la variation spatiale de la viscosité et la flottaison. Diverses sources définies par un modèle de fusion ont été introduites dans les équations de conservation pour tenir compte des échanges de matière et de chaleur entre les particules de glace et le fluide environnant. Le modèle est d'abord validé par les données expérimentales disponibles dans la littérature, puis appliqué aux écoulements laminaires et turbulents. Quelques caractéristiques importantes de transfert de chaleur sont obtenues telles que les distributions du coefficient de transfert de chaleur, de la température et de la fraction volumique de glace. Les effets du flux de chaleur imposé à la paroi du tube et d'autres paramètres de fonctionnement sur le coefficient de transfert de chaleur local sont également discutés en détail.

Mots-clés : coulis de glace ; fusion ; transfert de chaleur et de masse ; écoulements laminaires et turbulents.

6.1 Introduction

Ice slurries are mixtures of small ice particles (typically 0.1 to 1 mm in diameter) and a carrier liquid, which is a mixture of water and an additive (glycol, sodium chloride or calcium carbonate…) used to lower the freezing temperature. Applications of ice slurry include comfort cooling of buildings, food processing and the replacement of secondary refrigerants in ice rinks or supermarkets (Kauffeld et al., 2010). Due to their high pumpability even at high ice volume fractions they can be used also for air-conditioning applications in deep mining (Trabelsi et al., 2017). Ice slurries offer the possibility to enhance energy transport density and energy storage due to the combined effects of sensible and latent heat.

The behavior of ice slurries in heat transfer installations is complex. In horizontal pipes, the separation of the solid ice particles and the carrier liquid can occur with any particle size at very low velocities and with larger particles at high velocities. Ice particles concentrate along the upper part of the tube since their density is smaller than that of the aqueous solution. In addition, the melting of ice particles creates differences of temperature and concentration near the solid-liquid interface (exchanges of mass and heat). Thus, various flow patterns can be encountered in ice slurry pipe flows, which affect the hydrodynamics of the flow and the heat transfer mechanisms. Many experimental and numerical studies have been conducted on ice slurry heat transfer due to its special features such as high energy storage density, low pumping power requirements, and high heat transfer rates between the wall and the mixture. For most authors, the heat transfer coefficient increases with ice mass fraction and ice slurry velocity. Some of these studies are reviewed in the following paragraph.

Knodel et al. (2000) investigated experimentally the heat transfer of ice-water slurries in a horizontal tube of 24 mm inner diameter and 4.60 m in length with velocities ranging from 2.8 to 5.0 $\mathrm{m\ s^{-1}}$. They found that the Nusselt number decreases with the ice fraction during the transition from the turbulent to the laminar regime (relaminarization phenomenon). They attributed this reduction by the fact that the flow transitions from turbulent to laminar plug as the ice fraction increases. Lee and Sharma (2006) experimentally investigated the heat transfer

characteristics of 6.5% ethylene glycol ice slurry flowing in a horizontal tube of 13.84 mm inner diameter and 1500 mm of length at constant wall temperature (7.5-22.5 ℃) with mass flux and ice fraction ranging from 800 to 3500 $\mathrm{kg\,m^{-2}\,s^{-1}}$and 0 – 25%, respectively. The measured heat transfer rates increase with the mass flow rate and ice fraction; however, the effect of ice fraction appears not to be significant at high mass flow rates. For low mass flow rates, a sharp increase in the heat transfer coefficient was observed when the ice fraction was higher than 10%. Grozdek et al. (2009b) measured the local and mean heat transfer coefficients under constant wall heat flux of 4–16 $\mathrm{kW\,m^{-2}}$. It was reported that the local Nusselt number decreases rapidly in the entrance region but increases slightly in the fully-developed region under constant wall heat flux of 16 $\mathrm{kW\,m^{-2}}$. Renaud-Boivin et al. (2012) investigated experimentally the hydraulic and thermal behavior of ice slurry in a shell and tube heat exchanger. The heat transfer coefficient of ice slurry was found to increase by 33% with ice mass concentration increasing from 0% to 25%.

The numerical modeling of the heat transfer for melting ice slurry flows has been rather rarely reported. Niezgoda-Zelasko (2006, 2016) performed experiments and adopted the enthalpy-porosity approach to numerically investigate the heat transfer of ice slurry flowing through a horizontal pipe under a constant heat flux density. They found that the heat flux density has only a weak influence on the heat transfer coefficient. In addition, a relaminarization phenomenon was observed for mass fractions w_{is} >10%. Kousksou et al (2010) did not calculate the velocity and ice concentration distributions and only solved the energy equation to determine the effect of the mass flowrate and the wall heat flux on the heat transfer coefficient and the outlet temperature. Zhang and Shi (2015) used an Euler-Euler approach based on the kinetic theory of granular flows to study numerically the heat transfer characteristics of ice slurry. They reported that the local heat transfer coefficient decreases rapidly in the entrance region and remains approximately constant in the thermally fully-developed region. Yanbo Li et al. (2016) used the VOF two-phase model to investigate the heat transfer performance of ice slurry. Their results show that for turbulent flow the mean Nusselt number is strongly dependent on the inlet velocity and on the inlet ice mass fraction but does

not vary much with the wall heat flux. Recently, Kamyar et al. (2018) simulated the laminar flow of ethyl-alcohol/water ice slurry in a helical-coil heat exchanger. Their model accounts for the non-Newtonian behavior of the slurry through a Bingham model and for the melting using the enthalpy-porosity method. However, all such studies have not yet provided a complete description and analysis of ice slurry flow under the conjugated effects of ice melting and stratification. Moreover, these numerical methods have some drawbacks: the enthalpy-porosity method introduces an empirical term used to model the pressure drops due to the solid phase in the energy equation and the Eulerian model solves a set of two continuity, momentum and energy equations, one for each phase, which greatly increases the computational cost of the simulations.

In the present study, the thermal behavior and melting of ice slurry flowing through a horizontal circular heated tube are investigated numerically for both laminar and turbulent flow regimes. A Computational Fluid Dynamics (CFD) model which accounts for the ice particle settling, shear-induced migration, and melting and is simpler than the one used by Zhang & Shi (2015) but more complete than that used by Kousksou et al (2010) is proposed in section 6.2. It is an extension of the one in our previous study (Onokoko et al., 2018) which dealt with isothermal flow and therefore did not include the energy equation and the mass transfer between the solid and liquid phases. The model is then validated against the experimental data of Grozdek et al. (2009b) in Section 6.3 in terms of the local heat transfer coefficient. The results are presented and discussed in Section 6.4. The influences of the volume ice fraction and the wall heat flux on the temperature, melting rate, velocity and heat transfer coefficient are particularly investigated. Conclusions are finally provided in Section 6.5.

6.2 Numerical modeling

6.2.1 Description of the problem

The present study concerns the melting and transport of ethylene glycol ice slurry in a horizontal heated pipe. Figure 6.1 shows a schematic diagram of the problem and defines the

Cartesian system of coordinates. The inner diameter and length of the pipe are fixed to D=10mm and L=460D, respectively. The pipe thickness is considered as being negligible. The heated section of the pipe (300D) is long enough to ensure considerable melting of the ice slurry. It is preceded and followed by two adiabatic sections.

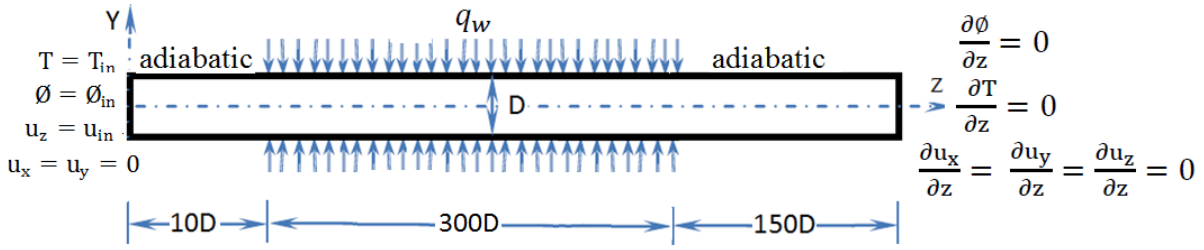

Fig. 6.1. Schematic diagram of the flow configuration with relevant notations and boundary conditions

6.2.2 Conservation equations

The numerical model is based on the following assumptions:

- The ice slurry is treated as an incompressible Newtonian fluid with phase change capacity and variable thermophysical properties (the Newtonian assumption is valid for ice concentrations below 15-20% (Yanbo et al., 2016; Fauffeld et al., 2005)).

- The flow is three-dimensional steady-state, either laminar or turbulent.

- Ice particles are assumed to be smooth, inelastic and spherical.

Based on these assumptions, the governing equations for the conservation of mass (Eq. 6.1), momentum (Eq. 6.2) and energy (Eq. 6.3) can be formulated respectively as:

$$\frac{\partial}{\partial x_i}(\rho_{is} u_i) = 0 \tag{6.1}$$

$$\frac{\partial}{\partial x_j}\left(\rho_{is} u_i u_j\right) = -\frac{\partial P}{\partial x_i} + \frac{\partial \tau_{ij}}{\partial x_j} \tag{6.2}$$

$$\frac{\partial}{\partial x_j}(\rho_{is} h_{is} u_j) = \frac{\partial}{\partial x_j}\left[k_{is}\left(\frac{\partial T}{\partial x_j}\right)\right] + S_h \tag{6.3}$$

where S_h is the source term due to phase changes.

The volume ice fraction in the ice slurry satisfies the following equation, which represents a balance between the convective and diffusive particle fluxes:

$$\frac{\partial}{\partial x_j}\left(\rho_{is}\emptyset u_j\right) = -\frac{\partial J_\emptyset}{\partial x_j} + S_{\dot{\gamma}} + S_\emptyset \tag{6.4}$$

Here $S_\emptyset$ is the source term due to phase changes and the term $S_{\dot{\gamma}}$ is (Onokoko & Galanis, 2013):

$$\mathrm{S}_{\dot{\gamma}} = \frac{\partial}{\partial \mathrm{x_j}}\left[\rho_{is}\mathrm{K_c}R^2\emptyset^2\left(\frac{\partial\dot{\gamma}}{\partial \mathrm{x_j}}\right)\right] \tag{6.5}$$

In Eq. (6.4), the mass flux of the ice particles $J_\emptyset$ in the ice slurry may be modeled as:

$$J_\emptyset = -\rho_{is}\Gamma_\emptyset\left(\frac{\boldsymbol{\partial\emptyset}}{\boldsymbol{\partial x_j}}\right) + \rho_{is}\emptyset\omega_0\mathrm{f}(\emptyset)\delta_{jy} \tag{6.6}$$

where $\Gamma_\emptyset$ is the mass diffusivity associated with shear-induced migration of ice particles. The second term on the right-hand side of Eq. (6.6) accounts for the flux due to particles settling with ω_0 the terminal velocity of a single ice particle in an aqueous solution calculated from Stokes' law and δ the Kronecker symbol. The mass diffusivity $\Gamma_\emptyset$ is:

$$\Gamma_\emptyset = \rho_{is}R^2\emptyset\dot{\gamma}\left(K_c + K_\mu\emptyset\frac{\partial\mu_{is}}{\mu_{is}\partial\emptyset}\right) \tag{6.7}$$

while, according to Revay & Higdon (1992), the hindrance function is given by:

$$\mathrm{f}(\emptyset) = (1-\emptyset)^{6.55}(1 + 3.458\emptyset^2 + 8.990\emptyset^3) \tag{6.8}$$

The values of the coefficients are $\mathrm{K_c}$ = 0.41 and $\mathrm{K_\mu}$ = 0.62 as suggested by Phillips et al. (1992).

The reader can refer to Onokoko and Galanis (2013), Onokoko et al. (2018) and Bordet et al. (2018) for a full description of the numerical model in the isothermal case.

6.2.3 Thermophysical properties of ethylene glycol ice slurry

The equilibrium phase diagram for ethylene glycol ice slurry is shown in Fig. 6.2. It shows that the phase change temperature decreases with increasing additive concentration. Eutectic composition is characterized by a mass fraction of ethylene glycol $w_{a,eut} \cong 64.4wt.\%$ and a eutectic temperature $T_{eut} \cong -63.6$°C (Corday et al., 1996). The ice line (liquidus) defines the temperature (T_f) at which phase changes occur. Above the ice line, the ice slurry is purely liquid (water and additive) while below it the aqueous solution and ice particles coexist in equilibrium. It should be noted that the ice particles are always considered to be pure water (Kauffeld et al., 2005).

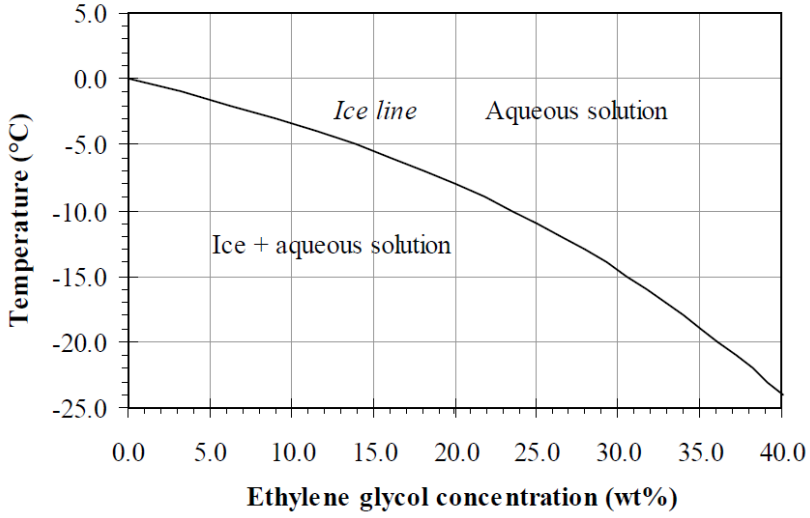

Fig. 6.2. Phase diagram of water-ethylene glycol mixture (Pronk, 2006)

Tabulated data published in the ASHRAE Handbook of Fundamentals (2005) give the ice slurry phase change temperature T_f (in °C) as a function of the ethylene glycol global mass fraction w_{ao} which is constant during heating or cooling processes. This data can be expressed as:

$$w_{ao} = \sum\left(c_i T_f^i\right) <=> T_f = \sum(c_i' w_{ao}^i) \tag{6.9}$$

The coefficients c_i and c_i' have been calculated by Renaud-Boivin et al. (2012) from the ASHRAE data.

When the temperature of the solution with an ethylene glycol global mass fraction w_{ao} is below the corresponding phase change temperature the concentration of ethylene glycol in the

aqueous solution increases to a value w_a since some water has solidified and has therefore been removed from the solution. This new additive concentration is related to the corresponding mass fraction of the ice by the following relation obtained from a mass balance:

$$w_{ic} = 1 - (w_{ao} / w_a) \tag{6.10}$$

The thermophysical properties of the ice slurry are obtained from the relations given in the Handbook on Ice Slurries (Kauffeld et al., 2005). They involve the volumetric ice fraction, the corresponding properties of ice, and the corresponding properties of the carrier liquid:

$$\rho_{is} = \emptyset\rho_{ic} + (1 - \emptyset)\rho_{as} \tag{6.11}$$

$$\mu_{is} = \mu_{as}\left(1 + 2.5\emptyset + 10.05\emptyset^2 + 0.00273e^{16.6\emptyset}\right) \tag{6.12}$$

$$k_{is} = k_{as}(1 + 3\emptyset\beta + 3\emptyset^2\beta^2\gamma) \tag{6.13}$$

$$\text{where} \quad \gamma = 1 + \frac{\beta}{4} + \frac{3\beta}{16}\left(\frac{\alpha+1}{2\alpha+3}\right), \quad \beta = \frac{\alpha-1}{\alpha+2}, \quad \alpha = \frac{k_{ic}}{k_{as}} \tag{6.14}$$

$$h_{is} = w_{ic}h_{ic} + (1 - w_{ic})h_{as} \tag{6.15}$$

To evaluate the enthalpy of ice h_{ic} and that of the aqueous solution h_{as}, the method proposed by Melinder and Granryd (2005) is used:

$$h_{ic} = -L_f + C_{p,ic}T \tag{6.16}$$

$$h_{as} = h_{0,T_{ref}} + \Delta h_{mix} + \int_{T_{ref}}^{T} C_{p,as}\, dT \tag{6.17}$$

where $h_{0,T_{ref}}$ is the enthalpy of water at the reference temperature, which is set as 0 kJ/kg at 0°C. $\Delta h_{mix}\ and\ L_f$ can be expressed as functions of the residual mass fraction w_a. The correlations for the ethylene glycol aqueous solution are taken from Renaud-Boivin et al. (2012) for Δh_{mix} and from Kumano et al. (2010) for L_f.

The properties of ice are obtained from the relations given in the Handbook on Ice Slurries (Kauffeld et al., 2005):

$$\rho_{ic} = 917 - 0.13T \tag{6.18}$$

$$k_{ic} = 2.21 - 0.0012T \tag{6.19}$$

$$C_{p,ic} = 2.12 + 0.008T \tag{6.20}$$

The properties of the aqueous solution (ρ_{as}, k_{as}, and $C_{p,as}$) depend on the temperature and the ice concentration. They are derived from tabulated data published in the ASHRAE Handbook of Fundamentals (2005) which can be expressed under the general form:

$$P_l(\emptyset_a, T) = \sum_{i=0}^{M} T^i \sum_{j=0}^{N} b_{i,j} \emptyset_a^j \tag{6.21}$$

The coefficients $b_{i,j}$ for ethylene glycol aqueous solution were calculated by Renaud-Boivin et al. (2012).

Finally, it should be noted that the ice concentration by mass and volume are related through the following expression (Kauffeld et al, 2005):

$$\emptyset_{ic} = w_{ic} \frac{\rho_{is}}{\rho_{ic}} \tag{6.22}$$

6.2.4 Source terms due to interphase heat and mass transfer

As mentioned before the source terms in equations Eq. (6.3) and Eq. (6.4) are due to ice melting. Obviously melting cannot take place in regions where ice is not present such as at near-wall downstream positions of the heated part of the pipe in Fig. 6.1. It can also not take place if the local temperature is below the corresponding phase change temperature as may be the case in the upstream adiabatic section of the pipe in Fig. 6.1. These phenomenological observations are quantified in the model by setting S_h and $S_\emptyset$ equal to zero when the ice concentration calculated from Eq. (6.4) is zero and when the temperature *T* calculated from

Eq. (6.3) is smaller than the phase change temperature T_f corresponding to the value of Ø obtained from Eq. (6.4).

When Ø > 0 and $T > T_f$ melting will take place. The heat and mass transfer due to melting can be derived from the energy balance at the interface between the ice particles and the surrounding aqueous solution (Hao and Tao, 2003). For this purpose, it is assumed that under these conditions the ice particle temperature is equal to the phase change temperature T_f while the surrounding liquid is at the temperature T obtained from the CFD simulations. Therefore:

$$S_h = \dot{m} L_f = h_{vol}(T - T_f) \tag{6.23}$$

The volumetric interfacial heat transfer coefficient is:

$$h_{vol} = 3\emptyset h_p / R \tag{6.24}$$

where h_p is the particle-liquid heat transfer coefficient estimated by Gunn's correlation (Gunn, 1978). The source term for the species conservation equation (Eq. 4) is simply:

$$S_\emptyset = \dot{m} = h_{vol}(T - T_f)/L_f \tag{6.25}$$

Eq. (6.25) has also been used by Zhang & Shi (2015). The value of T_f is calculated from the local ice concentration and is therefore not uniform.

The above formulation of the source terms as well as the four conservation equations (Eqs. 6.1-6.4) are very similar to those used by Abba et al. (2006) to study frazil ice formation in turbulent flow. That model, as the present one, solves a single set of continuity-momentum equations to obtain the velocity components, a single energy equation to obtain the temperature and a continuity equation for the ice to obtain its concentration. It then distinguishes between the temperature of the solid and the liquid in order to express and calculate the source terms associated with heat and mass transfer between the solid particles and the surrounding liquid. However, it should be noted that Abba et al. (2006) simplify their model by assuming that the viscosity and thermal conductivity are constant whereas in the

present model they are both treated as functions of the temperature and the ice concentration.

6.2.5 Turbulence modeling

The realizable k-ε model (Shih et al., 1995) was used to close the system of equations in the turbulent regime. This closure level is adequate for flows involving boundary layers under strong adverse pressure gradients, separation, rotation, and recirculation. The governing equations for the turbulence kinetic energy and the dissipation rate are under their standard form (Zhang & Li, 2008) and are therefore not reproduced here. The near-wall modeling is crucial for open wall bounded flows such as in the present study. For all mesh employed in this work, wall coordinate y^+ values less than 1 (for the enhanced wall treatment) were achieved, such that the flow is modeled up to the wall without resorting to the use of wall functions.

6.2.6 Numerical method and boundary conditions

The system of partial differential equations modeling the flow field are coupled since the thermophysical properties of the ice slurry depend on the temperature and ice fraction. They were solved using the commercial software Ansys-Fluent 15.0 based on the finite volume method. The ice particle conservative equation (Eq. 6.4) was introduced using the user-defined scalar (UDS) functionality. All source terms were added to the conservative equations. The SIMPLE algorithm was employed to overcome the pressure-velocity coupling in the momentum equation. Second-order schemes were used for the spatial discretization of the conservative equations together with the QUICK scheme to approximate the convection term. The gradients were evaluated using the least squares cell-based method.

The domain was divided into 1886812 cells (1771132 hexahedron cells and 115680 wedge/prism cells). The mesh was generated using Ansys workbench 15.0 and optimized through a mesh independence analysis. A mesh refinement process near the wall was performed to fulfill the requirement value of $y^+ \approx 1$. The numerical calculations were considered as converged when all the residuals were lower than 10^{-4}.

As indicated in Fig 6.1, the velocity and the ice particle mass fraction are assumed to be uniform at the pipe inlet; the corresponding turbulence intensity and the viscosity ratio are fixed at 5% and 10 respectively. The outflow condition is applied at the pipe outlet. Specific no-ice particle-flux and no-slip boundary conditions have been applied at the pipe wall which is subjected to a constant uniform heat flux (zero in the inlet and outlet adiabatic regions and non-zero for $0.1 < z < 3.1$ m).

6.3 Model validation

It must first be noted that the proposed model has already been carefully validated in Onokoko et al. (2018) for isothermal ice slurry flows in a horizontal pipe both against the pressure drop measurements of Grozdek et al. (2009a) and in terms of velocity and ice fraction distributions against the numerical results of Wang et al. (2013a).

To further validate the model in the non-isothermal case, the present numerical results were compared to the experimental data obtained by Grozdek et al. (2009b) for the flow of a 10.3wt% ethanol ice slurry in a horizontal circular pipe having a diameter of 21 mm and with a constant wall heat flux. The mean diameter of the ice particles is estimated to be 0.125 mm. The properties of the ethanol aqueous solution were obtained from Melinder (2007). According to Grozdek et al. (2009b), the values of the mean inlet velocity, heat flux imposed at the wall and ice fraction are such that both laminar and turbulent flow regimes are covered. Figure 6.3 which shows the variation of the mean heat transfer coefficient with the ice volume fraction for three sets of operating conditions indicates that the present numerical results agree quite well with the experimental data for all ice fractions up to 20%.

In view of these comparisons the present numerical model based on the single-phase approach proposed by Phillips et al. (1992) and extended to non-isothermal flows can therefore be used confidently to predict the heat transfer and fluid flow of ice slurry.

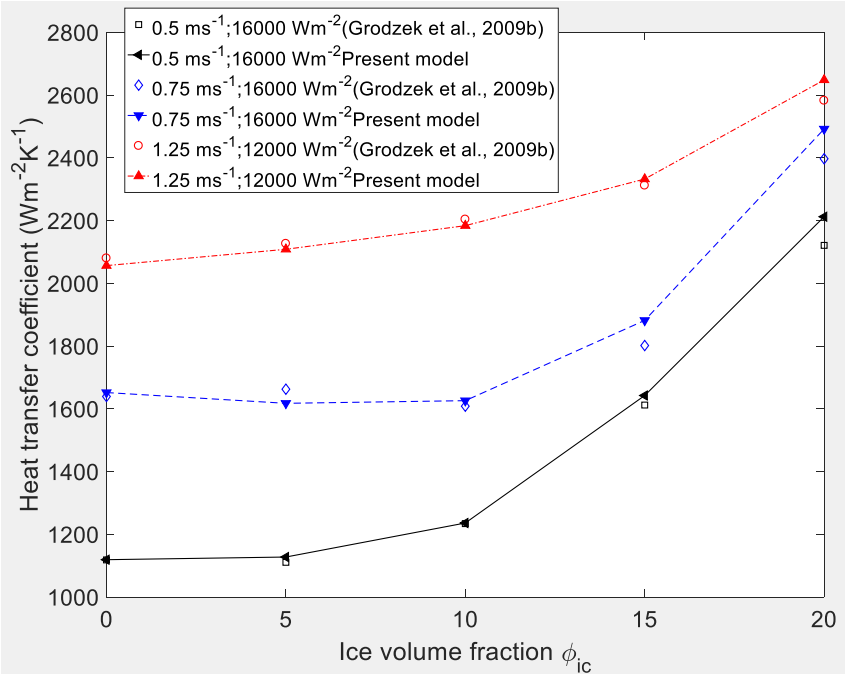

Fig. 6.3. Comparison of calculated mean heat transfer coefficients with the experimental data of Grodzek et al. (2009b).

6.4 Results and discussion

6.4.1 Operating conditions

In the following investigation of flow in the pipe of Fig. 6.1 the initial solution consists of a 6.5 wt% ethylene glycol-water solution for which the phase change temperature is approximately -2 °C. The ice particle diameter is fixed to 0.27 mm. The other operating conditions are specified in the following sections. However, it should be noted that for all the cases under consideration the inlet conditions are far from the eutectic composition. Therefore the temperature T_f in Eq. 6.23 and 6.25 is essentially constant, only slightly below the value -2 °C identified above.

The flow regime is determined by calculating the Reynolds number ($Re_{is} = \rho_{is} u D/\mu_{is}$). Following Niezgoda-Zelasko and Zalewski (2006) the flow is regarded as turbulent when this Reynolds number exceeds 3000.

6.4.2 Heat transfer characteristics of laminar ice slurry flows

The calculated results for a base case for which $\emptyset_{in}$= 15.0 vol%, u_{in}= 0.5 m s^{-1} (hence Re_{is} = 1507 at the inlet) and q_w = 32000 W m^{-2} are presented and analysed. Fig. 6.4 shows the corresponding ice mass fraction, temperature, velocity and melting rate distributions along the vertical diameter at different axial positions. The flow field can be divided into three main regions.

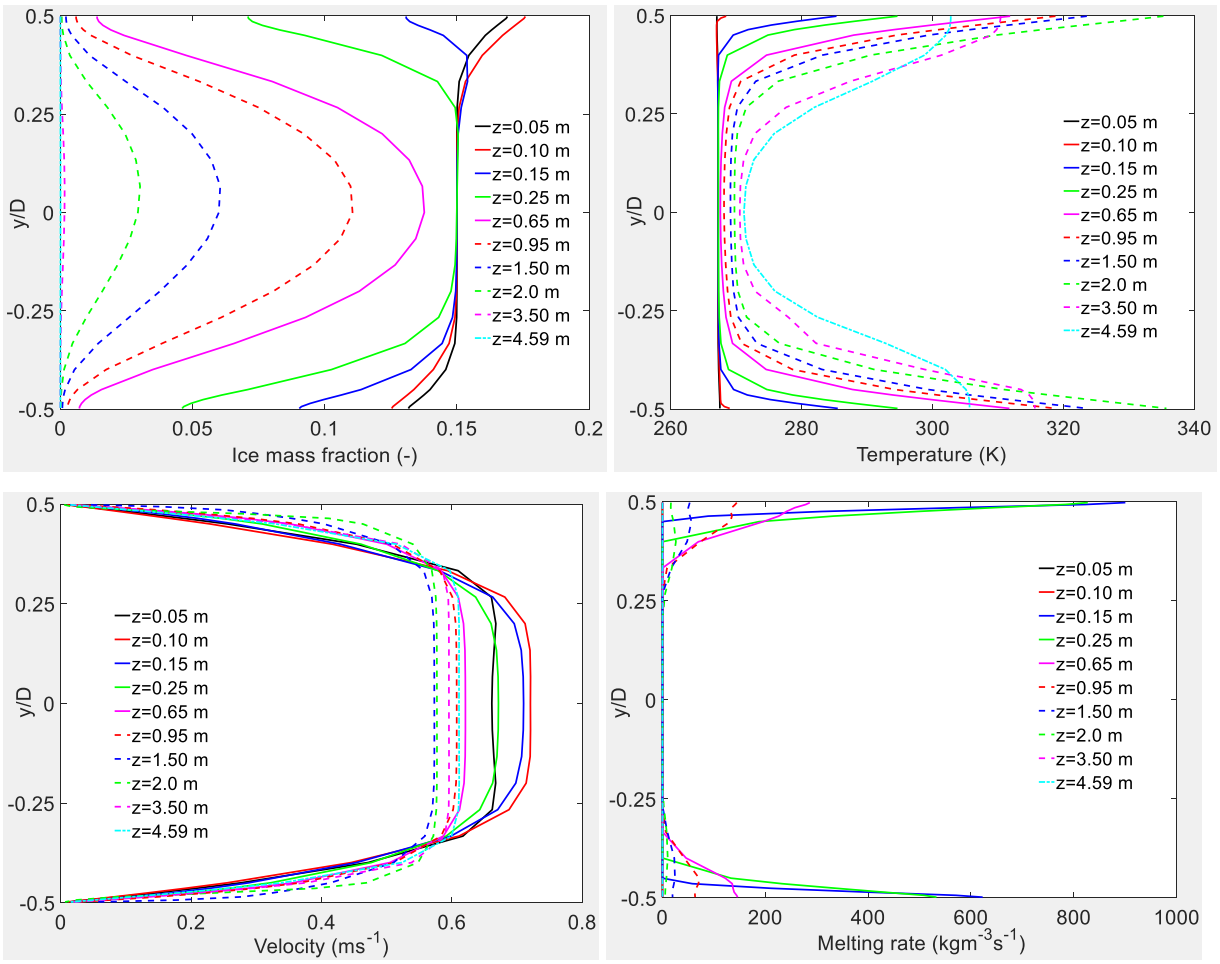

Fig. 6.4. Distributions of ice fraction, temperature, velocity and melting rate along the vertical diameter for laminar flow with $\emptyset_{in}$= 15 vol%, u_{in}= 0.5 m s^{-1} (Re_{is} = 1507), q_w= 32000 W m^{-2}

For z < 0.1 m (i.e. in the upstream adiabatic region) the temperature profile is uniform (identical to the one imposed at z = 0) while the ice fraction distribution is slightly different from the uniform one imposed at z = 0 due to the stratification generated by the density difference

between the ice particles and the aqueous solution (see Onokoko et al 2018). As a result of this behavior of the ice fraction and the temperature the density and viscosity of the ice slurry are essentially uniform in this region. Therefore, the velocity profile evolves as for any pure incompressible Newtonian fluid: it is essentially symmetrical with respect to the pipe axis and reflects the growth of the boundary layer. It is interesting to note that the velocity profiles at z = 0.05 m exhibits the well-known overshoot phenomenon caused by the rapid development of the boundary layer and that the flow is not hydrodynamically developed at z = 0.1 m. Finally, the melting rate is zero throughout this region since the flow up to z = 0.1 m is adiabatic.

As the fluid moves into the first part of the heated region ($0.1 \leq z \leq 0.2$ m) the fluid temperature at, and near, the wall increases quickly due to the heat addition. As a result, the melting rate in the near-wall region is appreciable, particularly near the top of the pipe, while it is zero near the pipe axis where the temperature has not increased. However, the ice fraction near the top of the pipe does not decrease as fast as near the bottom since ice particles are constantly moving upwards due to the density difference between the solid and liquid phases. Around the pipe axis the ice fraction remains equal to the inlet value throughout this first part of the heated region. The space-wise variation of the temperature and the ice fraction cause analogous variations of the ice slurry thermophysical properties which in turn influence the continuing development of the flow field. Thus, the viscosity is higher near the axis of the pipe where the ice concentration is higher and the temperature is lower; it is lower near the pipe wall where the ice concentration is lower and the temperature higher. Therefore the velocity profile does not develop as in the case of laminar flow of a pure Newtonian fluid with constant properties. In particular, the velocity at y = 0 decreases between z = 0.1 m and z = 0.25 m while the part of the diameter with low velocities (below 0.4 m s^{-1} for example) is smaller at z = 0.25 m. As z increases beyond z = 0.25 m the temperature of the near-wall fluid increases further, conduction takes effect and heat is transferred towards the center of the pipe. However, this process is slow due to the low conductivity of the ice slurry. As a result the increase of the fluid temperature close to the pipe axis is small for the conditions under study and melting only takes place in the near-wall region, particularly near the top of the pipe where the ice

concentration is higher. The observed depletion of ice in the central part of the pipe is therefore not due to melting but to the upwards migration of the light solid particles due to buoyancy. It is noted that throughout the heated region the temperature profile is essentially symmetrical with respect to the pipe axis. As the fluid moves downstream and the total quantity of ice decreases its effect on the fluid properties and on the velocity profile gradually disappears. However the important temperature variations observed at any given axial position cause considerable variations in the density, viscosity and Reynolds number and affect the hydrodynamic field. Thus, the velocity profiles are very different from those for laminar flow of a pure Newtonian fluid with constant properties. In particular, the velocity at y = 0 decreases between z = 0.25 m and z = 1.5 m and then remains constant between z = 1.5 m and z = 2.0 m.

Finally, in the downstream adiabatic region ($3.1 \leq z \leq 4.6$ m) the fluid temperature near the wall decreases while it increases in the vicinity of the axis due to conduction in the fluid which tends to eliminate the observed temperature non-uniformity. As mentioned before, this process is very slow and thus at the pipe outlet (z = 4.59 m) the wall temperature is still significantly higher than at the axis for the case under consideration. The corresponding ice fraction and the melting rate are essentially zero. Therefore, compared to their inlet values the viscosity is lower while the density is higher and thus the Reynolds number is higher than at the inlet (Re_{is} = 4021 at z = 4.59 m which indicates that the flow at this axial position is turbulent). The velocity profile is therefore different from that for laminar flow of a pure Newtonian fluid with constant properties.

An indication of the precision of these results is provided by comparing the calculated mass flowrate for different axial positions. It is thus found that for $0.05\text{m} \leq z \leq 4.59$ m the maximum and minimum values of this quantity are 0.03965 kg s^{-1} and 0.03951 kg s^{-1}. Since this range of values corresponds to a variation of less than 0.2% from their average we conclude that the numerical procedure is very accurate for the conditions under consideration.

Figure 6.5 shows the corresponding ice fraction distribution at six different cross-sections in the heated part of the pipe. The red and blue colours always indicate the region of maximum and minimum concentration respectively. However, it is important to note that the maximum and minimum values in the colour scale decrease as the distance from the inlet increases since, due to melting, the quantity of ice decreases as the fluid moves downstream. These results complement those in Fig. 6.4 and clearly show that the ice concentration is symmetrical with respect to the vertical pipe diameter. Analogous results for the temperature distribution are shown in Fig. 6.6. In this case the maximum value in the colour scale increases significantly as the distance from the inlet increases while the minimum value does not change much. It is seen that the temperature over a very important part of the cross-section centered on the pipe axis does not change much since most of the heat added to the fluid is used to melt the ice and conduction in the ice slurry is weak. The temperature distribution is also symmetrical with respect to the vertical pipe diameter.

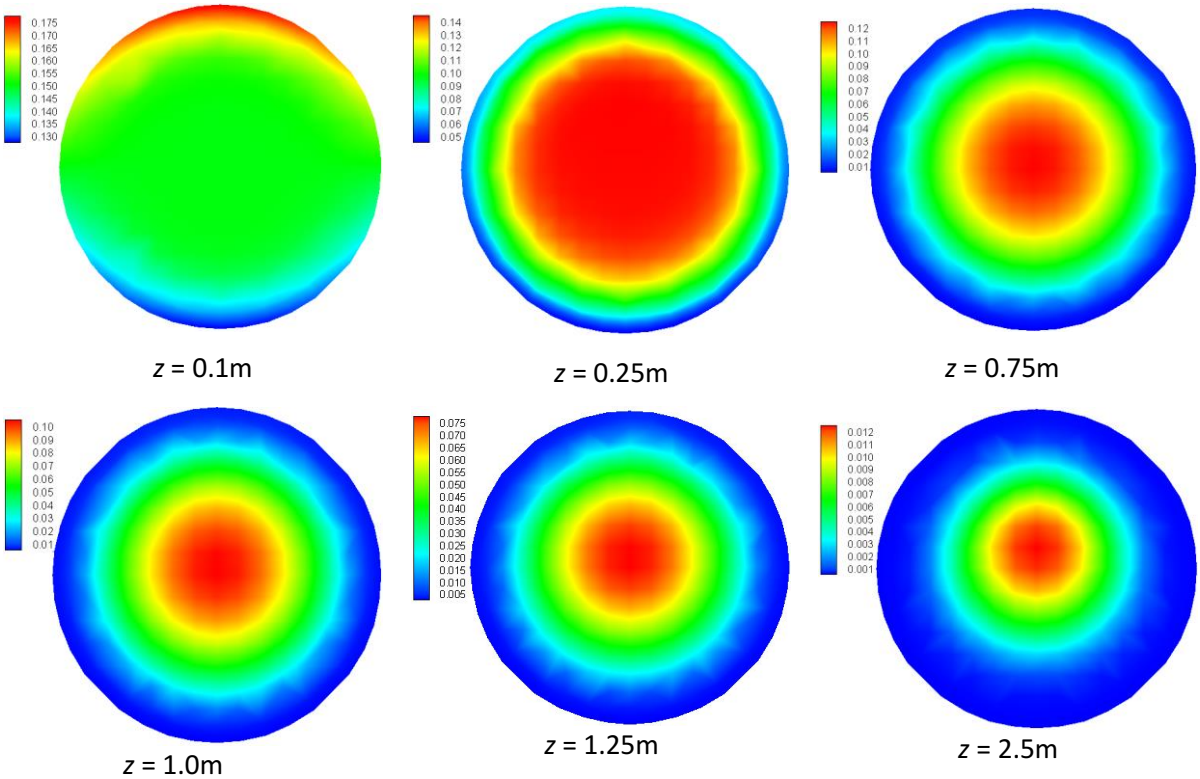

Fig. 6.5. Ice volume fraction distribution at different cross-sections of the heated region for laminar flow with $\emptyset_{in}$= 15 vol%, u_{in}= 0.5 m s^{-1} (Re_{is} = 1507), q_w= 32000 W m^{-2}

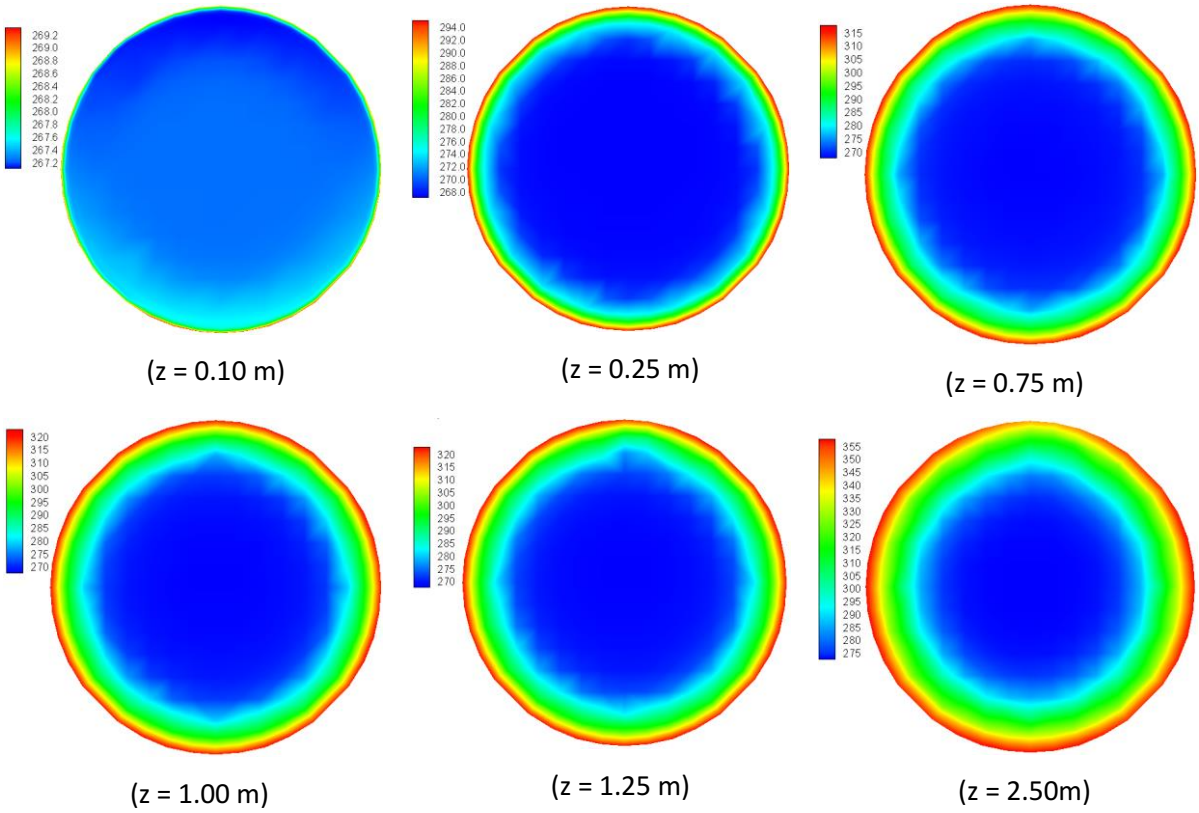

Fig. 6.6. Temperature (K) distribution at different cross-sections of the heated region for laminar flow with $\emptyset_{\mathrm{in}}$= 15 vol%, u_{in}= 0.5 m s^{-1} (Re_{is} = 1507), q_{w}= 32000 W m^{-2}

Figure 6.7 illustrates the effect of two inlet conditions on the ice concentration at *z* = 0.45 m. Figure 6.7a shows that the ice concentration increases as the inlet velocity increases, particularly near the periphery of the pipe. This tendency is attributed to the fact that the ascending, due to buoyancy, motion of the ice particles becomes relatively less significant as the inlet velocity increases (ice particles are transported downstream faster and they have less time to move upwards). Therefore, melting which takes mostly place near the top of the pipe (see fig. 6.4) decreases as the inlet velocity increases. Figure 6.7b shows, as expected, that the ice concentration at *z* = 0.45 m increases with the inlet ice concentration. In fact, the minimum concentration for $\emptyset_{in}$ = 20% is almost equal to the maximum concentration for $\emptyset_{in}$= 5%.

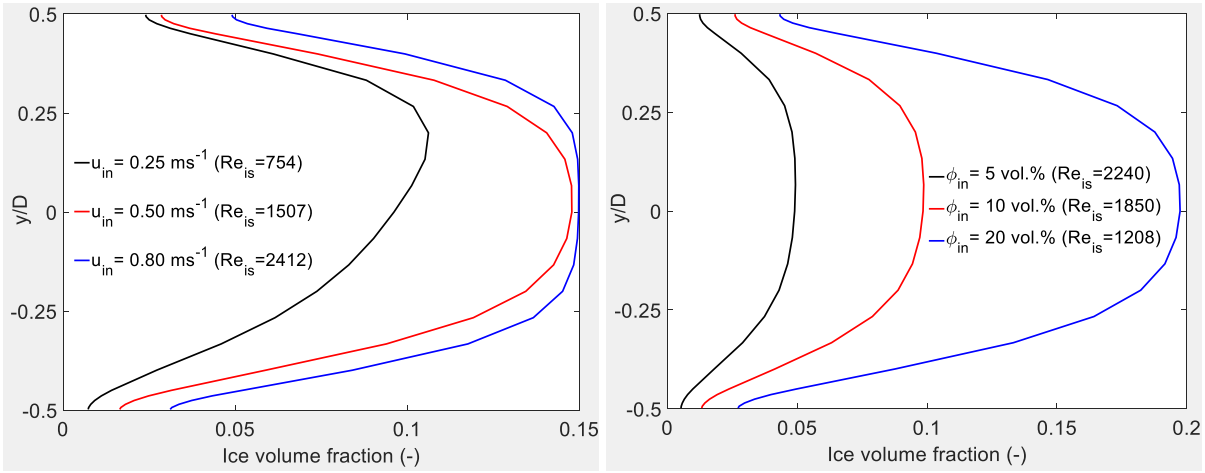

(a) (b)

Fig. 6.7. Ice volume fraction distribution at z = 0.45 m for laminar flow with q_w= 32000 W m^{-2} (a) different inlet velocities ($\emptyset_{in}$= 15%.) and (b) different inlet volume fractions (u_{in}= 0.5 m s^{1})

Figure 6.8 shows the streamwise variations of four important quantities: the wall temperature, the bulk temperature, the ice fraction and the heat transfer coefficient. In the upstream adiabatic region, the first three are equal to the corresponding imposed inlet values while the heat transfer coefficient is zero. In the first part of the heated region (from *z* = 0.1 m up to approximately 1 m) the bulk temperature increases while the wall temperature increases faster and the heat transfer coefficient decreases dramatically as is the case in all forced convection flows with uniform heat flux. It should be noted that in this region the increase of the bulk temperature is not linear since some of the supplied heat serves to melt the ice. The corresponding ice concentration decreases due to melting. Further downstream, i.e. from *z* ≈ 1m to *z* ≈ 1.75 m the wall temperature and the heat transfer coefficient are almost constant indicating that a thermally developed condition has been attained. Beyond *z* ≈ 1.75 m the ice concentration at the wall decreases to almost zero (see Fig 6.4 and Fig 6.5). As a result, the corresponding wall temperature increases dramatically, the bulk temperature increases almost linearly, and the heat transfer coefficient decreases again as in the case of pure-fluid flow with uniform heat flux. This fairly sharp decrease of the heat transfer coefficient was also observed by Xing et al. (2005) for liquid flows with PCM particles in a microchannel. Finally, in the downstream adiabatic region (*z* > 3.1 m) the ice concentration is essentially zero (see fig.

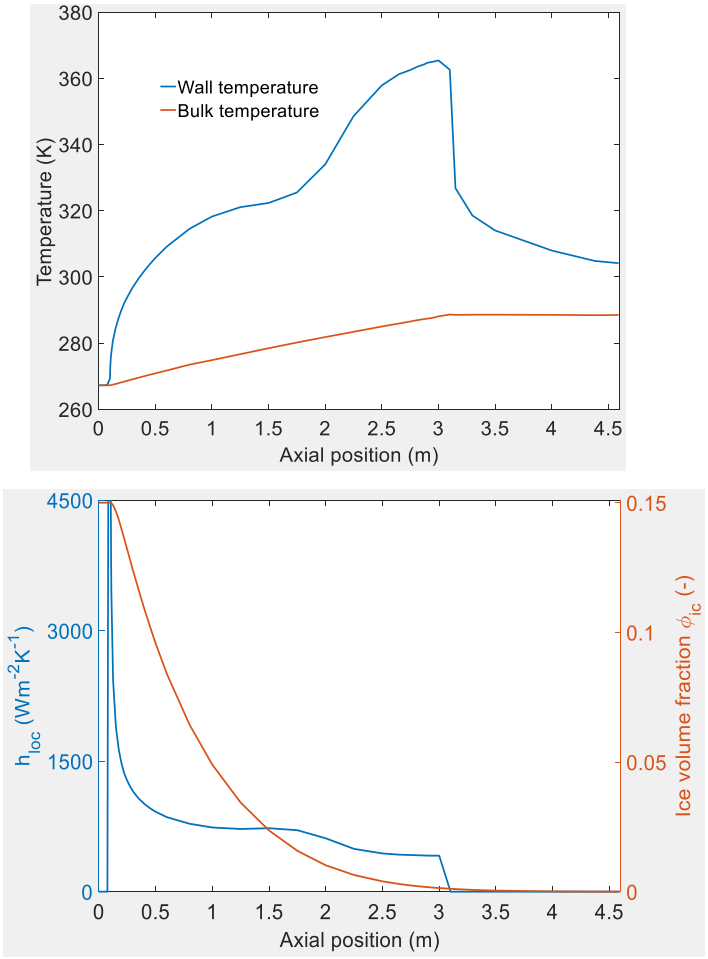

Fig. 6.8. Heat transfer characteristics of laminar ice slurry flow with $\emptyset_{in}$= 15 vol%, u_{in}= 0.5 m s^{1} (Re_{is} = 1507), q_w= 32000 W m^{-2}

6.4), the bulk temperature is constant, the heat transfer coefficient is zero and the wall temperature decreases due to conduction towards the cooler core fluid (see fig 6.4).

Figure 6.9 illustrates the influence of the imposed heat flux on the wall temperature and the local heat transfer coefficient. It shows that the peak wall temperature decreases with q_w and that it occurs further downstream as q_w decreases. In all cases the wall temperature increases rapidly at the beginning of the heated region and then the rate of its increase becomes smaller as the quantity of ice near the pipe walls decreases. The position where the rate of increase becomes once again important (which according to the discussion in the previous paragraph coincides with essentially zero ice concentration at the wall) also moves downstream as q_w decreases. The corresponding second important decrease of the heat transfer coefficient (see

Fig 8) also moves downstream and becomes less pronounced as q_w decreases. The influence of the heat flux on the heat transfer coefficient is very small as in other studies (Niezgoda-Zelasko, 2016; Yanbo et al., 2016). Results not shown here indicate that the average melting rate increases very rapidly from zero in the upstream adiabatic region to a maximum value which decreases and occurs further downstream as q_w decreases. They also show that, as expected, higher wall heat fluxes result in a shorter melting region and a longer aqueous solution region.

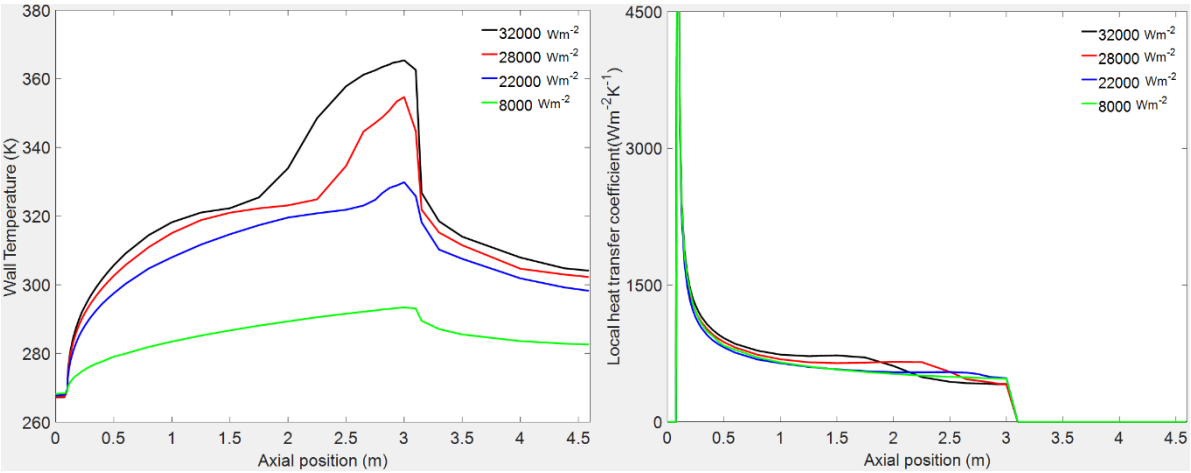

Fig. 6.9. Axial evolution of the wall temperature and the local heat transfer coefficient for laminar ice slurry flow with four wall heat fluxes for $\emptyset_{in}$= 15 vol%, u_{in}= 0.5 m s^{-1} (Re_{is} = 1507)

Figure 6.10 presents the relationship between the local Nusselt and Graetz numbers for laminar ice slurry flows with 5 and 15 vol% ice particle inlet concentrations under two wall heat fluxes, 8000 and 32000 W m^{-2}. The relation predicted by the present model is compared with values obtained from the following empirical equation by Shah et al. (1978):

$$Nu(z) = 5.364\left[1 + \left(220\frac{Gz(z)}{\pi}\right)^{-10/9}\right]^{3/10} - 1.0 \tag{6.26}$$

The definitions of the local Graetz and Nusselt numbers are as follows:

$$Gz(z) = \frac{zk_{is}}{\rho_{is}Cp_{is}u_mD^2} \tag{6.27a}$$

$$Nu(z) = \frac{h_z D}{k_{is}} \tag{6.27b}$$

The Nusselt number obtained with the present model is always higher than the one predicted by Eq 6.26 since the latter does not include the effect of melting. For the lower wall heat flux the present results show a monotonic decrease of Nu similarly to the predictions of Eq 6.26 since under this condition melting is slow. On the other hand, for the higher wall heat flux the present results show a local maximum value for Nu which, according to the previous comments, occurs at the position where the ice concentration at the wall becomes zero and the wall temperature rises sharply (see Fig 6.9).

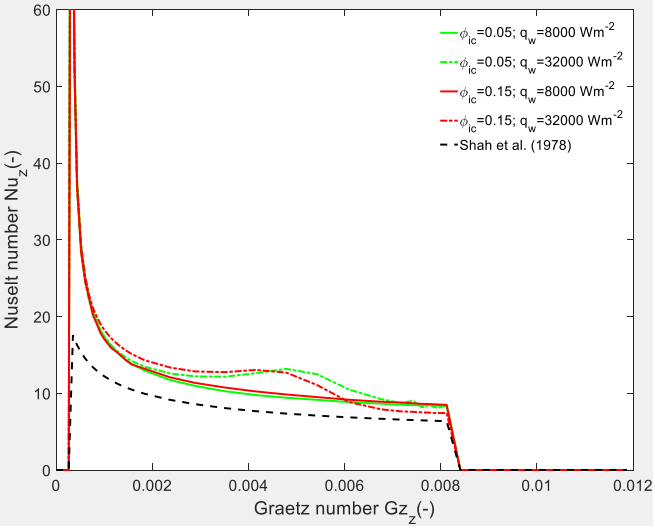

Fig. 6.10. Relationship between the local Nusselt and Graetz numbers for laminar ice slurry flows with u_{in}= 0.5 m s^{-1} (Re$_{is}$ = 1507).

6.4.3 Heat transfer characteristics of turbulent ice slurry flows

Figure 6.11 shows the ice mass fraction, temperature, velocity and melting rate distributions along the vertical diameter at different axial positions for $\emptyset_{in}$= 10.0 vol.%, u_{in}= 1.0 m s^{-1} (hence Re_{is} = 3708) and q_w=130000 $W\ m^{-2}$. Qualitatively the distributions for the ice fraction and the velocity are similar to those for laminar flow (see Fig 6.4). On the other hand those for the temperature and the melting rate are very different. Thus we note that for z > 0.25 m the temperature is higher than the imposed inlet value over the entire diameter whereas in the

laminar case it only increased near the wall. This is due to the turbulent mixing of the fluid which transports warm fluid from near the wall towards the center of the pipe. Thus the temperature of the fluid is higher than the melting temperature T_f over the entire diameter and, as shown, the melting rate is important even at the pipe axis for z = 0.65 m and z = 0.95 m.

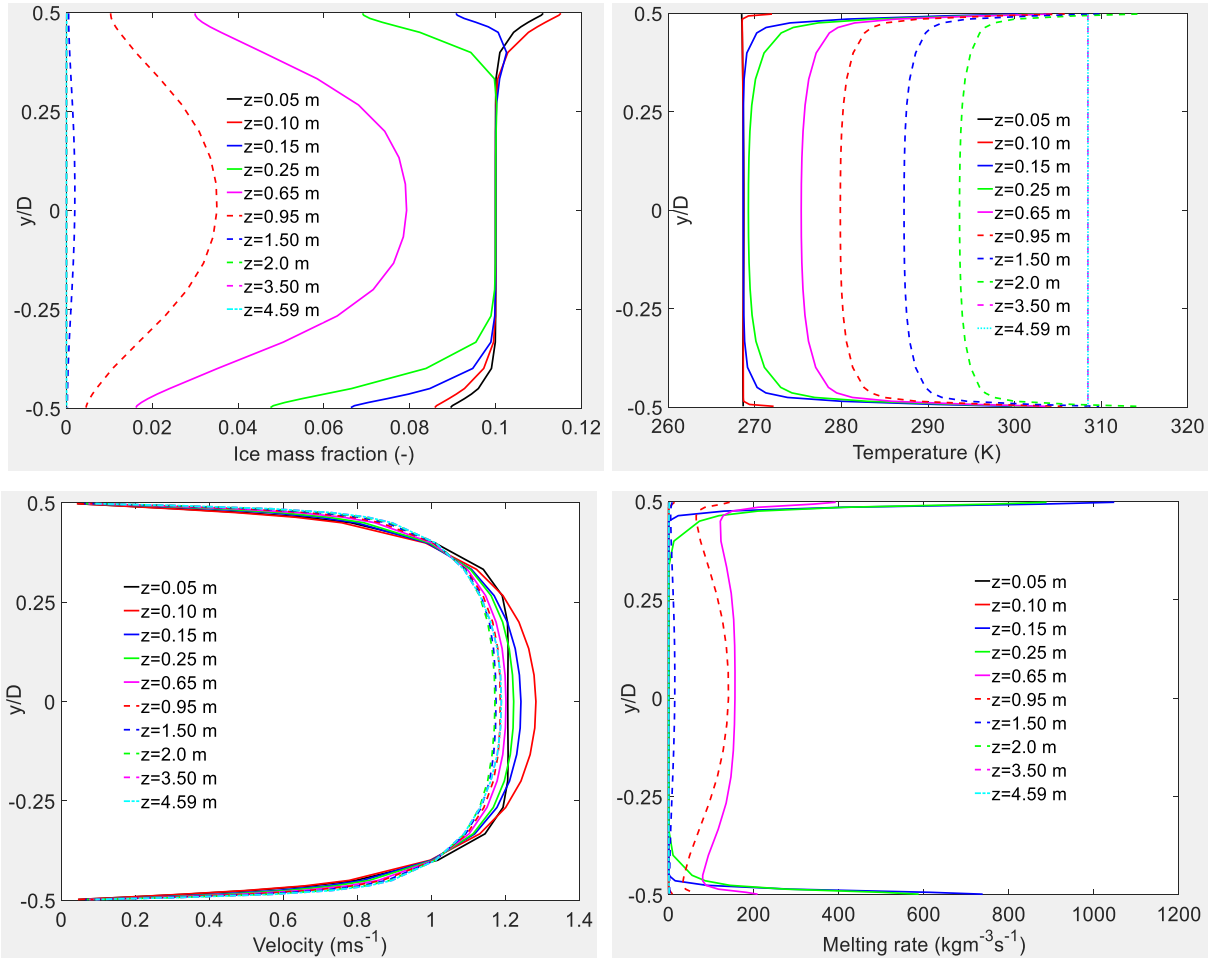

Fig. 6.11. Distributions of ice fraction, temperature, velocity and melting rate along the vertical diameter for turbulent flow with $\emptyset_{in}$= 10 vol%, u_{in}= 1.0 m s^{-1} (Re_{is} =3708), q_w= 130000 W m^{-2}

An indication of the precision of these results is provided by comparing the calculated mass flowrate for different axial positions. It is thus found that the first three significant figures for this quantity are the same for 0 < z < 4.59 m. Its value is 0.0793 kg s^{-1}. We therefore conclude that the numerical procedure is very accurate for turbulent conditions.

Figure 6.12 shows the corresponding ice fraction distribution at six different cross-sections of the pipe in the heated part of the pipe. The red and blue colours always indicate the region of maximum and minimum concentration respectively. However, it is important to note that the maximum and minimum values in the colour scale decrease as the distance from the inlet increases since, due to melting, the quantity of ice decreases as the fluid moves downstream. These results complement those in Fig. 6.11a and clearly show that the ice concentration is symmetrical with respect to the vertical pipe diameter. Analogous results for the temperature distribution are shown in Fig. 6.13. Contrary to the corresponding results for laminar flow (see Fig 6.6) the temperature is in this case almost uniform over the entire cross-section and increases significantly with the distance from the pipe inlet. The temperature distribution is also symmetrical with respect to the vertical pipe diameter.

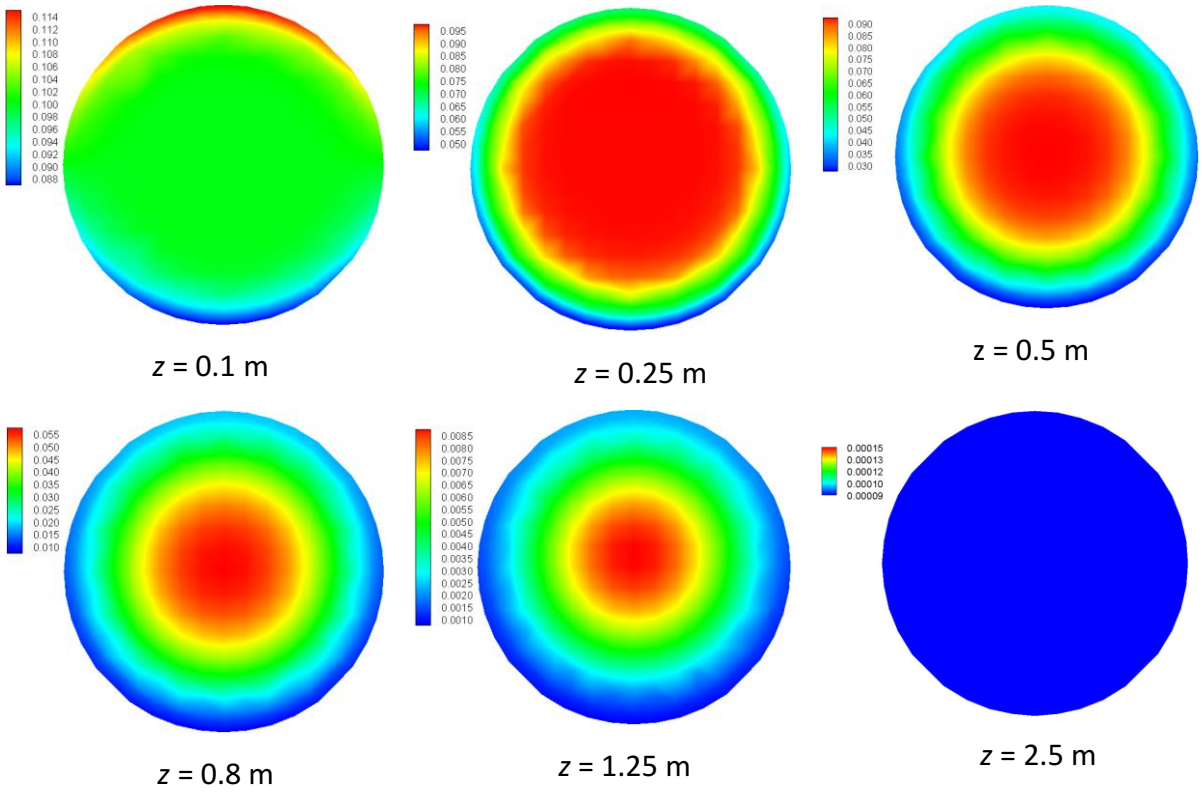

Fig. 6.12. Distributions of ice volume fraction at different cross-sections of the heated region for turbulent flow with $\emptyset_{in}$= 10 vol%, u_{in}= 1.0 m s^{-1} (Re_{is} = 3708), q_w= 130000 W m^{-2}

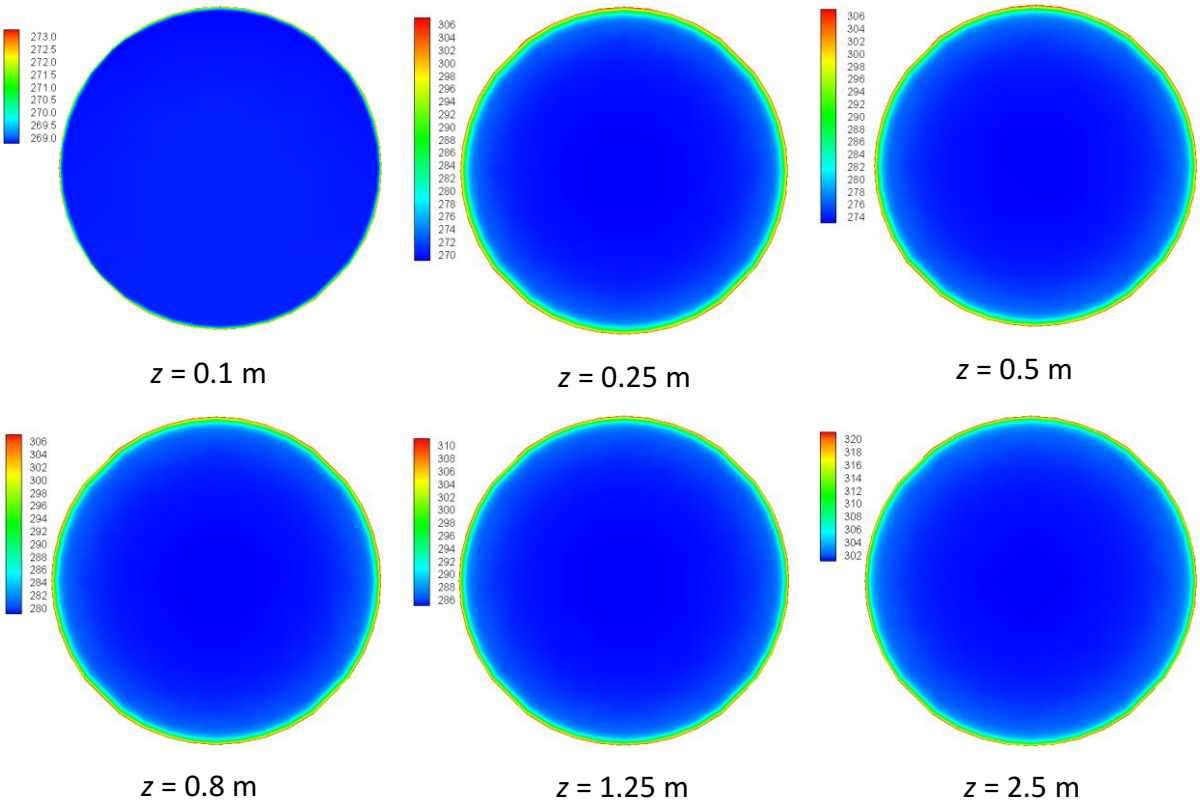

Fig. 6.13. Distributions of temperature at different cross-sections of the heated region for turbulent flow with $\emptyset_{in}$= 10 vol%, u_{in}= 1.0 m s^{-1} (Re_{is} =3708), q_w= 130000 W m^{-2}

Figure 6.14 illustrates the effect of the ice particle size on their volume fraction distribution in the vertical symmetry plane of the pipe. These results show that large particles require a longer distance to melt, a result which seems intuitively correct. They also show that the maximum concentration increases somewhat with the particle size.

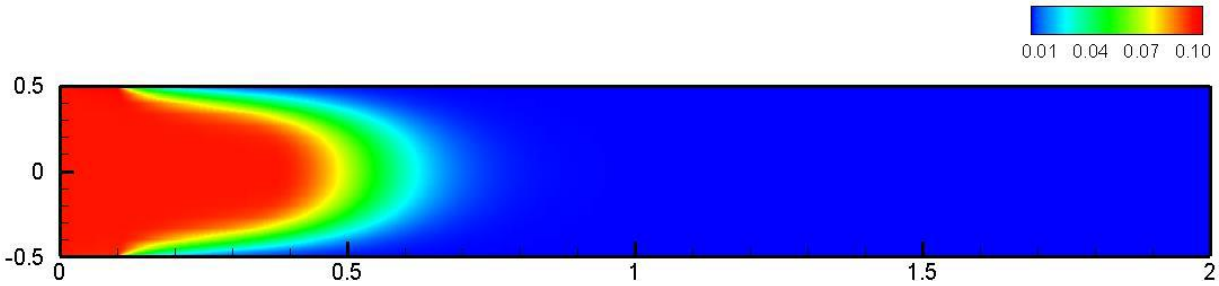

particle diameter = 0.10 mm

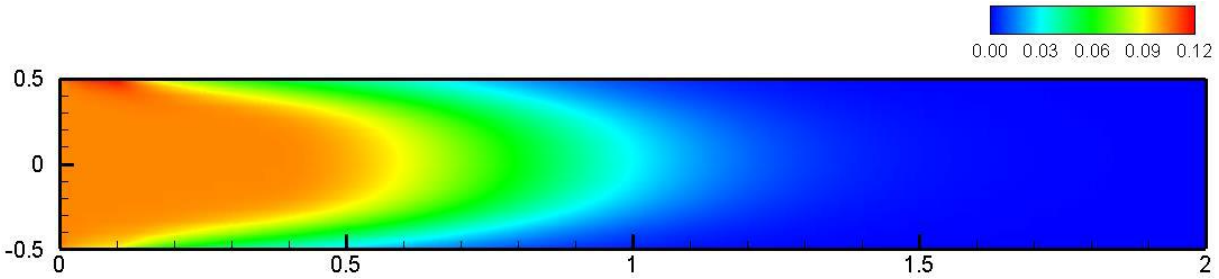

particle diameter = 0.27 mm

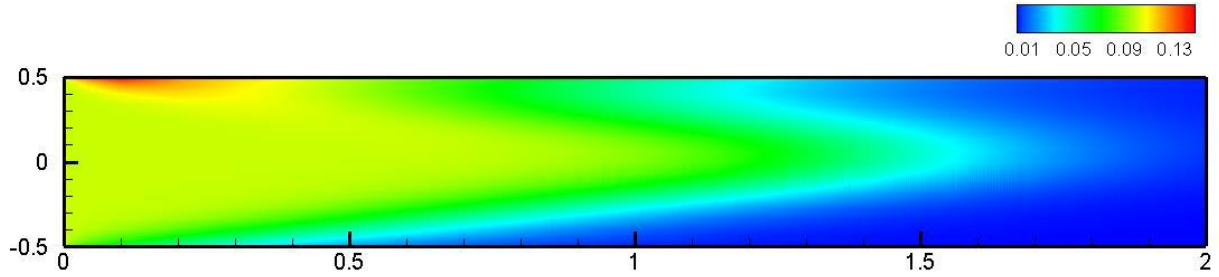

particle diameter = 0.45 mm

Fig. 6.14. Effect of ice particle size on their volume fraction distribution in the vertical symmetry plane of the pipe for turbulent flow ($\emptyset_{in}$= 10 vol.%, u_{in}= 1.0 m s^{-1}, q_w=130000 W m^{-2})

Figure 6.15 shows the streamwise variations of the wall temperature, the bulk temperature, the mean ice fraction and the heat transfer coefficient. It is analogous to Fig. 6.8 for laminar flow. In the upstream adiabatic region the first three quantities are equal to the corresponding imposed inlet values while the heat transfer coefficient is zero. As soon as heat is applied at *z* = 0.1 m the wall temperature increases very rapidly and the heat transfer coefficient decreases dramatically as is the case in all forced convection flows with uniform heat flux. The spectacular increase of the wall temperature occurs before any significant change to the fluid temperature (see Fig 6.12) and its magnitude is due to the high value of the imposed heat flux. Beyond *z* ≈ 0.25 m heat is transported towards the axis of the pipe by turbulent mixing and the fluid bulk

temperature increases almost linearly while the ice concentration decreases due to melting. Since more heat is now transferred towards the center of the pipe the difference between the wall and bulk temperature decreases and therefore the heat transfer coefficient increases. Zhang & Shi (2015) obtained analogous results (an increase of the heat transfer with distance after the almost vertical decrease near the inlet, see their Fig 6.16) with a more complicated Euler-Euler model. Melting continues, and the mean ice concentration becomes zero at approximately $z \approx 1.6$ m. Beyond this position the rate of increase of the wall temperature increases but remains smaller than that of bulk temperature since the flow field is not yet fully developed. So the difference ($T_{wall} - T_{bulk}$) decreases and therefore the heat transfer coefficient continues to increase. Finally, in the downstream adiabatic region ($z > 3.1$ m) the ice concentration is zero (see Fig 6.11), the bulk temperature is constant, the heat transfer coefficient is zero and the wall temperature decreases very rapidly due to the turbulent mixing of the hot and cold fluid. Thus, the wall temperature becomes equal to the bulk temperature very rapidly while in the case of laminar flow this equality was not achieved within the calculation domain (see Fig 6.8) since in that case heat transfer from the hot to the cold fluid took place by conduction, a much slower process.

Values of the heat transfer coefficient for the conditions used to obtain the results of Fig. 6.15 have not been found in the literature. It was therefore not possible to validate them. It should also be noted that very few studies have considered heat fluxes as high as that in Fig. 6.15. Only Zhang & Shi (2015) have the same wall heat flux as well as same inlet velocity, ice concentration and temperature as in Fig 6.15 but their additive is ethanol (10 vol%) while the pipe and particle diameters are different from those in the present study. Therefore it is not possible to quantitatively compare their calculated heat transfer coefficient values with ours. Furthermore, their heat transfer coefficient varies very little beyond the almost vertical initial decrease and is approximately equal to 3 kW m^{-2} K^{-1}. This value is considerably smaller than the experimental local value of approximately 6 kW m^{-2} K^{-1} determined by Kousksou et al (2010) at a distance of 0.5 m from the beginning of the heated region for water-ethanol (9 %) with a mass flow rate of 0.8 kg s^{-1} ($u \approx 2.5$ m s^{-1}), an ice mass fraction of 10% and $q_w \approx 22.3$ kW

m^{-2}. Since these two studies (Kousksou et al., 2010; Zhang & Shi, 2015) use the same additive with almost the same concentration and the differences between the adopted values of q_w and the inlet velocity have an opposite effect on the heat transfer coefficient it is indeed surprising that the calculated value by Zhang & Shi is only half of the corresponding measured value. On the other hand, Kousksou's value is quite close to our numerical prediction at the same axial position which, according to Fig. 6.15, is approximately equal to 5.1 kW m^{-2} K^{-1}. In view of this favorable comparison the results of Fig. 6.15 are deemed to be realistic.

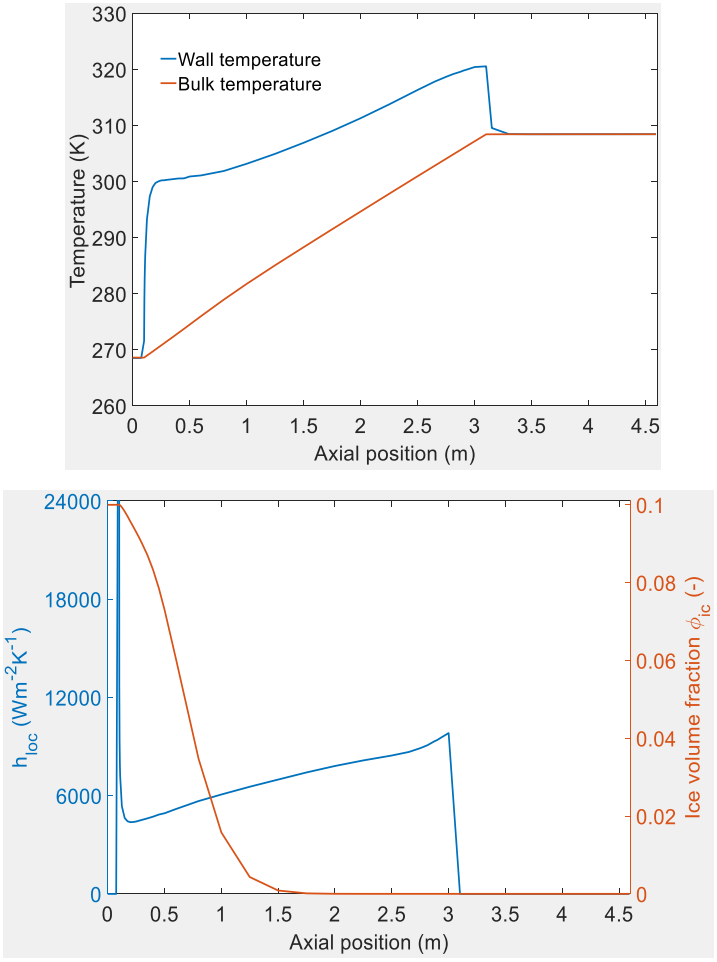

Fig. 6.15. Heat transfer characteristics of turbulent ice slurry flow with $\emptyset_{in}$= 10 vol%, u_{in}= 1.0 m s^{-1} (Re_{is} = 3708), q_w= 130000 W m^{-2}

Finally, Figure 6.16 illustrates the effect of the imposed wall heat flux on the axial evolution of the wall temperature, the local heat transfer coefficient, the mean ice fraction and the melting rate. In each case the shape of the evolutions is similar for all the values of q_w under

consideration. Thus, the maximum value of the wall temperature always occurs at the end of the heated region and it, as well as the temperature in the downstream adiabatic region, increases with q_w. Similarly, the local heat transfer coefficient decreases very rapidly in the beginning of the heated region, reaches a minimum which does not vary much with q_w and then increases reaching a maximum value, which increases with q_w, at the end of the heated region. A similar qualitative behavior of the heat transfer coefficient is predicted by the following empirical relation proposed by Gnielinski (1976):

$$h_{Gn} = Nu_{emp.} \frac{k_{is}}{D} = \frac{(f/8)(Re_{is}-1000)Pr_{is}}{1+12.7\sqrt{f/8}\left(Pr_{is}^{2/3}-1\right)} \cdot \frac{k_{is}}{D} \tag{6.28}$$

where

$$f = (1.58 \ln Re_{is} - 3.28)^{-2} \tag{6.29}$$

The differences between the present results and those calculated by this empirical relation are due to the fact that Gnielinski's relation does not take into account melting. Predictably, the increase of q_w causes a quicker decrease of the ice fraction which reaches zero at approximately 1.7 m, 1.8 m, 2.1 m and 2.8 m for wall fluxes of 130000, 110000, 80000 and 50000 W m^{-2} respectively. The influence of q_w on the heat transfer coefficient, although not very important, is greater than for laminar flow (see Fig 6.9) as in (Yanbo et al., 2016). The increase of q_w also causes an increase of the melting rate in the beginning of the heated region with the maximum rate occurring closer to the inlet as q_w increases. Beyond this position the melting rate decreases and is smaller for high values of q_w (see for example melting rates at z = 1.5 m).

The rather surprising result that high values of q_w cause higher melting rates near the beginning of the heated region (z < 0.5 m) and lower melting rates further downstream (z > 1.2 m) is explained by noting that according to equations 6.24 and 6.25 the melting rate is proportional to the product of the ice concentration and the temperature difference ΔT between the carrier fluid T and the melting temperature T_f (as noted before, for all the cases under consideration here T_f is essentially constant). Near the beginning of the heated region (z < 0.5 m) the ice concentration does not vary much with q_w since it is close to the imposed inlet value. On the

other hand, the fluid temperature is much higher for high values of q_w. Thus the melting rate in this early part of the heated region is mostly influenced by ΔT and hence it is higher for high values of q_w. Further downstream (z > 1.2 m) the remaining quantity of ice is much higher for low values of q_w and thus the ice concentration becomes the predominant factor in the determination of the melting rate which is therefore higher for low values of q_w.

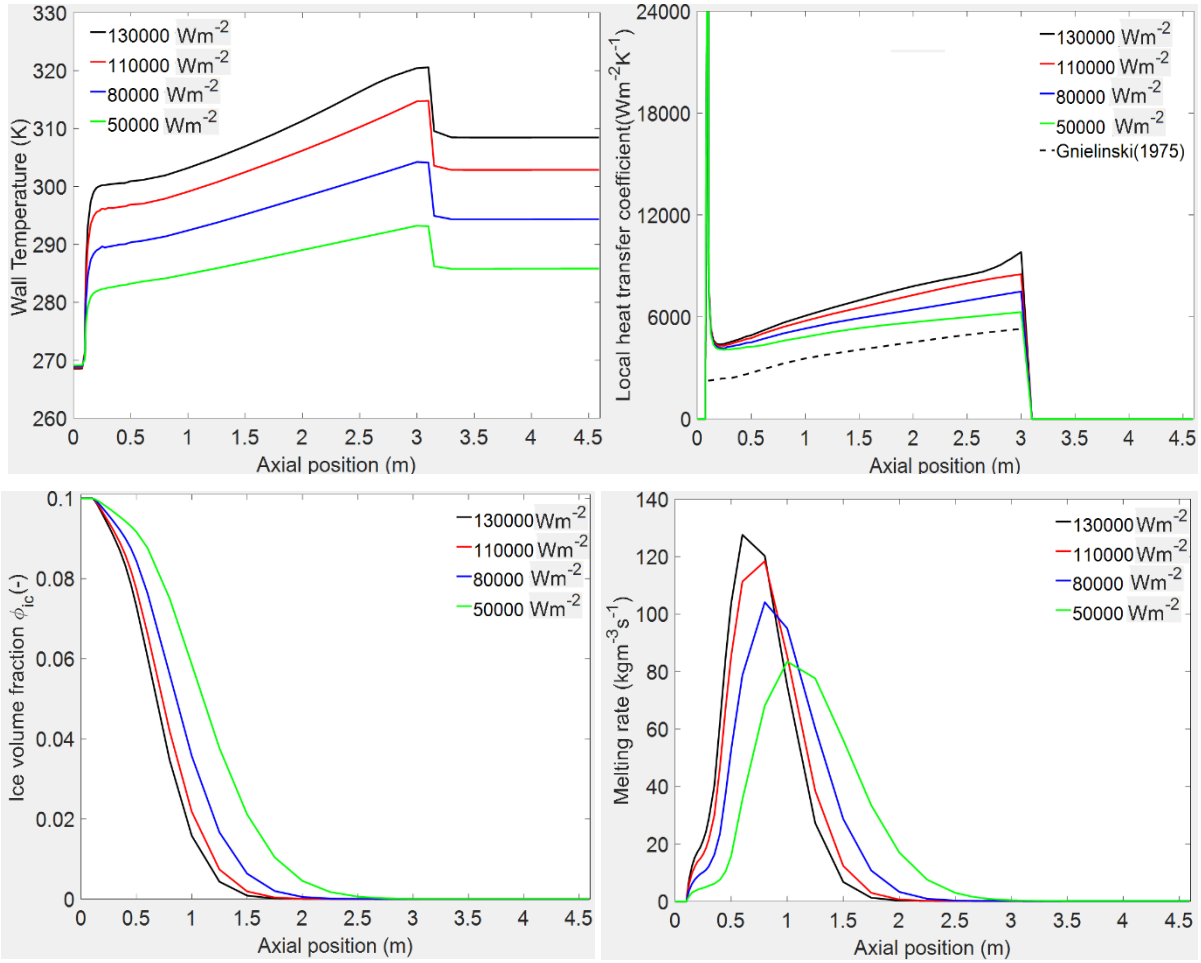

Fig. 6.16. Axial evolution of the heat transfer characteristics for turbulent flow with four wall heat fluxes and $\emptyset_{in}$= 10 vol%, u_{in}= 1.0 m s^{-1} (Re_{is} = 3708)

6.5 Conclusions

The hydrodynamic and thermal fields of ice slurry flow in a straight heated pipe were modelled using an approach which is more complete than the one used by Kousksou et al (2010) who solved only the energy equation. It is also simpler than the Euler-Euler models used in previous

studies (Zhang et Shi, 2015) since it includes fewer partial differential equations. Despite this simplicity the predicted values of the heat transfer coefficient are in very good agreement with corresponding experimental values from the literature over a large range of ice volume fractions and two different wall heat fluxes corresponding to both laminar and turbulent regimes at the pipe inlet. Similarly, the calculated profiles of velocity and ice concentration as well as the pressure drop are in very good agreement with corresponding published data. In view of these successful comparisons the proposed model was used to determine the velocity, temperature, ice fraction and melting rate for the flow of ethylene glycol-water ice slurry in a long heated pipe.

The analysis of the obtained results leads to the following main conclusions:

- Due to the melting of ice particles the heat transfer coefficient is higher than for conventional fluids for all the cases in this study. The axial evolution of the wall temperature and the local heat transfer coefficient is different than the corresponding evolutions for conventional fluids.
- The Reynolds number may increase from less than 1600 at the inlet to over 4000 at the outlet due to changes in the thermophysical properties caused by the simultaneous increase of the temperature and the decrease of the ice concentration. Therefore the classification of the flow regime as laminar or turbulent should be treated carefully.
- In the case of flows with laminar inlet conditions the temperature and the ice concentration around the pipe axis remain equal to their respective inlet values for long distances in the heated region since in such cases radial heat transfer is by conduction, a fairly slow process. As a result melting occurs only near the pipe walls.
- In the case of flows with turbulent inlet conditions the temperature and the ice concentration at the pipe axis start changing very close to the beginning of the heated region due to turbulent mixing. As a result melting occurs over the entire cross section normal to the pipe axis.
- An increase of the ice particle diameter causes an increase of the heating length required to totally melt the ice.

- Increasing the wall heat flux results in an increase of the maximum wall temperature and of the maximum melting rate as well as a reduction of the length required to totally melt the ice.

Some of these conclusions may seem obvious and it is comforting that the proposed simple model predicts logical behaviors. In fact, the main result of the present study is that it is possible to obtain good predictions for the melting flow of ice slurries without resorting to more complex two-phase models.

The present model must be further tested for higher initial concentrations of the carrier liquid (>6.5%), mass fractions of ice above 15% and larger diameters of the pipe and ice particles.

Acknowledgements: This project is part of the R&D program of the NSERC Chair in Industrial Energy Efficiency established in 2006 at Université de Sherbrooke. The authors acknowledge the support of the Natural Sciences and Engineering Research Council of Canada, Hydro-Québec, Rio Tinto Alcan and CanmetENERGY Research Center of Natural Resources Canada.

CHAPITRE 7

CONCLUSION GENERALE ET PERSPECTIVES

La prédiction du comportement hydrodynamique et thermique du coulis de glace en écoulement dans des tuyaux horizontaux est relativement difficile au regard des phénomènes complexes, tels que la stratification et la fusion des particules de glace, qui interviennent pendant l'écoulement. Dans le présent travail un modèle numérique a été développé pour simuler et analyser les caractéristiques hydrodynamique et thermique du coulis de glace en écoulement stationnaire dans un tuyau horizontal. Ce modèle qui est basé sur une approche monophasique est simple et efficace comparativement aux modèles multiphasiques actuellement disponibles utilisés pour des études similaires à la nôtre. Ces modèles multiphasiques sont très complexes et ont des exigences de calcul élevées. Les résultats obtenus avec notre modèle ont été comparés à ceux publiés dans la littérature et aux mesures obtenues, dans le cadre de ce travail, avec un banc d'essai disponible à CanmetENERGY.

- Les résultats numériques sont en excellent accord avec ceux obtenus numériquement par Wang et al. (2013a) pour les profils de vitesse et de concentration et ceux obtenus expérimentalement par Grozdek et al. (2009a, b) pour les pertes de pression et le coefficient de transfert de chaleur moyen.

- Les coefficients de friction dérivés des mesures obtenues au banc d'essai avec un coulis de glace à base de propylène glycol sont en excellent accord avec ceux obtenus par des simulations numériques dans des conditions similaires, excepté à des très faibles vitesses où le coulis de glace exhibe un comportement non-Newtonien causé probablement par le phénomène de stratification.

- Un modèle rhéologique de Bingham a été développé à partir des mesures obtenues en régime laminaire en introduisant la viscosité apparente et la contrainte seuil. Ces deux facteurs dépendent non seulement de la fraction volumique en particules de glace mais

aussi de la concentration initiale en additif. Les résultats obtenus sont en excellent accord avec ceux obtenus par des mesures expérimentales.

- En raison de la fusion de la glace, le coefficient de transfert de chaleur est plus élevé que ceux des fluides conventionnels. L'évolution axiale de la température de la paroi et du coefficient de transfert de chaleur local est différente des évolutions correspondantes pour les fluides conventionnels.
- La variation du nombre de Reynolds entre l'entrée et la sortie du tuyau due à la modification des propriétés thermophysiques du fluide (augmentation de la température et diminution de la concentration en glace) demande une classification minutieuse des régimes d'écoulement.
- Compte tenu de ces résultats, nous estimons que le modèle proposé est particulièrement adapté pour la simulation d'écoulements de coulis de glace en régime turbulent où la distribution de la fraction volumique en glace est presque uniforme.

Comme perspectives, des études ultérieures devront être conduites pour :

- Établir une base de données expérimentales de référence à partir de mesures locales des champs hydrodynamique moyen (laminaire et turbulent) et de concentration (UDV).
- Étudier l'influence d'autres facteurs tels que l'additif (nature et concentration initiale) et le rapport diamètre de la particule de glace sur le diamètre du tuyau pour des validations complémentaires du modèle, en particulier en régime laminaire où le phénomène de stratification intervient.
- Étendre cette étude au cas de fluides non-Newtoniens ($\emptyset_{ic} > 20\ vol.\ \%$) avec une attention particulière sur le modèle de Bingham.
- Étendre cette étude à d'autres géométries telles que des tubes de section transversale rectangulaire, elliptique … et des éléments plus complexes (coude, jonction en T…).

LISTE DES REFERENCES

Abba A., Montini M., Pignanoli L., Valdettaro L., Olla P., 2006. Numerical analysis of frazil ice formation in turbulent convection. arXiv:physics/0610070v1 [physics.geo-ph]

Abulnaga, B.E. (2002). Slurry Systems Handbook. New York: *McGraw-Hill*.

Ahrens, J.P. (2000). The fall-velocity equation. *J. Waterway, Port, Coastal, and Ocean Engineering*, 126(2), p. 99-102.

AIE Agence internationale de l'énergie *http://www.iea.org*

Albertson, M.L. (1953). Effect of Shape on Fall Velocity of Gravel Particles. *Proceedings of 5th Hydraulics Conference*, Univ. of Iowa, Bull. No. 34, USA.

ANSYS Fluent Theory Guide (2013) *http//www.ansys.com*

ASHRAE (2005). Handbook of Fundamentals. *Edition: I-P and SI Editions*, Atlanta, Ga

Ayel, V., Lottin, O. and Peerhossaini, H. (2003). Rheology, flow behaviour and heat transfer of ice slurries: a review of the state of the art. *International Journal of Refrigeration*, 26, p. 95–107.

Batchelor, G.K. (1977). The effect of Brownian motion on the bulk stress in a suspension of spherical particles. *Journal of Fluid Mechanics*, 83, p. 97–117.

Batchelor, G.K. (1972). Sedimentation in a dilute dispersion of spheres. *Journal Fluid Mechanics,* 52, p.245–268.

Bédécarrats, J.-P., Strub, F. and Peuvrel, C. (2009). Thermal and hydrodynamic considerations of ice slurry in heat exchangers. *International Journal of Refrigeration*, 32 (7), p. 1791-1800.

Bel, O. and Lallemand, A. (1999). Étude d'un frigoporteur diphasique. 2 : Analyse expérimentale du comportement thermique et rhéologique. *International Journal of Refrigeration*, 22, p. 175–187.

Bellas, J., Chaer, I. and Tassou, S.A. (2002). Heat transfer and pressure drop of ice slurries in plate heat exchangers. *Applied Thermal Engineering,* 22, p. 721–732.

Ben Lakhdar M. A. (1998). Comportement thermo- hydraulique d'un fluide frigoporteur diphasique : le coulis de glace. Étude théorique et expérimentale. PhD thesis, INSA Lyon, France.

Bingham, E.C. (1916). An investigation of the laws of plastic flow. *Bulletin of the US Bureau of Standards*, 13, p. 309-352.

Bond, A. (1959). Behaviour of Suspensions. *Civil Engineering Transactions of the Institution of Engineers*. Australia

Bordet A., Poncet S., Poirier M. and Galanis N. (2018). Advanced numerical modeling of turbulent ice slurry flows in a straight pipe. *International Journal of Thermal Sciences*, 127, p. 294-311.

Bordet A., Poncet S., Poirier M., Galanis N. (2018). Flow visualizations and pressure drop measurements of isothermal ice slurry pipe flows, *Experimental Thermal Fluid Sciences*, **99**, p.595-604.

Brown, P.P. and Lawler, D.F. (2003). Sphere Drag and Settling Velocity Revisited. *Journal of Environmental Engineering,* 129(2), p. 222-231.

Bui, A. and Rudman, M. (2003). Modeling of viscous resuspension using a one-field description of multiphase flows. *The International Conference on CFD in Minerals and Process Industries (CSIRO*), Melbourne, Australia, p. 10-42.

Burt, T. N. (1986). Field settling velocities of estuary muds. *In*: Mehta, A. J.(ed.), *Estuarine Cohesive Sediment Dynamics. Lecture Notes on Coastal and Estuarine Studies*, 14. Berlin, Germany: Springer Verlag, p. 126-150.

Buscall R., Goodwin J.W., Hawkins M.W. and Ottewill R.H. (1982). Viscoelastic properties of concentrated lattices, Part 1. Methods of examination, *Journal of the Chemical Society*, *Faraday Transactions I*, 78, p. 2873-2887.

Carver, R.E.(edt.). (1971). Procedures in Sedimentary Petrology. Wiley-Interscience, John Wiley and Sons Inc., New-York, 653 p.

Casson, N., (1959). A flow equation for pigment-oil suspensions of the printing ink type. *British Society of Rheology Proceedings,* Rheology of Disperse Systems, p. 84-104.

Chan D., and Powell, R.L. (1984). Rheology of suspensions of spherical particles in a Newtonian and a non- Newtonian fluid, *Journal of Non-Newtonian Fluid Mechanics*, 15, p. 165-179.

Chapman, B. (1990). Shear-induced migration phenomena in concentrated suspensions. PhD thesis, University of Notre Dame.

Chen, L., Duan, Y., Pu., W. and Zhao, C., (*2009*). CFD simulation of coal-water slurry flowing in horizontal pipelines. *Korean Journal of Chemical Engineering,* 26(4), p. 1144–1154.

Cheng, N.S. (1997a). Simplified Settling Velocity Formula for Sediment Particle. *Journal of Hydraulic Engineering,* 123(2), p. 149-152.

Cheng, N.S. (1997b). Effect of Concentration on Settling Velocity of Sediment Particles. *Journal of Hydraulic Engineering*, 123(8), p. 728-731.

Chilton, R. A. and Stainsby, R., (1998). Pressure Loss Equations for Laminar and Turbulent Non-Newtonian Pipe Flow. *Journal of Hydraulic Engineering*, 124 (5), p. 522-529.

Chow A. W., Sinton, S. W., Iwamiya, J. H. and Stephens, T. S. (1994). Shear-induced migration in Couette and parallelplate viscometers: NMR imaging and stress measurements, *Physics of Fluids*, 6, p. 2561-2576.

Christensen, K.G. and Kauffeld, M. (1997). Heat transfer measurement with ice slurry. IIR/IIF *International Conference Heat Transfer Issues in Natural Refrigerants*, Maryland, USA, p. 127–141.

Chung, J.D., Moon, S.J. and Lee, Y.P. (2014). Feasibility of ice-slurry application to the district cooling system in Korea, *International Journal of Air-Conditioning and Refrigeration,* 22, p. 1–10.

Clift, R., Grace, J.R. and Weber, M.E. (1978). Bubbles, Drops, and Particles. Academic Press, New-York.

Cordray D.R., Kaplan L.R., Woyciesjes P.M., Kozak T.F. (1996). Solid - liquid phase diagram for ethylene glycol + water. *Fluid Phase Equilibria*, 117, p. 146-152.

Coulomb, D. (2008). Refrigeration and cold chain serving the global food industry and creating a better future: two key IIR challenges for improved health and environment. *Trends in Food Science & Technology*, 29, p. 413-417.

Coussot, P. and Ancey, C., (1999). Rhéophysique des pâtes et des suspensions. *EDP Sciences*, Les Ulis.

Cowan, D., Chaer, I. and Maidment, G. (2010). Reducing refrigerant emissions and leakage– An overview and feedback from two EU projects. *Proc. Sustainable Refrigeration and Heat Pump Conference, Stockholm*, Sweden, ISBN 978-2-913149-81-6.

Danish, M., Kumar, S. and Kumar, Su. (2011). Approximate explicit analytical expressions of friction factor for flow of Bingham fluids in smooth pipes using Adomian decomposition method. *Communications in Nonlinear Science and Numerical Simulation*, 16, p. 239–251.

Davis, R.H. and Gecol, H., (1994). Hindered settling function with no empirical parameters for polydisperse suspensions. *AIChE Journal*, 40, p. 570–575.

DEFRA (2005). The Validity of Food Miles as an Indicator of Sustainable Development. ED50254 Issue 7 : http://library.uniteddiversity.coop/Food/DEFRA_Food_Miles_Report.pdf

Desmales, H. (2002). Etude des transferts de chaleur d'un fluide frigoporteur diphasique a changement de phase liquide-solide dans un échangeur a plaques lisses. Thèse de doctorat. INSA-Lyon.

Di Felice, R. (1999). The sedimentation velocity of dilute suspensions of nearly monosized spheres. *International Journal of Multiphase Flow.* 25, p. 559–574.

Doetsch, C. (2001). Experimentelle Untersuchung und Modellierung des Rheologischen Verhaltens von Ice-Slurries. PhD. Fraunhofer Institut-UMSICHT, Fachbereich Chemie technik der Universität Dortmund.

Doron, P. and Barnea, D. (1996). Flow pattern maps for solid-liquid flow in pipes. *International Journal of Multiphase Flow,* 22(2), p. 273-283.

Duminil, M. (1996). Réflexions sur l'emploi des frigoporteurs diphasiques. *Revue Générale du Froid,* 961, p. 35-41.

Egolf, P.W. and Kauffeld, M. (2005). From physical properties of ice slurries to industrial. *International Journal of Refrigeration,* 28, p. 4–12.

Egolf, P.W., Kitanovski, A., Ata-Caesar, D., Stamatiou, E., Kawaji, M., Bédécarrats, J.P. and Strub, F. (2005). Thermodynamics and heat transfer of ice slurry. *International Journal of Refrigeration,* 28, p. 51–59.

Egolf, P.W., Kitanovski, A., Ata-Caesar, D., Vuarnoz, D. and Meili, F. (2008). Cold storage with ice slurries. *International Journal of Energy Research*, 32, p. 187–203.

Einstein, A. (1906). Eine neue Bestimmung der Molekul-Dimensionen. *Annalen der Physik*, 19, p. 289–306.

Ekambara, K., Sanders, R.S., Nandakumar, K. and Masliyah, J.H. (2009). Hydrodynamic simulation of horizontal slurry pipeline flow using ANSYS-CFX. *Industrial & Engineering Chemistry Research.* 48(17), p. 8159–8171.

Fang, X., Xu, Y. and Zhou, Z. (2011). New correlations of single-phase friction factor for turbulent pipe flow and evaluation of existing single-phase friction factor correlations. *Nuclear Engineering and Design*, 241, p. 897–902.

Frei, B. and Egolf, P.W. (2002). Viscometry applied to the Bingham substance ice slurry. *Second Workshop on Ice-Slurries of the International Institute of Refrigeration*, Paris, France.

Friess Y., Koffler M. and Kauffeld M. (201). Density modification of ice particles in ice slurry. *International Journal of Refrigeration,* 62, pp. 97-105.

Gadala-Maria, F. (1979). The rheology of concentrated suspension. Ph.D. thesis, Stanford University.

Gadala-Maria, F. and Acrivos, A. (1980). Shear induced structure in a concentrated suspension of solid spheres. *Journal of Rheology*, 24, p. 799–814.

Goel, M., Roy, S.K. and Sengupta, S. (1984). Laminar forced convection heat transfer in microcapsuled phase change materiel suspensions. *Industrial Engineering Chemical Fundamentals*, 23(4), p. 420-425.

Graf, W. H. (1971). Hydraulics of Sediment Transport. *McGraw-Hill*, New-York.

Grozdek, M., Khodabandeh, R., Lundqvist, P. (2009a). Experimental investigation of ice slurry flow pressure drop in horizontal tubes. *Experimental Thermal and Fluid Science*, 33, p. 357–370

Grozdek, M., Khodabandeh, R., Lundqvist, P., Palm, B. and Melinder, A. (2009b). Experimental investigation of ice slurry heat transfer in horizontal tube. *International Journal of Refrigeration*, 32(6), p. 1310–1322.

Guilpart, J., Fournaison, L. and Ben Lakdhar, M.A. (1999). Calculation Method of Ice Slurries Thermophysical Properties-Application to Water/Ethanol Mixture. *20th International Congress of Refrigeration*, Sydney, Canada.

Gunn, D.J. (1978). Transfer of heat or mass to particles in fixed and fluidized beds. *International Journal of Heat and Mass Transfer,* 21, p. 467-476.

Hägg, C. (2005). Ice slurry as secondary fluid in refrigeration systems-fundamentals and applications in supermarkets. Licentiate thesis, Stockholm: School of Industrial Engineering and Management.

Hallermeier, R.J. (1981). Terminal Settling Velocity of Commonly Occurring Sand Grains. *Sedimentology*, 28(6), p. 859-865.

Hampton, R. E., Mammoli, A. A., Graham, A. L., Tetlow, N. and Altobelli, S.A. (1997). Migration of particles undergoing pressure driven flow in a circular conduit. *Journal of Rheology,* 41, p. 621-640.

Han, M., Kim, C., Kim, M. and Lee, S. (1999). Particle migration in tube flow of suspensions. *Journal of Rheology,* 43, p. 1157-1174.

Hansen, T.M., Radosevic, M. and Kauffeld, M. (2002). Behavior of ice slurry in thermal storage systems. *ASHRAE Research Project 1166*

Hao, Y.L. and Tao, Y.-X, (2003). Non-thermal equilibrium melting of granular packed bed in horizontal forced convection. Part I: experiment. *International Journal of Heat and Mass Transfer*, 46, p. 5017–5030.

Hawley, N. (1982). Settling Velocity Distribution of Natural Aggregates. *Journal of Geophysics, Res.* 87(C12), p. 9489–9498.

Herschel, W.H.; Bulkley, R., (1926). Measurement of consistency as applied to rubber-benzene solutions. *American Society of Testing Material Proc.,* 26, pp. 621-633

Hill, K.B., (1996). Pipeline Flow of Particles in Fluids with Yield Stresses, Ph.D. Thesis, University of Saskatchewan, Canada.

Hu, S. (2006). Fluid-Solid Transport in Ducts: Slurry Flows. In: Crowe, C. ed. *Multiphase Flow Hydraulics Conference*, Univ. of Iowa, Bull. No. 34, USA.

Illan, F. and Viedma, A. (2009a). Experimental study on pressure drop and heat transfer in pipelines for brine based ice slurry Part I: operational parameters correlations. *International Journal of Refrigeration*, 32, p. 1015–1023.

Illan, F. and Viedma, A. (2009b). Experimental study on pressure drop and heat transfer in pipelines for brine based ice slurry. Part II: Dimensional Analysis and Rheological Model. *International Journal of Refrigeration*, 32, p. 1024-1031.

Inaba, H. (2000). New challenge in advanced thermal energy transportation using functionally thermal fluids. *International Journal of Thermal Science,* 39, p. 991-1003.

Inaba, H. (2005). Preventing agglomeration and growth ice particles in water with suitable additives. *International Journal of Refrigeration*, 28, p. 20-26.

Inaba, H. and Morita, S. (1995). Flow and cold heat-storage characteristics of phase change emulsion in coiled double-tube heat exchanger. *Transaction ASME, Journal of Heat Transfer*, 117, p. 440–446.

Jensen, E.N., Christensen, K.G., Hansen, T.M., Schneider, P. and Kauffeld, M. (2000). Pressure drop and heat transfer with ice slurry. *Final Proceedings of the IIR-Gustav Lorentzen Conference on Natural Working Fluids,* Purdue University, West Lafayette, IN, p. 572-580.

Jiang, Y.Y. and Zhang, P. (2012). Numerical investigation of slush nitrogen flow in a horizontal pipe. *Chemical Engineering Science*, 73(7), p. 169–180.

Jimenez, J.A. and Madsen, O.S. (2003). A Simple Formula to Estimate Settling Velocity. *Journal of Environmental Engineering*, 129(2), p. 222-231.

Kamyar, A., Aminossadati, S.M., Leonardi, C.R. (2018). Thermo-Hydrodynamics of a Helical Coil Heat Exchanger Operated with a Phase-Change Ice Slurry as a Refrigerant. *Heat Transfer Engineering,* DOI: 10.1080/01457632.2018.1428989.

Kauffeld, M., Kawaji, M. and Egolf, P. (2005). Handbook on Ice Slurries-Fundamentals and Engineering, *International Institute of Refrigeration (IIF/IIR),* France.

Kauffeld, M. (1998). Ice slurry. *In: Proceedings of the managing challenges in thermal energy transportation with advanced thermal energy storage technology*, IEA/ECES annex 5th workshop. Freiburg, Germany.

Kauffeld, M., Christensen, K.G., Lund, S. and Hansen, T.M., (1999). Experience with ice slurry. *Proceedings of the First Workshop on Ice Slurries*, Yverdon-les-Bains, Suisse, p. 42–73.

Kauffeld, M., Wang, M. J., Goldstein, V., and Kasza, K.E. (2010). Ice slurry applications. *International Journal of Refrigeration*, 33, p. 1491–1505.

Kaushal, D.R., Thinglas, T., Tomita, Y., Kuchii, S., Tsukamoto, H., (2012). CFD modeling for pipeline flow of fine particles at high concentration. *International Journal of Multiphase Flow*, 43, p. 85–100.

Kitanovski A. & Poredos A. (2002). Concentration distribution and viscosity of ice-slurry in heterogeneous flow. *International Journal of Refrigeration,* 25(6), p. 827-835.

Kitanovski A., Vuarnoz D., Ata-Caesar D., Egolf P., Hansen T. & Doetsch C. (2005). The fluid dynamics of ice slurry. *International Journal of Refrigeration*, 28, p. 37-50

Knodel D., France M., Choi S. & Wambsganss W. (2000). Heat Transfer and pressure drop in ice-water slurries. *Applied Thermal Engineering*, 20, p. 671–685.

Kobayashi, A. and Shirai, Y. (1996). A method for making large agglomerated ice crystals for freeze concentration, *Journal of Food Engineering*, 27, p. 1–15.

Koh, C.J., and Hookham, P. (1994). An experimental investigation of concentrated suspension flows in a rectangular channel, *Journal of Fluid Mechanics*, 266, p. 1-32.

Kousksou T., Jamil A., El Rhafiki T., Zeraouli Y., 2010. Prediction of the heat transfer coefficient for ice slurry flows in a horizontal pipe. Energy Conversion and Management 51, 1311-1318.

Krieger, I. M. and Dougherty, T. J. (1959). A Mechanism for Non-Newtonian Flow in Suspensions of Rigid Spheres. *Transactions of The Society of Rheology*, 3(1), p. 137–152.

Kumano, H., Tamura, F., Sawada, S. and Asaoka, T. (2013). Study on flow and heat transfer characteristics of ice slurry in the transition region. *International Journal of Refrigeration,* 36, p. 801-808.

Kumano, H., Hirata, T., Shouji, R. and Shirakawa, M. (2010). Experimental study on heat transfer characteristics of ice slurry. *International Journal of Refrigeration,* 33, p. 1540–1549.

Kumano, H., Yamanada, Y., Makino, Y. and Asaoka., T. (2016). Effect of initial aqueous solution concentration on rheological behavior of ice slurry. *International Journal of Refrigeration*, 68, p. 218–225.

Kyoto Protocol (1997), United Nations Framework Convention on Climate Change.

Landman, K.A. and White, L.R. (1992). Determination of the Hindered Settling Factor for Flocculated Supsensions. *AIChE Journal*, 38(2), p. 184-192.

Lee, D.W., Yoon, C.I. and Yoon, E.S. (2002). Experimental Study on Flow and Pressure Drop of Ice Slurry for Various Pipes. *International Institute of Refrigeration*, Proceedings of 5th Workshop on Ice Slurries, Stockholm.

Lee, D.W. and Sharma, A. (2006). Melting of ice slurry in a tube-in-tube heat exchanger. *International Journal of Energy Research*, 30, p. 1013-1021

Leighton, D. and Acrivos, A. (1987a). Measurement of self-diffusion in concentrated suspension of spheres. *Journal of Fluid Mechanics*, 177, p. 109–131.

Leighton, D. and Acrivos, A. (1987b). The shear-induced migration of particles in concentrated suspensions. *Journal of Fluid Mechanics*, 181, p. 415–439.

Leighton, D., and Acrivos, A., (1986). Viscous Resuspension. *Chemical Engineering Science*, 41(6), p. 1377–1384.

Li, Y., Wang, S., Wang, J. and Zhang, T., 2016. CFD Study of Ice Slurry Heat Transfer Characteristics in a Straight Horizontal Tube. *Procedia Engineering*, 146, p. 504 – 512.

Liu, J., (1974). Flow of Bingham Fluid in the Entrance Region of an Annular Tube. M. S. Thesis, University of Wisconsin-Milwaukee, USA.

Liu, Y.H., Zhang, Z., Zhao, J. and Chen, P. (1997). Experimental study on friction loss characteristics of pipes with ice slurry. *Proceedings of International Symposium in Air Conditioning in High Rise Buildings*, 2, p. 490-494.

Lugo, R., Fournaison, L., Chourot, J.-M. and Guilpart, J. (2002). An excess function method to model the thermophysical properties of one-phase secondary refrigerants. *International Journal of Refrigeration*, 25, p. 916–923

Lunt, M.F. et al. (2015). Reconciling Reported and Unreported HFC Emissions with Atmospheric Observations. *Proceedings of the National Academy of Sciences of the United States of America*, 112(19), p. 5927–5931.

Lyon, M.K. and Leal, G.L. (1998). An experimental study of the motion of concentrated suspensions in two-dimensional channel flow, Part 1. Monodisperse systems, *Journal of Fluid Mechanics*, 363, p. 25-56.

Ma, Z.W. and Zhang, P. (2012). Pressure drops and loss coefficients of a phase change material slurry in pipe fittings. *International Journal of Refrigeration,* 35(4), p. 992-1002.

Maron and Pierce (1956). Application of Ree-Eyring Generalized Flow Theory to Suspensions of Spherical Particles. *Journal of Colloid Science,* 11(1), p. 80-95.

Meewise, J.W. and Infante Ferreira, C.A. (2003). Validation of the use of heat transfer models in liquid/solid fluidized beds for ice slurry generation. *International Journal of Heat and Mass Transfer*, 46, p. 3683–3695.

Melinder, A. (1997). Thermophysical Properties of Liquid Secondary Refrigerants, Tables and Diagrams for the Refrigeration Industry. *IIR Handbook*, Paris.

Melinder, A. (2010). Properties of Secondary Working Fluids. International Institute of Refrigeration, Paris. ISBN 978-2-913149-76-2.

Melinder, A. and Grandryd, E. (2005). Using property values of aqueous solutions and ice to estimate ice concentrations and enthalpies of ice slurries. *International Journal of Refrigeration,* 28, p. 13-19.

Mellari, S. (2016). Experimental investigations of ice slurry flows in horizontal pipe based on monopropylene glycol. *International Journal of Refrigeration*, 65, p. 27-41.

Mika, L. (2013). Ice slurry flow in a poppet-type flow control valve, *Experimental Thermal Fluid Science*, 45, p. 128–135.

Monteiro, A.C.S. and Bansal, P. (2010) Pressure drop characteristics and rheological modelling of ice slurry flow in pipes. *International Journal of Refrigeration*, 33, p. 1523–1532.

Montreal Protocol (1989), United Nations Environment Program on Substances that Deplete the Ozone layer- Final Act.

Morris, J. F., and Boulay, F. (1999). Curvilinear flows of non-colloidal suspensions: The role of normal stresses. *Journal of Rheology*, 43(5), article 1213.

Nascimento, S.C.C., Macedo, E.N. and Quaresmo, J.N.N. (2006). Generalized Integral Transform Solution for Hydrodynamically Developing Non-Newtonian Flows in Circular Tubes. *Journal of the Brazil Society of Mechanical & Engineering,* 28(1), p. 125-130.

Niezgoda-Zelasko, B. and Zalewski, W. (2006). Momentum transfer of ice slurry flows in tubes, modeling. *International Journal of Refrigeration*, 29(3), p. 429-436.

Niezgoda-Zelasko, B. (2006). Heat transfer of ice slurry flows in tubes. *International Journal of Refrigeration*, 29(3), p. 437–450.

Niezgoda-Zelasko, B. and Zelasko, J. (2007). Generalized non-Newtonian flow of ice-slurry, *Chemical Engineering and Process*ing, 46(10), p. 895–904.

Niezgoda-Zelasko B., 2016. The enthalpy-porosity method applied to the modelling of the ice slurry melting process during tube flow. Procedia Engineering 157, 114-121.

Nikora, V., Aberle, J., Green, M. (2004). Sediment Flocs: Settling Velocity, Flocculation Factor, and Optical Backscatter. *Journal of Hydraulic Engineering,* 130(10), p.1043–1047.

Onokoko C. L. & Galanis N. (2013). Stratification in isothermal ice-slurry pipe flow. ASME Int. Mech. Eng. Congress & Expo, paper IMECE2013-63801, San Diego (USA), November 15-21.

Onokoko, C.L., Poirier, M., Galanis, N., Poncet, S., (2018). Experimental and numerical investigation of isothermal ice slurry flow. *International Journal of Thermal Sciences*, 126, p. 82-95.

Oseen, C. (1927). Hydrodynamik. In Akademische Verlagsgesellschaft, chapter 10. Leipzig, Germany.

Otswald, W., (1925). Uber die Geschwin-digkeitfunktion der viskisität disperser Systeme. Koloid Zeistricht, 36, p. 99-117

Ovarlez, G., Bertrand, F. and Rodts, S. (2006). Local determination of the constitutive law of a dense suspension of noncolloidal particles through magnetic resonance imaging. *Journal of Rheology*, 50(3), p. 259-292.

Paradis, M.A., Turcot, R. and Faucher, G. (1989). Development of prototype ice slurry generator for district cooling. *IDHCA, 80th Annual Conference*. Virginia Beach, USA, p. 392-404.

Phillips, R. J., Armstrong, R. C., Brown, R. A., Graham, A. L. and Abbot, J. R. (1992). A Constitutive Equation for Concentrated Suspensions that Accounts for Shear-Induced Particle Migration. *Physics of Fluids A*, 4, p. 30-40.

Pronk, P. (2006). Fluidized bed heat exchangers to prevent fouling in ice slurry systems and industrial crystallizers. PhD Thesis, Technische Universiteit Delft.

Pronk, P., Hansen, T.M., Infante Ferreira, C.A. and Witkamp, G.J. (2005). Time-dependent behaviour of different ice slurries during storage. *International Journal of Refrigeration*, 28, p. 27-36.

Reghem, P. (2002). Étude hydrodynamique de fluides diphasiques solide–liquide en conduite circulaire : application au coulis de glace. PhD thesis, Université de Pau et des Pays de l'Adour, Pau, France.

Renaud-Boivin, S., Poirier, M. and Galanis, N. (2012). Experimental study of hydraulic and thermal behavior of an ice slurry in a shell and tube heat exchanger. *Experimental Thermal and Fluid Science*, 37, p. 130-141.

Revay, J. M. and Higdon, J. J. L. (1992). Numerical simulation of polydisperse sedimentation: equal-sized spheres. *Journal of Fluid Mechanics*, 243, p. 15-32.

Richardson, J. F. and Zaki, W. N. (1954). Sedimentation and Fluidization: Part 1. Transactions of the Institution of Chemical Engineers, 32, p. 35-53.

Rubey, W.W. (1933). Settling Velocities of Gravel, Sand, and Silt Particles. *American Journal of Science,* XXV (145), p. 325-338.

Sari, O., Meili, F., Vuarnoz, D. and Egolf, P.W. (2000). Thermodynamics of moving and melting ice slurries. *Proceedings of the 2nd IIR Workshop on Ice Slurries*, Paris, p. 140–153.

Sayed-Ahmed, M.E. (2000). Mixed convection heat transfer of power-law fluids in a vertical eccentric annulus. *Indian Journal of Pure Applied Mathematics*, 31(3), p. 227-242.

Schaflinger U. (1990). Centrifugal separation of a mixture. *Fluid Dynamics Research*, 6, p. 213-249.

Shapley, N. C., Armstrong, R. C. and Brown, R.A. (2002). Laser Doppler velocimetry measurements of particle velocity fluctuations in a concentrated suspension. *Journal of Rheology*, 46, p. 241-272.

Shi, Z., Chen, J. and Chen, Q. (2015). On the turbulence models and turbulent Schmidt number in simulating stratified flows. *Journal of Building Performance Simulation*, 9(2), p. 134-148.

Shi, X.J. and Zhang, P. (2016). Conjugated heat and mass transfer during flow melting of a phase change material slurry in pipes. *Energy*, 99, p. 58-68.

Shih, T.H., Liou, W.W., Shabbir, A., Yang, Z. and Zhu, J. (1995). A new k-epsilon eddy-viscosity model for high Reynolds number turbulent flows, *Computers & Fluids*, 24(3), p. 227-238.

Shojaei, A. and Arefinia, R. (2006). Analysis of the sedimentation process in reactive polymeric suspensions. *Chemical Engineering Sciences*, 61(23), p. 7565–7578.

Shook, C. A. (1985). Experiments with concentrated slurries of particles with densities near that of the carrier fluid. *The Canadian Journal of Chemical Engineering,* 63, p. 861-869.

Sinton, S. W. and Chow, A. W. (1991). NMR flow imaging of fluids and solid suspensions in Poiseuille flow, *Journal of Rheology,* 35, p. 735-772.

Snoek, C.W. (1993). The design and operation of ice-slurry based district cooling systems. IEA report: district heating, The Netherlands Publishers.

Snoek, C. and Bellamy, J. (1997). Heat transfer measurements of ice slurry in tube flow. *Proceedings of the 4th World Conference on Experimental Heat Transfer. Fluid Mechanics and Thermodynamics,* Brussels, p. 1993-1997.

Stamatiou, E. and Kawaji, M. (2005). Thermal and flow behavior of ice slurries in a vertical rectangular channel. Part II. Forced convective melting heat transfer. *International Journal of Heat and Mass Transfer,* 48, p. 3544–3559.

Stamatiou, E., Meewise, J.W. and Kawaji, M. (2005). Ice slurry generation involving moving parts. *International Journal of Refrigeration*, 28, p. 60–72.

Stutz, B., Reghem, P. and Martinez, O. (2013). Flow of Slurries of Particles with Density Close to that of Water. *Consulted online at: http://docsmartinez.free.fr/NO_vi.PDF*

Swamee P. K. & Aggarwal N. (2011). Explicit equation for laminar flow of Bingham plastic fluids. *Journal of Petroleum Science and Engineering*, 76, p. 178–184

Tchobanoglous, G. (1991). Wastewater engineering: treatment, disposal, and reuse (3rd ed.). Metcalf & Eddy, McGraw-Hill Inc., New-York.

Thomas, D. G. (1965). Transport characteristics of suspension: VIII. A note on the viscosity of Newtonian suspensions of uniform spherical particles. *Journal of Colloid Science*, 20(3), p. 267–277.

Tian, Q.Q., He, G.G., Wang, H. and Cai, D.H. (2014). Simulation on transportation safety of ice slurry in ice cooling system of buildings, *Energy & Buildings*, 72, p. 262–270.

Trabelsi, H., Galanis, N. and Orfi, J. (2010). Simulation of forced convection ice slurry flow in a heated tube. *Proceedings of the 14th International Heat Transfer Conference* IHTC14 August 8-13, Washington, DC, USA.

Trabelsi, S., Hafid, M., Poncet, S., Poirier, M., Lacroix, M., Rheology of Ethylene- and Propylene-Glycol Ice Slurries: experiments and ANN model, *International Journal of Refrigeration*, **82**, p.447-460, 2017.

Wafo Soh, C. and Mureithi, E.W. (2006). Exact and numerical solutions of a fully developed generalized second-grade incompressible fluid with power-law temperature-dependent viscosity. *International Journal of Non-Linear Mechanics, 41*, p. 271-280.

Wallis, G.B., (1969). One Dimensional Two-Phase Flow. McGraw Hill, New-York.

Wang, J.H., Wanga, S., Zhang, T. and Liang, Y. (2013a), Numerical investigation of ice slurry isothermal flow in various pipes. *International Journal of Refrigeration*, 36(1), p. 70–80.

Wang, J., Wang, S., Zhang, T. and Battaglia, F. (2017). Mathematical and experimental investigation on pressure drop of heterogeneous ice slurry flow in horizontal pipes. *International Journal of Heat and Mass Transfer*, 108, p. 2381–2392

Wang, J.H., Zhang, T.F. and Wang, S.G. (2013b). Heterogeneous ice slurry flow and concentration distribution in horizontal pipes. *International Journal of Heat and Fluid Flow*, 44, p. 425–434.

Wasp, E.J., Kenny, J.P. and Gandhi, R.L. (1977). Solid-Liquid Flow Slurry Pipeline Transportation. 1st ed. Germany: Trans. Tech Publications.

Xing, K.Q., Tao, Y.-X. and Hao, Y. L. (2005). Performance Evaluation of Liquid Flow with PCM Particles in Microchannels. *Journal of Heat Transfer*, 127, p. 934-940.

Yanbo Li, Shugang Wang, Jihong Wang, Tengfei Zhang, 2016. CFD Study of Ice Slurry Heat Transfer Characteristics in a Straight Horizontal Tube. Procedia Engineering 146, 504-512.

Yu, B. and Ozoe, H. (2001). Non-parabolic Flow Pattern at the Entrance Region in a Circular Tube with a Uniform Inlet Velocity. *Numerical Heat Transfer*, *Part A*, 39, p. 857-862.

Zarraga, I. E., Hill, D. A., and Leighton, D. T. (2000). The characterization of the total stress of concentrated suspensions of noncolloidal spheres in Newtonian fluids. *Journal of Rheology,* 44(2), p. 185-220.

Zhang, J. and Li, A., (2008). CFD simulation of particle deposition in a horizontal turbulent duct flow. *Chemical Engineering Research and Design*, 86, p. 95-106.

Zhang, P. and Shi, X.J. (2015). Thermo-fluidic characteristics of ice slurry in horizontal circular pipes. *International Journal of Heat and Mass Transfer*, 89, p. 950-963.

Zhang, P. and Ma, Z.W. (2012). An overview of fundamental studies and applications of phase change material slurries to secondary loop refrigeration and air conditioning systems, *Renewable and Sustainable Energy Reviews*, 16(7), p. 5021–5028.